Stony Brook University

Structural Studies of Molybdopterin Synthase, an Essential Enzyme for Dithiolene Formation during Molybdenum Cofactor Biosynthesis

A Dissertation Presented

By

Juma Nkosi Daniels

to

The Graduate School

In Partial Fulfillment of the

Requirements for the Degree of

Doctor of Philosophy

In

Molecular and Cellular Biology

Stony Brook University

December 2007

Stony Brook University

The Graduate School

Juma Nkosi Daniels

We, the dissertation committee for the above candidate for the
Doctor of Philosophy Degree,
Hereby recommend acceptance of this dissertation.

Hermann Schindelin, Ph.D.
Advisor
Professor, Rudolf Virchow Center, University of Würzburg, Germany
Formerly Associate Professor, Department of Biochemistry and Cell Biology,
Stony Brook University

Robert S. Haltiwanger, Ph.D.
Co-advisor
Professor, Department of Biochemistry and Cell Biology, Stony Brook University

A. Wali Karzai, Ph.D.
Chairperson of Defense
Associate Professor, Department of Biochemistry and Cell Biology
Stony Brook University

Erwin London, Ph.D.
Professor, Department of Biochemistry and Cell Biology, Stony Brook University

Peter J. Tonge, Ph.D.
Professor, Department of Chemistry, Stony Brook University

Daniel P. Raleigh, Ph.D.
Professor, Department of Chemistry, Stony Brook University

This dissertation is accepted by the Graduate School

Lawrence Martin
Dean of the Graduate School

Abstract of the Dissertation

Structural Studies of Molybdopterin Synthase, an Essential Enzyme for Dithiolene Formation during Molybdenum Cofactor Biosynthesis

By

Juma Nkosi Daniels

Doctor of Philosophy

In

Molecular and Cellular Biology

Stony Brook University

2007

The molybdenum cofactor is found in a variety of enzymes present in bacteria, plants and animals and is composed of closely related molecules which all contain molybdopterin, a tricyclic pyranopterin containing a cis-dithiolene group. Molybdopterin is important for the coordination of molybdenum or tungsten in virtually all biological life forms. Deficiencies in molybdenum cofactor biosynthesis in humans cause severe neurological abnormalities that usually result in death during early childhood. The majority of the mutations causing this deficiency have been identified in proteins that are involved in the synthesis of the molybdopterin moiety of the cofactor. One of the enzymes affected by these previously characterized mutations is molybdopterin synthase which is responsible for the formation of the dithiolene group of molybdopterin. To further the understanding of the mechanistic action of the molybdopterin synthase,

structural studies of the enzyme have been performed using X-ray crystallographic techniques.

MPT synthase is comprised of two subunits, MoaE and MoaD, and the activated enzyme carries a thiocarboxylate at the C-terminus of MoaD. The 2.0 Å resolution crystal structure of MPT synthase in its apo-form and the 2.5 Å structure of the enzyme in complex with its substrate, precursor Z, reveal a distinct substrate-binding pocket which is 11 Å wide and allows the substrate to snuggly fit into it. This newly defined pocket reveals the residues involved in substrate-binding and suggests possible roles for some of these residues during catalysis. Due to the structural similarity of the small MoaD subunit to the small subunit of thiazole synthase, an enzyme involved in thiamine biosynthesis, the sulfur transfer mechanism is proposed to be closely related, although MPT synthase is involved in a distinct sequence of two sulfur transfer events. The co-crystal structure of MPT synthase with precursor Z is the first ever reported for this class of sulfur transferases and provides a structural basis for understanding the effects of mutations which lead to molybdenum cofactor deficiency.

Table of Contents

List of Abbreviations

μM:	Micromolar
Å:	Ångstrom (10^{-10} m)
Amp:	Ampicillin
ATP:	Adenosine triphosphate
Cα:	Alpha carbon
C-:	Carbon
Cam:	Chloramphenicol
Cu:	Copper
Da:	Dalton
DNA:	Deoxyribonucleic acid
DTT:	Dithiothreitol
DXP:	1-deoxy-D-xylulose-5-phosphate
E. coli:	*Escherichia coli*
EDTA:	Ethylene diamine tetracetic acid
FAD:	Flavine adenine dinucleotide
Fig:	Figure
FPLC:	Fast protein liquid chromatography
Fe-S:	Iron sulfur cluster
GMP:	Guanosine monophosphate
GTP:	Guanosine triphosphate
H-:	Hydrogen

HEPES:	4-(2-hydroxyethyl)-1-piperazineethanesulfonic acid
HPLC:	High performance liquid chromatography
IPTG:	Isopropyl-β-D-thiogalactopyranoside
kDa:	Kilodalton (=1,000 Da)
LB:	Luria Bertani broth
MCD:	Molybdopterin cytosine dinucleotide
MGD:	Molybdopterin guanine dinucleotide
M:	Molar
Mm:	Millimolar
Mo:	Molybdenum
Moco:	Molybdenum cofactor
MPT:	Molybdopterin
MPTS:	Molybdopterin synthase
N-:	Nitrogen
NaCl:	Sodium chloride
NAD:	Nicotinamide adenine dinucleotide
$(NH_4)_2SO_4$:	Ammonium sulfate
Ni^{2+}:	Nickel ion
NMR:	Nuclear magnetic resonance
nM:	Nanomolar
MoaD-SH:	Thiocarboxylated MoaD
MoaEΔ141:	MoaE subunit without the C-terminal helix (141-150)

OD_{600}:	Optical density measured at 600 nm
PAGE:	Polyacrylamide gel electrophoresis
PCR:	Polymerase chain reaction
PDB:	Protein Data Bank
PEG:	Polyethylene glycol
Psi:	Pounds per square inch
rms:	Root mean square
ROS:	Reactive oxygen species
S-:	Sulfur
SA:	*Stapylococcus aureus*
S. aureus:	*Stapylococcus aureus*
SDS:	Sodium dodecyl sulfate
$t_{1/2}$:	Half-life
Tris:	Tris (hydroxymethyl) aminomethane
U:	Enzymatic Unit
VC:	*Vibrio cholerae*
V. cholerae:	*Vibrio cholerae*
W:	Tungsten
XDH:	Xanthine dehydrogenase

List of Figures

List of Tables

Acknowledgements

I would like to deeply thank our collaborators from the Rajagopalan laboratory at Duke University, particularly Dr. Margot Wuebbens, for providing much of *S. aureus* and *V. cholerae* proteins and substrate used in my research. I thank all my current and previous committee members, Dr. Robert Haltiwanger, Dr. A. Wali Karzai, Dr. Erwin London, Dr. Peter Tonge, and Dr. Daniel Raleigh, for guidance and support. I sincerely thank, my advisor Dr. Hermann Schindelin together with Dr. Caroline Kisker they have provided continuous support, immense knowledge and guidance in the field of protein crystallography and I am fortunate to have learned from them during my graduate school career. I thank the members of Schindelin and Kisker lab, I will always remember every one of them, they have all made graduate school research a more enjoyable time in my life, and I appreciate and value their friendship.

I dedicate this thesis to my loving family, my mother, my younger sister, Danielle, and my older brother, Chris, throughout my life they have always been my foundation of love and inspiration.

Main Introduction

A. **Molybdenum's importance in life**

The transition metals molybdenum and tungsten are found in trace amounts in virtually all biological life forms and depending on the organism, one or the other of these metals is required for a variety of redox transformations. With the exception of nitrogenase, all Mo- and W-dependent enzymes complex the metal as the molybdenum cofactor (Moco), whose biosynthetic pathway is well conserved in prokaryotes, archaea and eukaryotes [1,2]. As a vital component of proteins involved in the global carbon, sulfur, and nitrogen cycles, Moco has been very well characterized in a variety of enzymes, including xanthine dehydrogenase, sulfite oxidase and nitrate reductase (Fig 1.1) [2-7].

i. Xanthine dehydrogenase

Xanthine dehydrogenase (XDH), which is found in most mammalian tissues, is involved in the oxidative hydroxylation of purines, pyrimidines, pterins, and aldehyde substrates. It is mainly involved in the final stage of purine catabolism by catalyzing the oxidation of hypoxanthine to xanthine and the oxidation of xanthine to uric acid. Xanthine dehydrogenase contains one Moco which is directly involved in the initial oxidation of the substrate. Subsequently the electrons derived from the substrate are transferred to two Fe-S clusters, a tightly bound flavine adenine dinucleotide (FAD), and finally to nicotinamide adenine dinucleotide (NAD) (Fig 1.2a). Normally, the enzyme can be found in this form, but upon proteolytic cleavage it is transformed into an oxidase, which represents the form of the enzyme found in cow's milk. This altered enzyme is capable of substituting molecular oxygen for NAD as the final electron acceptor and its

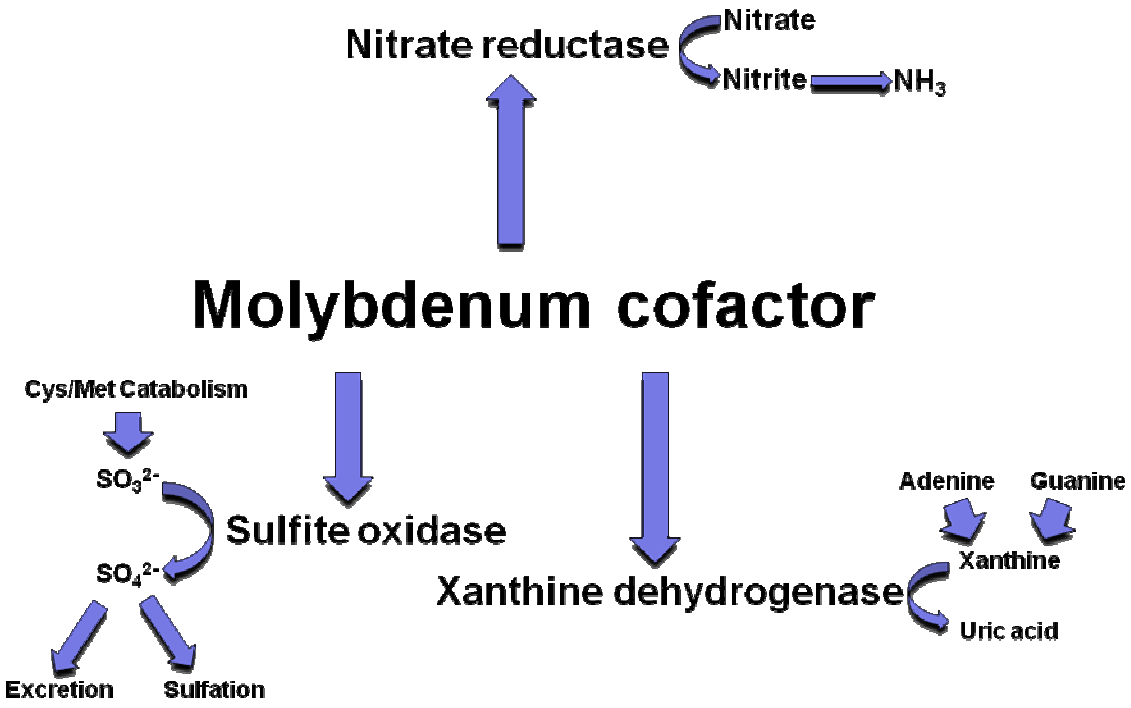

Figure 1.1: Selected molybdoenzymes found in the global carbon, sulfur and nitrogen cycles. The molybdenum cofactor is the essential common component found in enzymes involved in cysteine, methionine and DNA catabolism. It is also required in bacterial nitrate assimilation and anaerobic respiration.

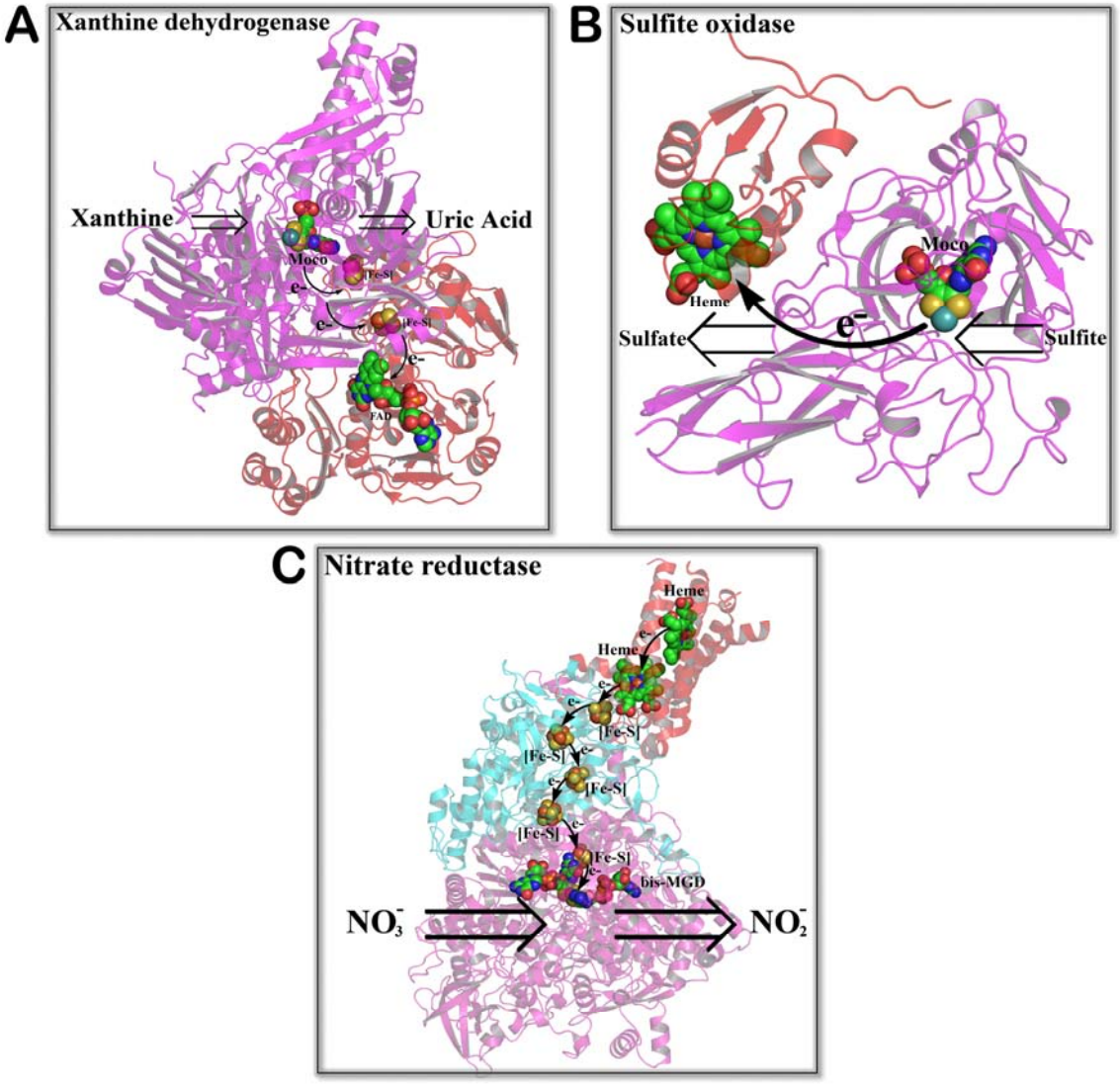

Figure 1.2: Structures of molybdoenzymes with multiple electron carriers depicting the electron flow between them. Crystal structures of **(a)** xanthine dehydrogenase (PDB entry 1JRO), **(b)** sulfite oxidase (PDB entry 1SOX) and **(c)** respiratory nitrate reductase (PDB entry 1Y4Z). Moco, FAD, heme and iron-sulfur clusters in ball representation with Moco binding subunits colored in *magenta*. Substrates bind in close proximity of the molybdenum cofactor, which represents one end of the electron transfer chain or wire utilized in transformations in all plants, animals and bacteria.

activity generates a variety of reactive oxygen species (ROS), such as superoxides and hydrogen peroxides. The ROS production results in a potent antimicrobial activity, an observation which correlates with studies implicating this molybdoenzyme in the inflammatory response [8-10].

ii. Sulfite oxidase

Despite sulfate's importance in cellular activities, for a long time it has been considered to only be an inert ion. Sulfate is required for proper cell growth and development in many organisms. It is involved in a variety of important biological processes, including biosynthesis and detoxification via sulfation of many endogenous (glycosaminoglycans, cerebrosides, steroids, catecholamines) and exogenous compounds (acetaminophen, isoproterenol, ibuprofen, salicylate) [11]. Sulfation produces glycosaminoglycans, such as chondroitin sulfates, which form the major component of cartilage. This process also forms a major constituent in the myelin membranes of the brain, namely cerebroside sulfate [12,13]. Methionine and cysteine metabolism can sometimes produce sulfite as a byproduct and sulfite can be found in many foods that are ingested by humans. Sulfite is subsequently oxidized to sulfate by the enzyme sulfite oxidase, which also contains the molybdenum cofactor, and an additional b-type heme as an electron transferring prosthetic group which is utilized to transfer electrons to cytochrome c, the ultimate electron acceptor in this pathway (Fig 1.2b). Mutations that cause sulfite oxidase deficiency augment the normal metabolic pathways for sulfite, causing an accumulation of sulfite in the body. Sulfite oxidase deficiency is caused by various mutations that disrupt enzyme dimerization of sulfite oxidase, disrupt interactions

with the molybdenum center and the interactions with the molybdopterin portion of the Moco [14,15]. Since sulfite is a relatively reactive ion in comparison to sulfate, it may increase the formation of metabolites such as S-sulfocysteine and thiosulfate. It is possible that substituting S-sulfocysteine for cysteine in connective tissues causes the weakening of the zonule of the lens, thus resulting in the characteristic dislocated lenses. Similar damage may also occur throughout the nervous system leading to the severe neurodegenerative phenotypes associated with this disease. However, it should also be noted that the pathogenesis of brain damage in individuals affected by sulfite oxidase deficiency could also be related to a general lack of sulfate in the central nervous system, or even a mixture of both an abundance of sulfite and a lack of sulfate.

iii. Nitrate reductase

Since humans lack the ability to fix nitrogen, nitrogen sources are obtained through the diet in the form of amino acids derived from plants and animals. Bacteria, on the other hand have a superior capability to obtain nitrogen; some bacteria are able to fix atmospheric nitrogen in an ATP dependent reaction that is catalyzed by the nitrogenase enzyme system. This mechanistic challenge is accomplished by a molybdenum iron cofactor that is completely different from Moco. Nitrogen in the form of nitrate can also be used in the production of essential amino acids through the Moco-containing assimilatory nitrate reductases found in both bacteria and plants. These enzymes are closely related to sulfite oxidase, but feature a NADH as third cofactor in addition to the Moco and *b*-type heme. Additionally, under anaerobic conditions, nitrate reduction is tightly linked with anaerobic respiration via Moco-containing respiratory nitrate

reductase [14]. Respiratory nitrate reductases are normally anchored on the cytoplasmic face of the membrane, and contain three subunits with characteristic redox-active prosthetic groups: NarG, the catalytic subunit with a molybdo-bis(molybdopterin guanine dinucleotide) form of the molybdenum cofactor and an [Fe-S] cluster; NarH, the electron transfer subunit with four [Fe-S] clusters; NarI, the integral membrane subunit with two hemes [16,17]. NarGHI catalyzes electron transfer from a quinol binding site located in NarI through the redox cofactors aligned as an "electric wire" through the complex to the molybdo-bis-(molybdopterin guanine dinucleotide) cofactor in NarG, where nitrate is reduced to nitrite (Fig 1.2c). Often NarGHI forms a respiratory chain with a second molybdoenzyme, formate dehydrogenase, via a lipid soluble quinol. Electron transfer from formate to nitrate is coupled to proton translocation across the cytoplasmic membrane generating the proton motive force necessary for the production of cellular energy [18,19].

The discovery of molybdoenzymes, and their essential roles in a variety of processes ranging from the detoxification of purines and sulfite to alternate respiratory systems in bacteria has accelerated further studies in the past 40 years. In parallel with the discovery of new Moco-containing enzymes and their molecular characterization multiple studies have identified and characterized a series of enzymes involved in Moco biosynthesis which are necessary for the proper function of all molybdenum-containing (with the notable exception of nitrogenase) or tungsten-containing enzymes.

B. **Molybdenum cofactor biosynthesis**

The notion of a cofactor common to all molybdoenzymes was identified from studies of a series of pleiotropic mutants found in the fungus *Aspergillus nidulans* which caused a deficiency in both xanthine dehydrogenase and nitrate reductase [20]. It was subsequently demonstrated that the inactive nitrate reductase apo-protein isolated from the nit-1 mutant of *Neurospora crassa* regained activity after the addition of denatured purified molybdoenzymes [21,22]. The existence of a non-covalently bound cofactor common to nitrate reductase, sulfite oxidase, and xanthine oxidase and other Moco-containing enzymes was later identified as a novel pteridine derivative [23-26]. This pteridine is usually referred to as molybdopterin (MPT) and represents the metal-binding portion of Moco. MPT can be chemically described as a reduced pyranopterin-ene-dithiolate with a terminal phosphate group as seen in figure 1.3.

In *Escherichia coli* (*E. coli*), MPT biosynthesis starts with a molecule of 5'-GTP which is converted to a sulfur-free tricyclic pyranopterin derivative, designated as precursor Z, by the action of the MoaA and MoaC proteins [27-29]. In this unusual reaction MoaA and MoaC catalyzes the cyclic rearrangement of carbon atoms of 5'-GTP to produce precursor Z (Fig 1.4 step 1). This reaction involves a *S*-adenosylmethionine (SAM) derived 5'-deoxyadenosyl-derived radical to facilitate the insertion of the guanine C8 atom between the C2' and C3' atoms of GTP (Fig. 1.5). In humans the *MOCS1* locus has been reported to produce MoaA and MoaC related enzymes, MOCS1A and MOCS1B, from non-overlapping open reading frames within a bicistronic transcript [30]. Mutations in the *MOCS1* locus have been found in all group "A" Moco deficient patients

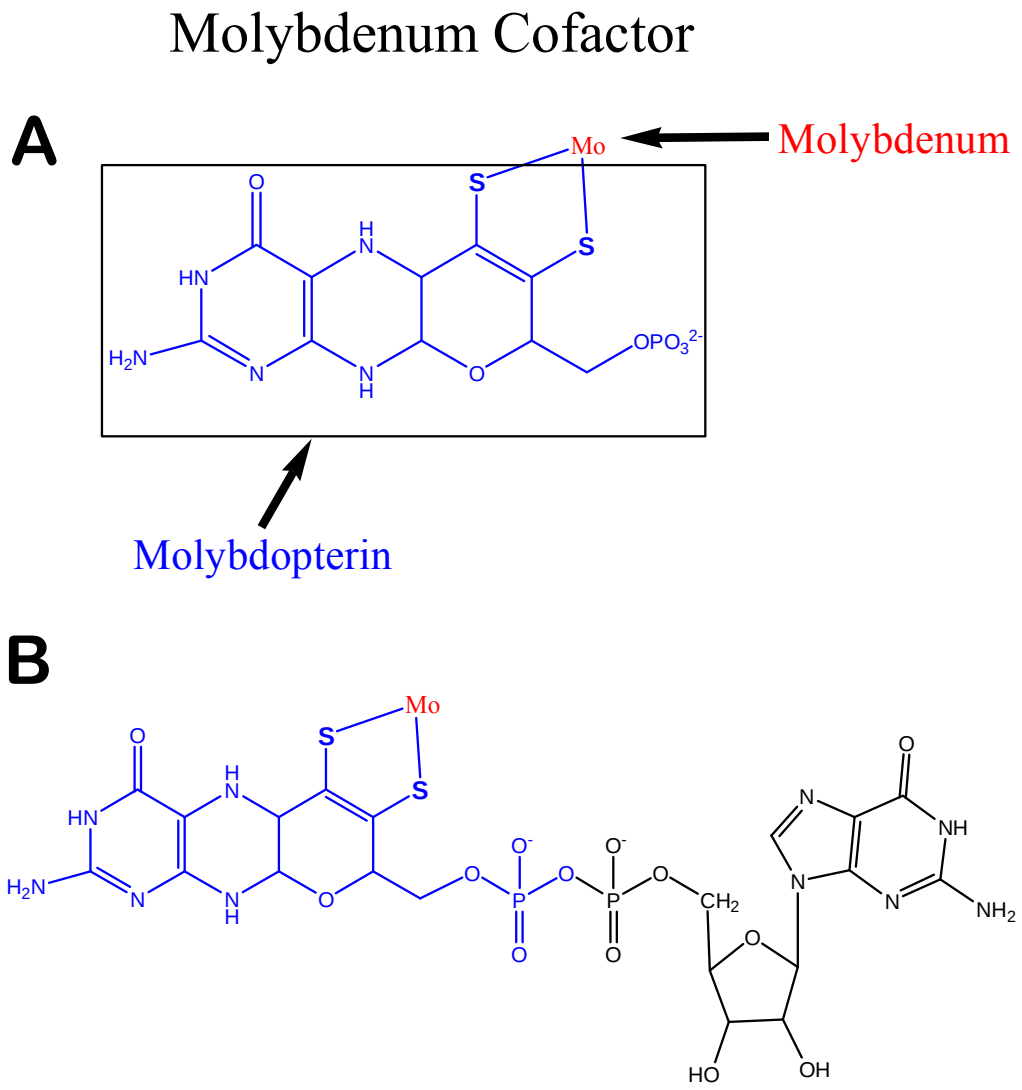

Figure 1.3: Structures of the molybdenum cofactor (Moco). **(a)** Structure of the basic Moco. The molybdopterin portion is colored in *blue* and molybdenum in *red* (tungsten can also be substituted at this position) (**b**) Structure of the molybdopterin guanine dinucleotide form of Moco, which is found in certain eubacteria including *E. coli*.

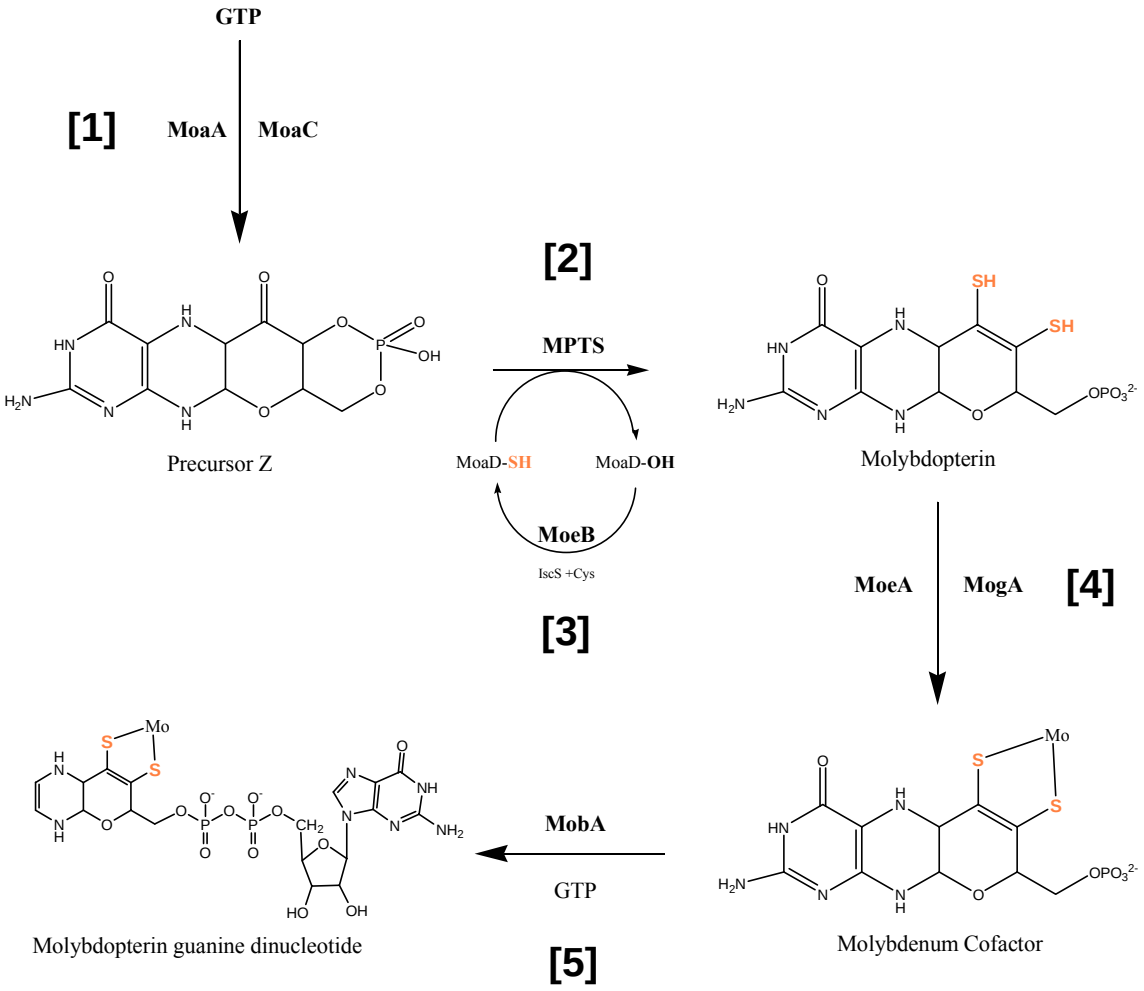

Figure 1.4: The Moco biosynthesis pathway. In humans biosynthesis ends with the insertion of the molybdenum to molybdopterin **[4]**, while in bacteria an additional and exclusive nucleotide modification occurs **[5]**. The names used in this pathway refer to the *E. coli* proteins.

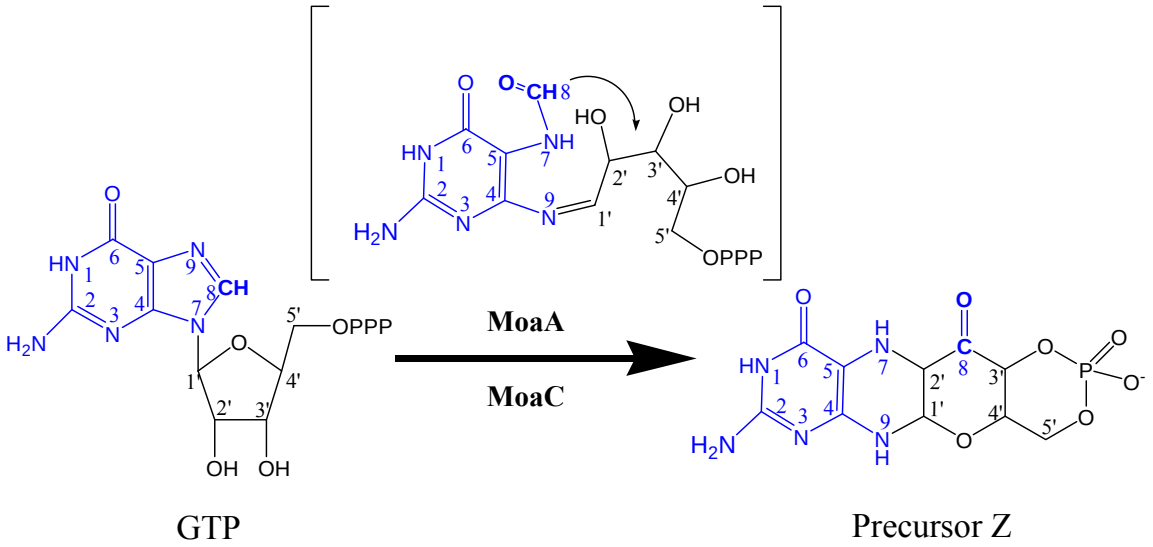

Figure 1.5: MoaA and MoaC catalyzed conversion of GTP to Precursor Z. MoaA and MoaC catalyze the conversion of GTP to precursor Z via a radical SAM to facilitate the insertion of C8 carbon via possible intermediate shown in brackets between the C2' and C3' positions of GTP to produce precursor Z.

[30,31], and since these patients cannot make precursor Z it triggered studies aimed at identifying a cure involving precursor Z injections. However, this approach requires large quantities of precursor Z [32,33].

In the ensuing step of MPT biosynthesis, precursor Z is converted to the dithiolene containing product MPT (Fig 1.4 step 2) by the enzyme MPT synthase. The formation of the dithiolene chelate by MPT synthase, primarily determines the electronic characteristics which are responsible for the spectroscopic and reactive properties of Moco and W-cofactors and serves as a buffer to modulate electron density at the Mo during electron transfer [34]. MPT synthase is a heterotetrameric protein which is composed of two distinct subunits encoded by the *moaD* and *moaE* genes found in the *moa* operon together with *moaA* and *moaC*. The human orthologs to MoaD and MoaE are expressed from transcripts of *MOCS2A* and *MOCS2B*, which are transcribed as one contiguous overlapping RNA, but are later spliced into two separate transcripts [35]. These two subunits form the biologically essential heterotetramer. In the active form, each MoaD molecule contains a thiocarboxylate at the C-terminal glycine which serves as the sulfur donor during synthesis of the MPT dithiolene group. Regeneration of the MoaD thiocarboxylate is catalyzed by an additional enzyme, which is translated from the *moeB* gene. The resulting MoeB protein regenerates the thiocarboxylate in an ATP-dependent manner with the aid of a cysteine desulfurase and a rhodanese-like protein [36-41] (Fig 1.4, step 3). The MoaD protein forms a stable, heterotetrameric complex with both MoaE (in MPT synthase) and with MoeB. With the exception of the C-terminus,

which is deeply buried in the partner protein, the MoaD structure is virtually identical in both complexes and is quite similar to the structure of ubiquitin [36,39].

In the last conserved step of Moco biosynthesis, MPT is converted to Moco by complexation with molybdate, although there is some controversy regarding its mechanism. This step is mediated by the MoeA and MogA proteins or their orthologs (Fig 1.4 step 4) [42-46]. The controversy has arisen from a crystal structure of the G-domain of Cnx1, the plant ortholog of MogA, in complex with a copper-MPT intermediate [47]. In the proposed mechanism, copper acts as a temporary placeholder for molybdenum; the S-atoms of the MPT dithiolene group would bind copper and subsequently molybdate would displace it in ATP dependent manner. Biochemical studies have confirmed that the energy stored in the adenylate is somehow involved in Mo-insertion. However, it should be noted that various metal ions have also been shown to bind tightly to sulfur rich sites [48,49]. Additionally, a recent study by a team of bioinorganic chemists demonstrated that *E. coli* cells grown in Cu-depleted media have no augmented molydoenzyme activity [50], which suggests that copper may have no significance in molybdenum insertion during Moco biosynthesis.

Moco biosynthesis follows a conserved pathway, but some organisms perform additional reactions that modify Moco. In eubacteria, the cofactor is often present in a dinucleotide form combining Moco and either a purine or pyrimidine nucleotide via a pyrophosphate linkage [51]. In *E. coli*, the MobA protein links a guanosine 5'-monophosphate (5'-GMP) to Moco forming molybdopterin guanine dinucleotide (MGD), which is shown in figure 1.4, step 5 [52]. This modification is essential for the activity of

most, but not all, bacterial Moco-containing enzymes. For instance the bacterial xanthine dehydrogenase from *Rhodobacter capsulatus* contains the mono-nucleotide form (MPT) of the cofactors which is the form found in all eukaryotic Moco-containing enzymes. In addition, enzymes from other bacteria utilize molybdopterin cytosine dinucleotide (MCD) instead of MGD [53]. Upon completion of biosynthesis, mature Moco is inserted into the Moco-dependent enzymes, possibly with the aid of chaperones [54]. The NarJ and the XdhC proteins, help with the insertion of Moco into the specific molydoenzymes nitrate reductase and xanthine dehydrogenase, respectively. Since the bacterial xanthine dehydrogenase requires the mononucleotide form of Moco, the XdhC protein is responsible for discouraging MGD formation by binding directly to MobA to ensure sufficient MPT for the XDH protein in bacteria [55].

Mutations in the genes encoding the enzymes involved in human Moco biosynthesis lead to the rare and generally severe Moco deficiency disease [56,57]. The affected patients display an almost identical set of symptoms found in patients with sulfite oxidase deficiency including neurological symptoms such as attenuated growth of the brain, untreatable seizures, dislocated ocular lenses, and mental retardation, most often leading to death in early infancy. The highly similar phenotypes occurring in Moco deficiency, demonstrate that among human Moco-containing enzymes, the activity of sulfite oxidase is most crucial for human health. Moco deficiency has been categorized according to the step during Moco biosynthesis in which the mutation occurs; group A patients have mutations in the genes involved in the first step of Moco biosynthesis (production of precursor Z) while group B patients carry mutations in genes encoding the

proteins involved in the conversion of precursor Z to MPT, or in metal incorporation [57]. Mutations identified in group B patients include substitutions, deletions and premature terminations in both MOCS2A and MOCS2B, which are translated from the genes encoding the human equivalents of MoaD and MoaE, respectively (Table 1.1) [31,57,58].

Table 1.1

Base change in *MOCS2A*	Amino acid change in MOCS2A
252insC	I85X
19G>T	V7F
45T>A	S15R
3G>A	No translation
16C>T	Q6X
88C>T	Q30X
106C>T	Q36X

Base change in *MOCS2B*	Amino acid change in MOCS2B
533_536delGTCA	K117X
635_637delGCT	delA150
658_664delTTT AAAAinsG	delL158K159
714_718delGGAAA	Nonsense after Gly157
726_727delAA	Nonsense after Lys159

List of mutations found in Moco deficient patients affecting molybdopterin formation and resulting protein changes. Mutations in MOCS2A (MoaD homologue) and MOCS2B (MoaE homologue) cause a variety of deletions, missense and nonsense mutations.

Chapter 1

Crystal Structure of a Molybdopterin Synthase-Precursor Z Complex: Insight Into Its Sulfur Transfer Mechanism And Its Role In Molybdenum Cofactor Biosynthesis

The majority of the work described in this chapter has been accepted for publication in *Biochemistry* with myself as the first author.

I. Introduction

The metal binding portion of Moco is usually referred to as molybdopterin (MPT), and can be chemically described as a reduced pyranopterin-ene-dithiolate with a terminal phosphate group as seen in figure 2.1. The existence of molybdopterin can be determined by standard oxidation reactions, that form predictable and stable fluorescent molecules named, Form A and Form B. Form B can be produced by boiling any Moco containing enzyme in air, while Form A production occurs when KI/I_2 is added to this reaction (Fig 2.1).

In *E. coli*, MPT biosynthesis starts with a molecule of GTP, which is converted to a sulfur-free tricyclic pyranopterin derivative designated precursor Z by the action of the MoaA and MoaC proteins [27-29]. In the ensuing step, precursor Z is converted to MPT by MPT synthase. This heterotetrameric protein is composed of two subunits encoded by the *moaD* and *moaE* genes.

In the active form of MPT synthase, each MoaD molecule contains a thiocarboxylate at the C-terminal glycine that serves as the sulfur donor during synthesis of the MPT dithiolene group (Fig 2.1). Regeneration of the MoaD thiocarboxylate is catalyzed by the MoeB protein in an ATP-dependent manner with the aid of a cysteine desulfurase and a rhodanese-like protein [36-41]. In the last conserved Moco biosynthesis step, MPT is converted to Moco by complexation with molybdate, a step mediated by the MoeA and MogA proteins, or their orthologs [42-46]. In *E. coli*, an additional step performed by the MobA protein results in the formation of the guanosine

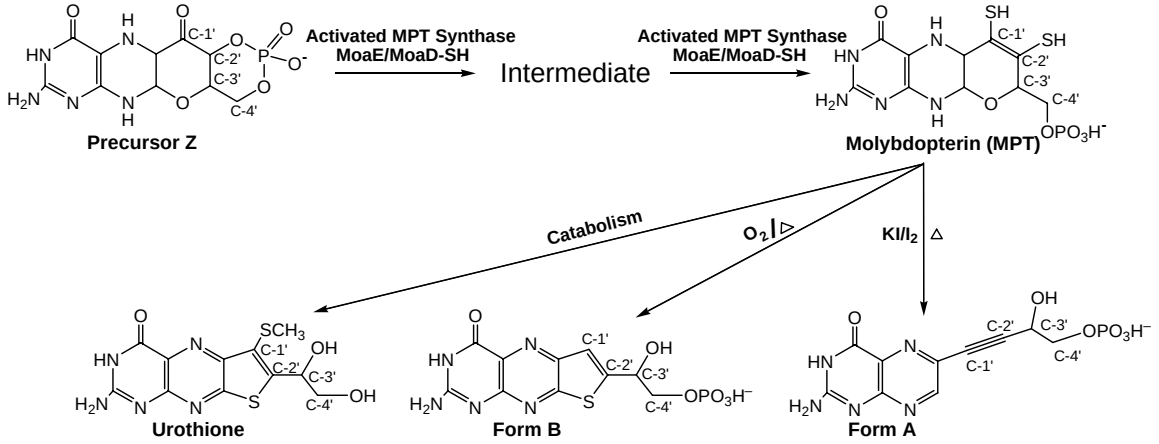

Figure 2.1: Structures of MPT and related molecules. MPT synthase catalyzes the conversion of precursor Z to MPT via a two step sulfur transfer mechanism. MPT can be converted to two fluorescent species: Form A, the end product of MPT oxidation in the presence of KI/I_2; Form B, MPT end product after oxidation in air with a structure that is similar to urothione, the catabolic end product of Moco.

monophosphate-containing dinucleotide form of the cofactor [51,52]. Upon completion of the biosynthesis, mature Moco is inserted into the Moco-dependent enzymes, possibly with the aid of chaperones [54].

Moco deficiency has been categorized according to the step of Moco biosynthesis in which the mutation occurs; group A patients have mutations in the genes involved in the first step of Moco biosynthesis (production of precursor Z), while group B patients carry mutations in genes encoding the proteins involved in the conversion of precursor Z to MPT, or in metal incorporation [57]. Although extremely rare, mutations that cause Moco deficiency have been found in gephryin a human fusion protein which contains an N-terminal G-domain, related to MogA, and C-terminal E-domain, related to MoeA. Gephyrin is involved in the metal incorporation of MPT, and surprisingly, it is also involved in the anchoring of the glycine receptor, a major inhibitory neurotransmitter receptor [59] to which it binds via its C-terminal MoeA-like domain. The extremely rare mutation in *geph*, causing Moco deficiency in humans, has been identified as a deletion of exons 2 and 3 which results in premature termination of the gephyrin protein [60]. Mutations identified in the remaining majority of group B patients include substitutions, deletions and premature terminations in both MOCS2A and MOCS2B, which are translated from genes encoding the human equivalents of MoaD and MoaE, respectively [31,57,58]. The crystal structure of both active and inactive *E. coli* MPT synthase as well as the MoaE homodimer have been previously determined (Fig 2.2a) [36,39]. In the MPT

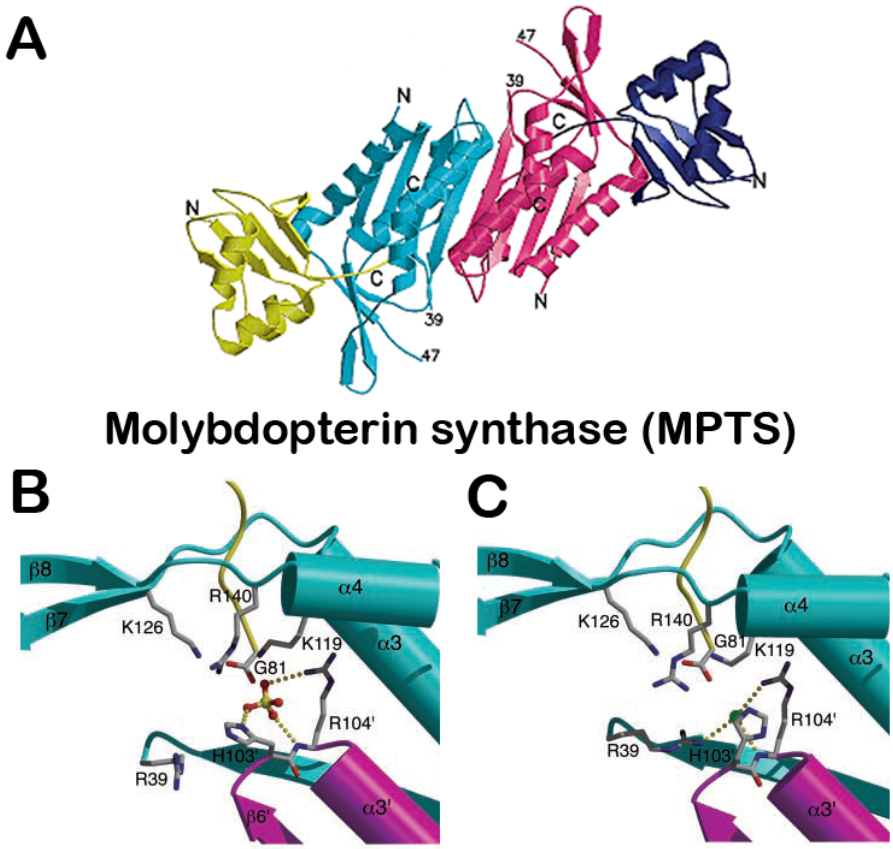

Figure 2.2: Crystal structure of the heterotetramer of *E. coli* molybdopterin synthase. (**a**) The heterotetrameric enzyme contains two MoaD (*yellow* and *blue*) and two MoaE (*cyan* and *magenta*) subunits. The MoaE subunits form a central dimer, while the MoaD subunits are located on either end of the protein. The MoaD C-terminus is deeply inserted into each MoaE subunit. (**b**) Sulfate binding-site in the orthorhombic form of MPT synthase (PDB entry, 1NVI). The MoaD C-terminus is shown in *yellow*, the proximal MoaE subunit in *cyan* and distal MoaE subunit in *magenta*. Active site residues are depicted in all-bonds representation, and the bound sulfate molecule in ball-and-stick representation. (**c**) A chloride, *green* sphere, in the monoclinic form of MPT synthase (PDB entry, 1FM0) binds at roughly the same position as sulfate in the orthorhombic form. (Figure generated from Rudolph et al, [36,39])

complex, the two MoaE molecules form a central dimer, with one MoaD located at each end of the protein and its C-terminus deeply inserted into the proximal MoaE subunit. Structural and biochemical studies have localized the MPT synthase active site adjacent to the MoaD C-terminus that carries the thiocarboxylate when activated [36,39,61] into a pocket lined with conserved residues at the interface between the proximal and distal MoaE subunits. The MPT synthase active site is composed of strictly conserved residues from both MoaE subunits (Fig 2.2b,c). A crystal structure from a covalent complex of *E. coli* MPT synthase (PDB entry, 1FMA) revealed that *E. coli* Lys119 had become covalently attached to the activated MoaD C-terminal glycine forming a catalytically inactive MoaE-MoaD amide linkage. Due to the higher free energy of the thiocarboxylate, the MoaD C-terminal thiocarboxylate is hydrolyzed over time at room temperature, and typically forms this MoaE-MoaD adduct as a side reaction. Although MoaE Lys119 and MoaE Lys126 (Lys116 and Lys123 in *S. aureus* MoaE and Lys118 and Lys125 in *V. cholerae* MoaE) both reside less than 3 Å away from the MoaD thiocarboxylate, only Lys119 is involved in this side reaction, which may mean that Lys126 is protonated while Lys119 exists in an unprotonated state. Additionally, mutational studies that measured the formation of MPT from various mutants of MoaE, together with thiocarboxylated MoaD, show that *E. coli* MoaE K119A variants are absolutely inactive, while *E. coli* MoaE K126A accumulates intermediate and continues to produce limited amounts of MPT [61]. This implicates Lys119 as a key catalytic residues and Lys126 acting in a supporting role during MPT formation.

The conversion of precursor Z to MPT involves the addition of sulfur atoms at the C-1' and C-2' side chain carbons with the concomitant linearization of the cyclic phosphate. A mono-sulfurated, linear phosphate intermediate of this conversion has been identified, verifying that the two sulfur atoms are added sequentially [61]. Given the presence of two active sites in each molecule, it was proposed that such an intermediate would migrate from one active site to the other within the MPT synthase molecule for addition of the second side chain sulfur [62]. However, evidence that precursor Z, the intermediate, and MPT remain tightly bound to MPT synthase during the reaction indicates that both dithiolene sulfur additions take place at the same active site [61]. Although mass spectral analysis indicated the presence of a single sulfur atom on the intermediate side chain, the identity of the side chain carbon carrying the sulfur could not be determined [61]. To clarify this and other aspects of the MPT synthase mechanism as well as to gain further insight into the etiology of MPT synthase mutations identified in cofactor deficient patients, the crystal structure of MPT synthase in complex with its substrate, precursor Z, was determined. The previously identified crystallization conditions of *E. coli* MPT synthase [36,39] contained either 5 M NaCl with 0.1 M HEPES, pH 7.5 or 1.1 M $(NH_4)_2SO_4$ with 0.1 M HEPES, pH 7.5. Since both conditions are not suitable for the growth of MPT synthase/precursor Z co-crystals, other organisms were screened to serve as the source of an MPT synthase protein that would crystallize under conditions more conducive for the visualization of a MPTS-precursor Z complex.

II. Materials and Methods

A. Cloning of His-tagged *Staphylococcus aureus* MPT synthase

The sequence encoding the *moaD* and *moaE* genes was cloned from *S. aureus* genomic DNA (ATCC, Manassas, VA) as a contiguous sequence into the pET-16b vector (Novagen, San Diego, CA) between the NdeI and BamHI sites. This vector introduces a hexa-His tag at the N-terminus of MoaE, which is surface exposed in the crystal structure of *E. coli* MPT synthase. 300 nM of each of the *S. aureus* pET-16b forward and reverse primers listed in Table 2.1, were added to the PCR reaction, containing 100 ng of *S. aureus* genomic DNA, 200 μM NTPs, 1X Expand Buffer, and 1 U High Fidelity Enzyme Mix (Expand High Fidelty PCR System, Roche Applied Science, Indianapolis, IN). The PCR product and the pET-16b vector were sequentially digested with the NdeI (New England Biolabs, Ipswich, MA) and BamHI (Roche Applied Science, Indianapolis, IN) restriction enzymes. The resulting products were purified using the High Pure PCR Product Purification Kit (Roche Applied Science, Indianapolis, IN), ligated using the Rapid DNA Ligation Kit (Roche Applied Science, Indianapolis, IN), and transformed into DH5α with the aid of a standard heat shock [63] protocol. Cells were grown and selected on LB/amp plates (100 μg/mL), and subsequently a single colony was used to inoculate 5 mL of fresh LB/amp media for overnight growth. Plasmid DNA was purified from the resulting cells using the High Pure Plasmid Isolation Kit (Roche Applied Science, Indianapolis, IN) and sequenced at the Stony Brook University DNA Sequencing Facility. The resulting plasmid is referred to as pJD1000.

Table 2.1

S. aureus pET-16b primers

F-NdeI SA MoaE	*A GGA TTG AAA TGA CAT ATG AAA CAA TTT GAA ATC GTG*
R-BamHI SA MoaD	*T TGC TTT CAT GCT CCC GGA TCC TTA ACC TCC ACT AAC*

S. aureus pET-11b primers

F-NdeI SA MoaE	*A GGA TTG AAA TGA CAT ATG AAA CAA TTT GAA ATC GTG*
R-BamHI SA MoaE	*T TCA TCT CTC GGA TCC TTA TTC CTC CCT CTT CGC TTC*
F-NdeI SA MoaD	*G GGA GGA ATA AGA GAG CAT ATG AAG GTA CTT TAC TTC*
R-BamHI SA MoaD	*T TGC TTT CAT GCT CCC GGA TCC TTA ACC TCC ACT AAC*

Primer sequence used in the PCR amplification of *S. aureus* MoaE and MoaD subunits. (F=Forward, R=Reverse)

B. Expression and purification of the His-tagged *S. aureus* MPT synthase

The pJD1000 construct was transformed into Rosetta BL21 *E. coli* cells by heat shock [63], and subsequently these cells were selected after overnight growth at 37ºC on LB plates containing 100 µg/mL ampicillin and 34 µg/mL chloramphenicol. One of the resulting colonies was used to inoculate 25 mL LB/amp/cam media and cells were grown overnight. With the overnight culture 1 L of LB/amp/cam media was inoculated, and cells were grown to an OD_{600} = 0.5. At that time protein production was induced with 0.5 mM isopropyl-β-D-thiogalactopyranoside (IPTG) and cell growth was continued at 37˚C for 4 hours. Cells were harvested by centrifugation at 8000 x g for 25 minutes at 4˚C and lysed in 50 mM Tris-HCl, pH 8.0, 300 mM NaCl and 10 mM imidazole by passing them twice through a French pressure cell at 1,500 psi and centrifuged at 16,000 x g. The protein was initially purified by affinity chromatography with a column containing 5 mL Ni^{2+} agarose beads (Qiagen, Valencia, CA). The supernatant from the previous centrifugation step was applied to the column, which was washed with lysis buffer containing in addition 100 mM of imidazole to remove non-specifically bound protein. Subsequently, the protein was eluted from the column by increasing the imidazole concentration to 250 mM. The protein eluted concentrated enough to be used directly in the last purification step in which the protein was applied to a 26/60 Superdex 200 size exclusion chromatography column (GE Healthcare, Piscataway, NJ) in a buffer containing 50 mM Tris-HCl, 50 mM NaCl, pH 8.0. Although other oligomeric states were observed, the main fraction of protein eluted from the column at around 210 mL (Fig 2.3) and was concentrated to 10 mg/mL using a Centricon-20 Centrifugal Filter

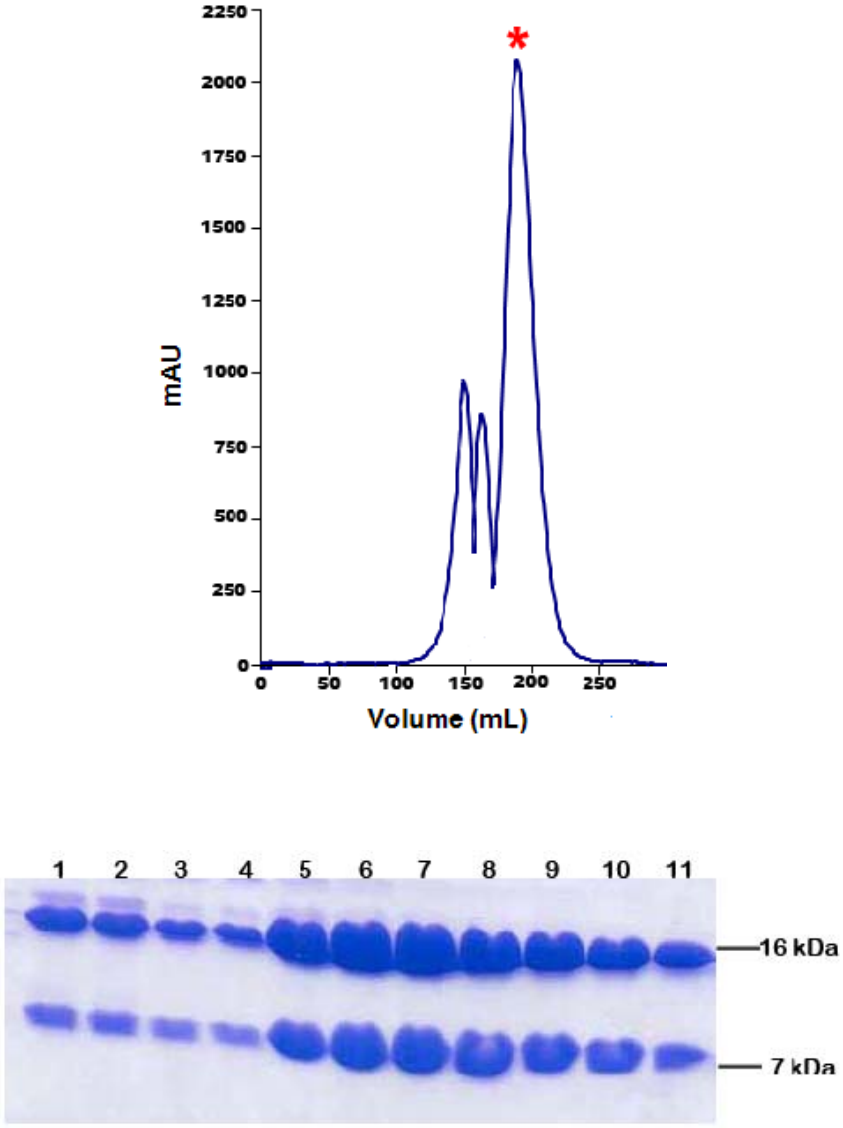

Figure 2.3: Size exclusion chromatography of His-tagged *S. aureus* MPT synthase. The enzyme eluted from the column at an elution volume around 210 mL in the main peak, which is indicated by an asterisk (note the peaks at larger elution volumes, which represent higher oligomeric states). Each fraction contained about 3 mL and 12 µl of each fraction were applied to the gel (Label on gel: Fractions #1-2 from first peak coming off the column, #3-4 second peak, #5-11 from peak indicated by asterisk).

Unit (Millipore, Billerica, MA) with a molecular weight cutoff of 5,000 Da. Protein concentrations were measured by absorption at 280 nm using a calculated molar extinction coefficient of ε = 42,400 $M^{-1}cm^{-1}$ (calculated with the Protparam program in Expasy; http://ca.expasy.org/tools/protparam.html).

C. Cloning of untagged *S. aureus* MPT synthase

The cloning of the untagged MPT synthase was performed by Dr. Margot M. Wuebbens (Department of Biochemistry, Duke University) using similar protocols as described in section A. To obtain non-tagged *S. aureus* MPT synthase, PCR was used to incorporate NdeI and BamHI sites at the 5′ and 3′ ends, respectively, of the contiguous coding region for the MoaE and MoaD subunits from pJD1000. This DNA segment was then cloned into the pET 11b expression vector, which has no tag, to generate plasmid pMWSaMPTS. All nucleotide sequences were verified by automated sequencing.

D. Expression and purification of the untagged *S. aureus* MPT synthase

The expression and purification of the untagged *S. aureus* MPT synthase was performed by Dr. Margot M. Wuebbens (Duke University) using similar protocols as described in section B. The pMWSaMPTS plasmid was transformed into *E. coli* BL21(DE3) cells for expression, and 1 liter cultures in LB/carbenicillin medium were induced at OD_{600} = 0.6 by the addition of 0.1 mM IPTG. After 5 hours of growth at 30°C, the cells were harvested by centrifugation, resuspended in 10 mM Tris, 2 mM EDTA and stored at -20 °C. Protein purification was as previously described for *E. coli* MPT

synthase [36] using a Superdex 75 16/60 FPLC sizing column (GE Healthcare) with a yield of approximately 25 mg/l of cell culture based on a calculated molar extinction coefficient ε = 43,973 $M^{-1}cm^{-1}$ at 280 nm. For activity assays, the *S. aureus* MPT synthase MoaE and MoaD subunits were individually cloned, purified, and assayed as previously described for the *E. coli* MPT synthase subunits [61].

E. Growth of precursor Z overproducing *E. coli* cells

Precursor Z purification from the *moaD*$^-$ chlM(DE3) cell strain transformed with a plasmid expressing the MoaA protein followed a procedure similar to that described earlier [64]. These experiments were carried out by Dr. Margot M. Wuebbens (Duke University). From a glycerol stock of this cell type, cells were streaked onto a LB/amp/cam agar plate and one colony from the overnight growth was inoculated into fresh media containing the previous antibiotics and allowed to grow overnight. These cells were subsequently inoculated into a 2 L flask containing LB, 0.4% Na-nitrate, and 50 μM of IPTG and was filled to the very rim to yield a final OD_{600} = 0.1. This flask was sealed and allowed to grow overnight anaerobically without agitation at room temperature.

F. Preparation of MPT synthase loaded with precursor Z

The isolation of precursor Z was performed by Dr. Margot M. Wuebbens (Duke University) using similar protocols as described in Wuebbens et al [64]. Cells containing precursor Z were harvested by centrifugation, washed with H_2O and resuspended in 2.8

mL H_2O/g wet weight. The cells were divided into 5 aliquots, and each aliquot was treated sequentially as follows: the cells were acidified to pH 2 by the addition of 4 N HCl and centrifuged at 7,600 x g for 10 min. The supernatant was neutralized with 2 N NaOH and rotoevaporated to approximately 0.9 mL and injected onto an Alltech C18 HPLC column (14 x 250 mm) equilibrated with 5 mM ammonium acetate, pH 5.0. Precursor Z eluting between 3.5 and 5.0 mL was collected, pooled, and concentrated prior to injection onto an Alltech Partisil SAX HPLC column (14 x 250 mm) equilibrated with 10 mM sodium citrate, pH 3. The total amount of precursor Z purified from 6 liters of culture was approximately 500 nmoles in a volume of 2-3 mL. This was combined with 15 mL of 50 mM Tris-HCl, 50 mM NaCl, pH 8.0 prior to the addition of an equimolar amount of non-tagged *S. aureus* MPT synthase. After incubation at 4°C for 20 min, the mixture was concentrated to less than 1 mL using a Vivaspin 20 30K concentrator. The volume was twice increased to 12.5 mL with additional buffer and then concentrated to a volume of less than 200 µL. The final sample concentration was 25-35 mg/mL of MPT synthase.

G. Crystallization of the His-tagged *S. aureus* MPT synthase

Tagged *S. aureus* MPT synthase was screened for suitable crystallization conditions using the Hampton Crystal Screen [65] and Emerald BioSystems Wizard Screens™ I and II. Using the hanging drop vapor diffusion technique with 1 µl of protein and 1 µl of precipitant on pre-silanized cover slides, crystals were produced from Hampton Crystal Screen II and were optimized at a protein concentration of 10 mg/mL in a buffer

containing 50 mM Tris-HCl, 50 mM NaCl, pH 8.0 against a precipitant consisting of 2.0 M sodium formate, 0.1 M sodium acetate, pH 5.3, at 22˚ C. After two days, these conditions yielded spherulite bodies that transformed into well-defined crystals with approximate dimensions of 0.04 x 0.1 x 0.1 mm^3 after 3 weeks (Figure 2.4a).

H. Crystallization of *S. aureus* MPT synthase in complex with precursor Z

Since the high salt sodium formate crystallization conditions identified for the tagged MPT synthase were likely to prevent co-crystallization of the complex, lower salt crystallization conditions for the non-tagged proteins were screened. This protein crystallized from the same hanging drop vapor diffusion technique described in section G of this chapter, at a protein concentration of 10 mg/ml under conditions consisting of 18% (w/v) PEG 8000, 0.1% polyvinylpyrrollidone K15, and 0.1 M Tris-HCl, pH 8.0 at 4˚ C. Although this same condition did not initially yield diffraction-quality crystals for the precursor Z loaded protein, the addition of microseeds of the untagged apoprotein resulted in co-crystals with dimensions of 0.22 x 0.14 x 0.14 mm^3 after three to four days (Figure 2.4b).

I. Data Collection, Structure Determination and Refinement

For all samples, the crystals were soaked sequentially in increasingly higher concentrations of glycerol until reaching a final glycerol concentration of 30%; at that time the crystals were flash cooled by dipping the crystals into liquid nitrogen. Diffraction data were collected at the National Synchrotron Light Source, Brookhaven

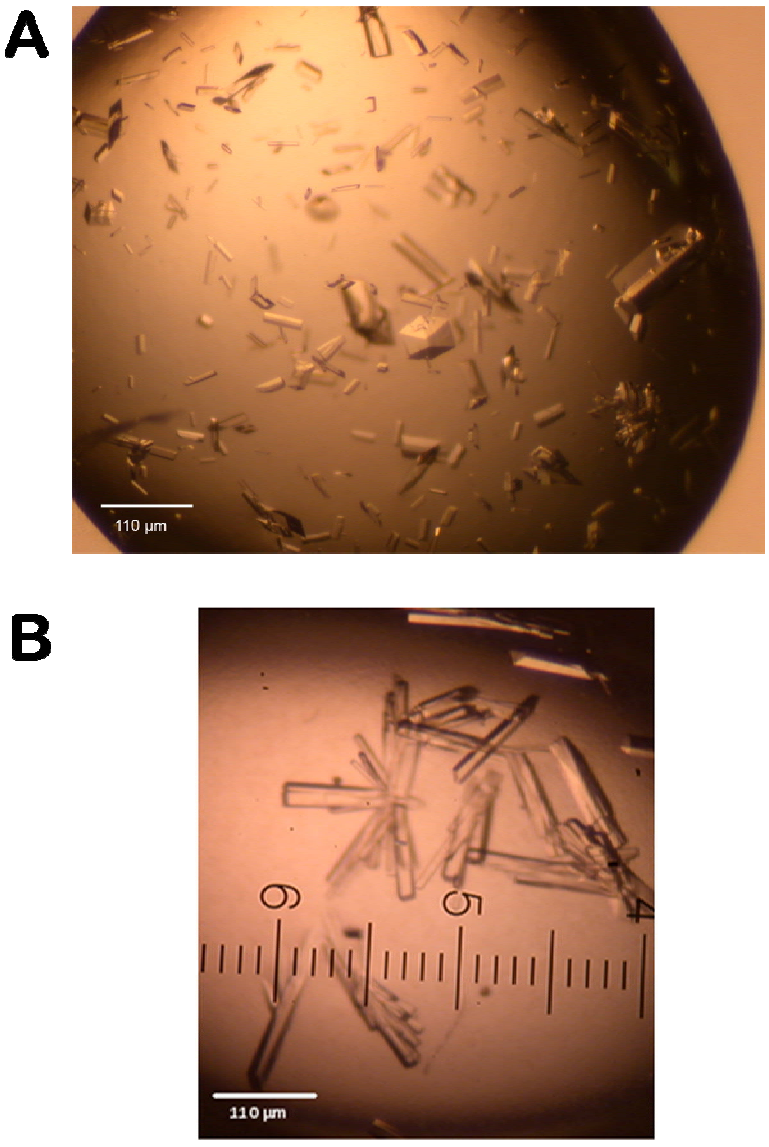

Figure 2.4: Crystals of *S. aureus* MPT synthase. (**a**) Crystals of the His-tagged apo-enzyme. (**b**) Crystals of MPT synthase loaded with precursor Z grown after microseeding with untagged apo-crystals.

National Laboratory at a wavelength of 1.1 Å on beamline X26C for apo *S. aureus* MPT synthase crystals and X25 for the precursor Z-MPT synthase co-crystals where the large c-axis necessitated a data collection protocol with a small rotation-increment. Consequently, a total of 180˚ of data were recorded in 0.2˚ increments. Diffraction data were indexed, integrated and scaled using HKL-2000 [66].

The structure of apo *S. aureus* MPT synthase was solved by molecular replacement with the program MOLREP [67,68] using the heterodimeric (*E. coli* MPT synthase structure, PDB entry 1NVI) [39] as the search model. Rotational and translational searches were performed with data in the resolution range from 50 to 4 Å and identified one MPT synthase heterodimer in the asymmetric unit. The model was refined with the program REFMAC [69], initially by rigid body refinement followed by TLS and restrained refinement [70,71]. Model building was carried out with the program O [72]. Once a final model for the apo-protein was generated, MOLREP was used to find solutions for the complex structure in the same procedure described for the apo-protein. This search found 2 heterotetramers in the asymmetric unit. The model was again refined using the program REFMAC [69], following the procedure outlined above coupled to model building with O [72]. The precursor Z model was constructed utilizing the Monomer Library Sketcher from the CCP4 [73] suite starting with the structure of Moco. Initially, the substrate was positioned manually into the electron density maps, while water molecules were added with the program ARP [74].

J. Generation of Form B from the mono-sulfurated MPT Intermediate

A precursor Z sample of approximately 75 nmoles was prepared by Dr. Wuebbens as previously described [64] and summarized in section F. K126A *E. coli* MoaE and activated MoaD (MoaD-SH) were purified as described earlier [61]. Samples containing 150 nmoles of each protein were combined and incubated for 10 minutes prior to the addition of the entire precursor Z sample and a quantity of 100 mM Tris, pH 7.2 sufficient to bring the total reaction volume to 2.5 mL. This was left for 16 hr in the dark at room temperature to facilitate production of the intermediate [61]. Following incubation, an identical reaction mixture containing wild-type *E. coli* MoaE was incubated for 10 min at room temperature. At that point, both reaction mixtures along with a control sample containing 200 nmoles of the human Moco-containing enzyme sulfite oxidase were all acidified to pH 2.5 with 4 N HCl and placed in a boiling water bath for 30 min to produce Form B [75]. After cooling and centrifugation to remove precipitated protein, each supernatant was applied to a separate PD-10 desalting column (GE Healthcare) equilibrated with 10 mM acetic acid. The columns were washed with 6.5 mL of the same solution prior to elution of Form B with an additional 4 mL. After the addition of 24 μL of 2 N NaOH, 10 μL calf intestine alkaline phosphatase (Roche Applied Science, Indianapolis, IN) solution and 25 μL of 1 M $MgCl_2$, the three samples were left in the dark at room temperature for 16 hr. Each sample was concentrated to dryness, resuspended with 0.9 mL of H_2O and analyzed by injection onto an Alltech C18 HPLC column (250 x 4.6 mm) equilibrated with 50 mM ammonium acetate and 20% methanol with a flow rate of 1 mL/min [75,76].

K. Coordinates

The atomic coordinates and structure factors for *S. aureus* MPT synthase in its apo-state (PDB entry, 2Q5W) and in complex with precursor Z (PDB entry, 2QIE) have been deposited in the Protein Data Bank, Research Collaboratory for Bioinformatics, Rutgers University, New Brunswick, NJ (http://www.rcsb.org). In addition the coordinates for activated *E. coli* MPT synthase, previously determined by Michael J. Rudolph have been deposited as well (PDB entry 3BII).

III. Results & Discussion

A. Cloning, purification and analysis of *S. aureus* MPT Synthase

Although the crystal structures of active and inactive *E. coli* MPT synthase as well as the MoaEΔ141 dimer alone have been reported [39], *E. coli* MPT synthase was not suitable for co-crystallization with precursor Z. Although it is more stable than MPT, precursor Z is sensitive to oxidation by air or metal ions, either of which yields the inactive fluorescent derivative compound Z in the time frame of minutes to days. Despite numerous attempts, all conditions determined for crystal formation of *E. coli* MPT synthase involve high salt (likely to result in dissociation of precursor Z from MPT synthase) and/or extended crystallization times (likely to result in precursor Z oxidation to compound Z) [36,39]. Since these efforts proved futile, MPT synthase proteins from other organisms were cloned, expressed, and screened for crystallization suitability. The advent of genome sequencing projects facilitated this effort, and genomic databases were searched (PUBMED) for microorganisms with sequences homologous to known MPT synthase sequences. Among other organisms, this search identified the genes for the MPT synthase subunits in *S. aureus*. Like the *E. coli* proteins, the genes for the two *S. aureus* MPT synthase subunit proteins are contiguous to each other with a minimal number of base pairs separating the two open reading frames (four base pairs for *S. aureus* and a single base pair for *E. coli*). Interestingly, the order of the two proteins is reversed in the two genomes with *moaE* preceding *moaD* in *S. aureus*. Using the reported sequences for the two subunits, the *S. aureus* MPT synthase genes were cloned into expression vectors designed to express His-tagged and native untagged MPT synthase as well as the

individual MoaE and activated MoaD subunits. The MPT synthase protein from *S. aureus* was found to crystallize under more appropriate conditions, and this protein was chosen for further co-crystallization experiments.

At the amino acid level, the primary sequence identity of *E. coli* and *S. aureus* MPT synthase is 35.5% and 25.9% for the MoaE and MoaD subunits, respectively. Additionally, the strictly conserved residues identified in multiple sequence alignments of *E. coli* MPT synthase are all present in the *S. aureus* protein including those presumed to be involved in substrate-binding and catalysis [39,61]. The two heterotetrameric MPT synthase protein complexes are also similar in size with molecular weights of 52,408 Da for *S. aureus* and 51,152 Da for *E. coli*. Non-tagged *S. aureus* MPT synthase, MoaE and activated MoaD were all purified under the same conditions as the *E. coli* proteins, with similar protein yields [36]. To assay for MPT synthase activity (MPT production from precursor Z), the individual *S. aureus* and *E. coli* activated MPT synthase subunits were combined with precursor Z [61]. Although the final extent of MPT production was the same, the rate of MPT production by activated *S. aureus* MPT synthase was approximately 5.5 times slower than that of *E. coli* MPT synthase with $t_{1/2}$ =1.65 and 0.3 min, respectively (Dr. Margot Wuebbens, personal communication).

B. Structure of apo *S. aureus* MPT synthase

Crystals of His_6-tagged, apo *S. aureus* MPT synthase belong to the monoclinic space group C2 with unit cell dimensions of a = 133.9 Å, b = 45.8 Å, c = 41.8 Å and β= 93.4° with one MoaD-MoaE heterodimer in the asymmetric unit. Although the crystals

diffracted X-rays well beyond 2.0 Å resolution, the structure was refined at this resolution to an R-factor of 0.149 and an R_{free} of 0.193 (Table 2.2). The resulting model has good stereochemistry with 97.6% of all non-Pro and non-Gly residues in the most favored regions of the Ramachandran diagram, 2.4% in generously allowed regions, and no residues in disallowed regions (Fig 2.5) as defined by MOLPROBITY [77]. As seen in figure 2.6a, both subunits of MPT synthase exhibit a mixed α+β architecture. The MoaD subunit adopts a ubiquitin-like (β-grasp) fold which is composed of a central β sheet consisting of five strands and three α-helices, while the MoaE subunit contains eight β-strands forming two β-sheets surrounded by a total of four α-helices. The MoaE structure exhibits an α/β hammerhead fold. A noteworthy difference between the two structures is that residues 36 to 44 of the *S. aureus* MoaE subunit are ordered, while the corresponding residues (39 to 47) in *E. coli* MoaE were disordered in all crystal structures [36,39]. With the presence of this loop, a distinct cavity adjacent to the postulated active site is formed, which is visible when a surface representation of the structure is calculated (Fig. 2.6b). Although the C-terminus of *S. aureus* MoaE is disordered, it can be modeled on the basis of the *E. coli* structure, which shows that *S. aureus* MoaE Gln137 would partially occlude the binding pocket (Fig. 2.6c). In *E. coli* MoaE, Gln137 is replaced by Arg140, and this longer residue almost completely blocks the active site, suggesting that the conformation observed for the C-terminal residues of *E. coli* MoaE probably facilitates proper positioning after precursor Z has bound. To understand why the C-terminus of *S. aureus* MoaE (residues 135 to 149, corresponding to the last helix of *E. coli* MoaE) is disordered, and also disordered in the structure of the *E. coli* MoaEΔ141 homodimer, the

Table 2.2

Data collection statistics	Apo-enzyme	Precursor Z complex
Unit cell dimensions (Å, °)	*a* = 133.9, *b* = 45.8, *c* = 41.8 α= 90, β= 93.4, γ= 90	*a* = 56.6, *b* = 58.1, *c* = 331.8 α= 90, β= 90, γ= 90
Resolution limits	50 - 2.0	50 - 2.5
Completeness	0.948 (0.714)	0.969 (0.830)
R_{sym}	0.033 (0.065)	0.071 (0.632)
I/ σI	42.0 (15.4)	22.2 (2.4)
Redundancy	3.3 (2.1)	5.3 (3.6)
All reflections	54,634	200,513
Unique reflections	16,442	38,004
Refinement statistics		
Number of reflections used	15,541	36,033
Resolution limits	30 - 2.0	30 - 2.5
Number of protein/ solvent/substrate atoms	1,751/152	7,004/78/92
R_{factor}	0.149	0.206
R_{free}	0.193	0.255
Rms deviations from ideal values in		
Bond distances (Å)	0.017	0.009
Bond angles (°)	1.55	1.21
Chiral centers ($Å^3$)	0.10	0.071
Average B-factors ($Å^2$) of protein/solvent/substrate atoms	28.0/30.9	61.7/66.6/87.0
Average B-factors ($Å^2$) of substrates and surrounding atoms within 5 Å radius	-	73/79/94/109 64/65/70/71
Ramachandran statistics	97.6/0.0	97.8/0.0

$R_{sym} = \sum_{hkl} \sum_i |I_i - \langle I \rangle| / \sum_{hkl} \sum_i I_i$ where I_i is the i^{th} measurement and $\langle I \rangle$ is the weighted mean of all measurements of I. $\langle I/\sigma I \rangle$ indicates the average of the intensity divided by its standard deviation. $R_{cryst} = \Sigma \, ||F_o| - |F_c|| \, / \, \Sigma \, |F_o|$ where F_o and F_c are the observed and calculated structure factor amplitudes. R_{free} same as R_{cryst} for 5% of the data randomly omitted from refinement. Numbers in parentheses apply to the respective highest resolution shell. Ramachandran statistics indicate the fraction of residues in the most favored and disallowed regions of the Ramachandran diagram as defined by the program MOLPROBITY.

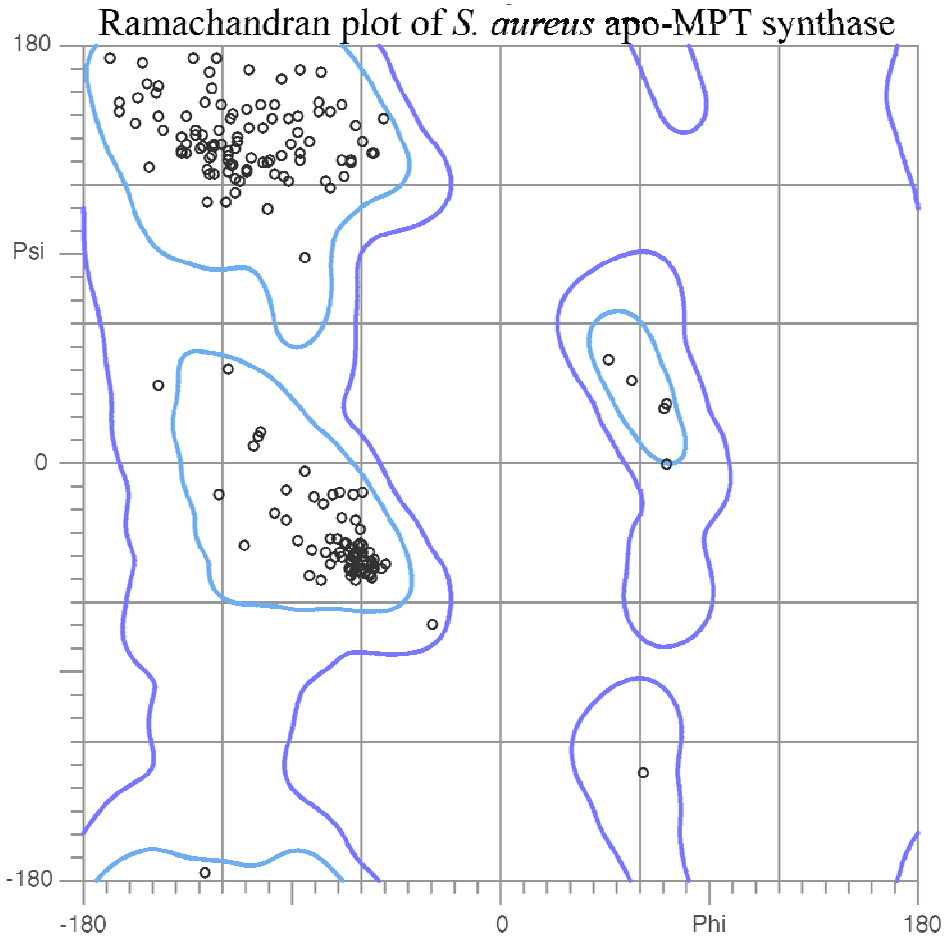

Figure 2.5: Ramachandran diagram (non-Gly residues) of the *S. aureus* apo-MPT synthase. The model displays good stereochemistry with 97.6% of all non-Pro and non-Gly residues in the most favored region of the Ramachandran diagram, 2.4% in generously allowed regions, and no residues in the disallowed regions, as defined by MOLPROBITY.

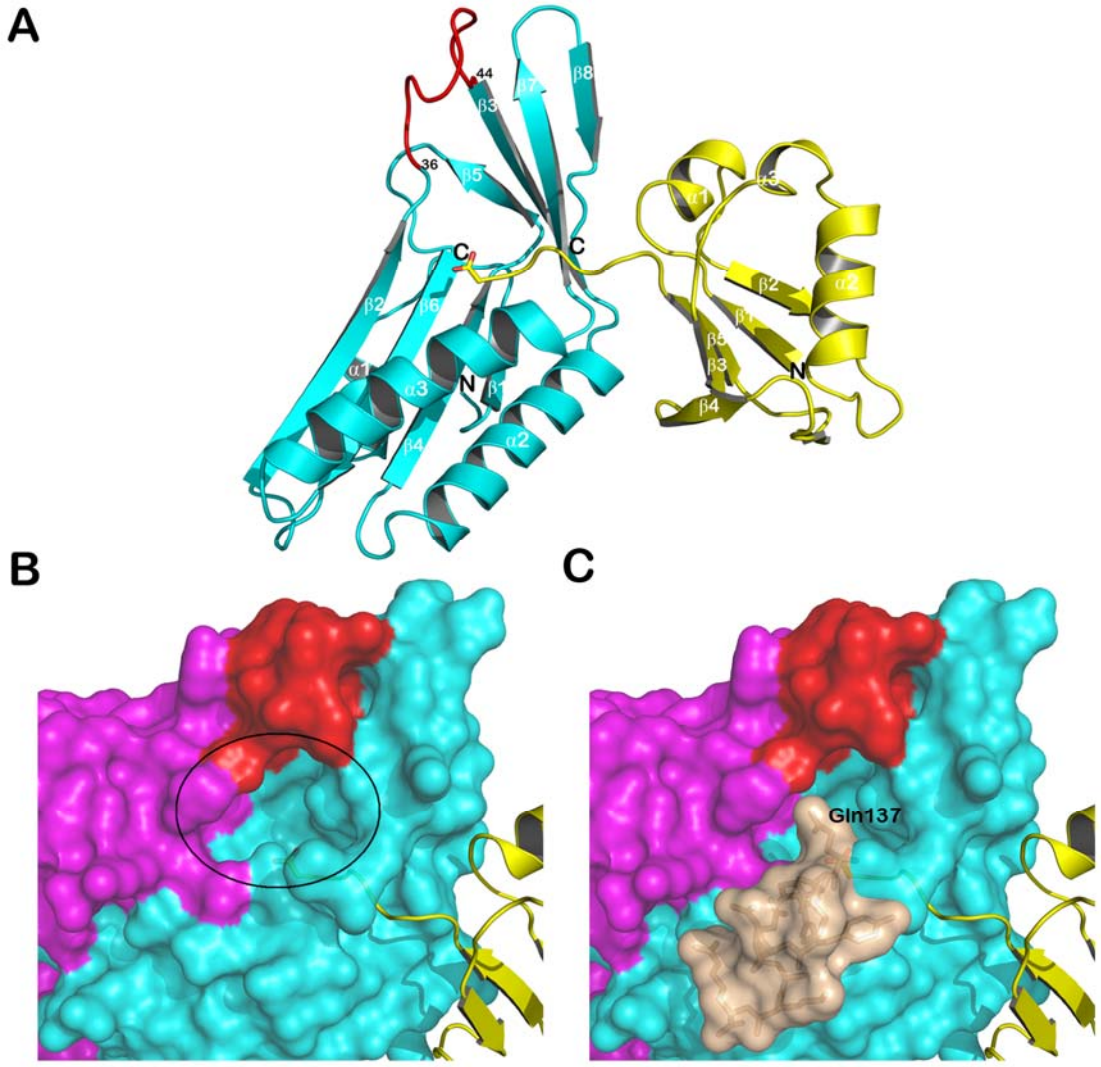

Figure 2.6: Structural features of *S. aureus* MPT synthase. (**a**) Ribbon diagram of the heterodimer of *S. aureus* apo-MPT synthase with MoaE (*cyan*) and MoaD (*yellow*) subunits, and the newly ordered loop, residues 36-44, in *red*. (**b**) Surface representation of the substrate-free MPT synthase heterotetramer with MoaE subunits (*cyan* and *magenta*) and residues 36-44 (*red*). MoaD is shown as a ribbon diagram (*yellow*). The C-terminal carboxylate, hidden by MoaE, is inside the putative substrate-binding pocket, which is indicated by the *black* circle. (**c**) Model of the C-terminal region of *E. coli* MoaE (transparent surface in *tan*, atoms in stick representation) superimposed onto the *S. aureus* MPT synthase structure.

E. coli and *V. cholerae* MPT synthase (described in Chapter 3) structures were both inspected. The MoaE subunits in both of these proteins have a well-ordered MoaE C-terminal helix that contains a Trp at the C-terminus (*E. coli* Trp150, *V. cholerae* Trp149). Typically two large hydrophobic residues (*V. cholerae* Trp73 and Phe112; *E. coli* Trp74 and Phe113) found on the α2 and α3 helices of MoaE interact with the MoaE C-terminal Trp residue. However, *S. aureus* does not contain any Trp or similar hydrophobic residue on the MoaE C-terminal helix, therefore the disorder of the C-terminus of *S. aureus* MoaE and the *E. coli* MoaEΔ141 homodimer could be attributed to the absence of this Trp residue that is almost always found at the MoaE C-terminus.

Despite the relatively low level of sequence identity between the *S. aureus* and *E. coli* proteins, their overall structures are quite similar. This is reflected in root mean square (rms) deviations between C-alpha atoms of 1.45 Å and 1.2 Å when the MoaE and MoaD subunits, respectively, are superimposed. In contrast, a superposition of the entire MoaE/MoaD heterotetramer results in a somewhat larger rms deviation of 1.7 Å, which is due to the fact that the *E. coli* and *S. aureus* MoaD subunits differ by a rotation of ~17° around the C-terminal tail (Fig. 2.7). Further examination of the residues forming the MoaD/MoaE interface in either *S. aureus* or *E. coli* MPT synthase (*S. aureus* MoaD Phe6, Ala7, Phe55 and Ile71 corresponding to *E. coli* Phe7, Ala8, Leu59, Phe75 and *S. aureus* MoaE Tyr52, Met55, Trp122, Trp133 corresponding to *E. coli* Tyr55, Met58, Trp125 and Trp136), reveals that these residues interact in a similar fashion despite the MoaD rotation. Interestingly, the type-conserved exchange of *E. coli* MoaD Phe75 to Ile71 in *S. aureus* MoaD is complemented by a reverse exchange of *E. coli* MoaD Leu59

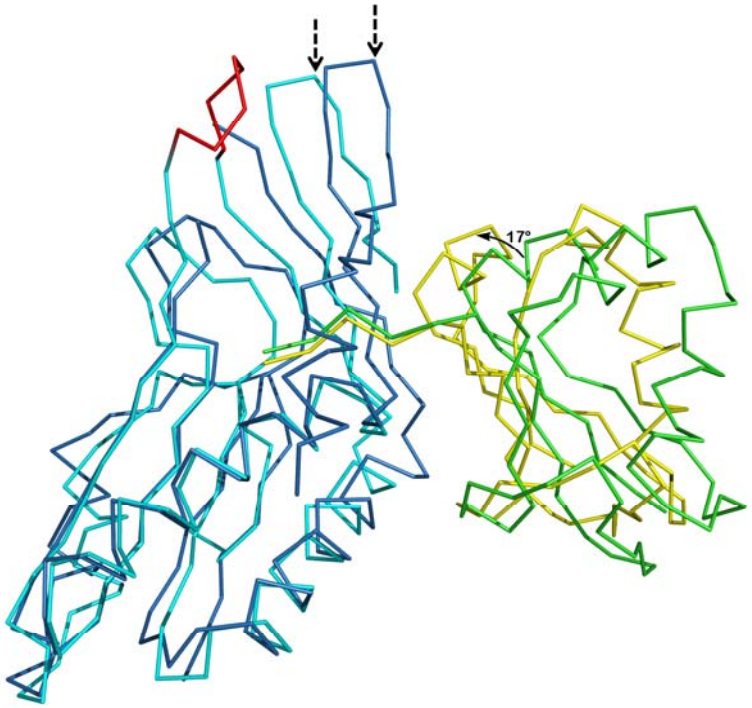

Figure 2.7: Superposition of *E. coli* and *S. aureus* MPT synthase. The MoaE dimer within the heterotetramer was used for the superposition, but only a MoaD/MoaE heterodimer is shown in each case. *E. coli* MoaE and MoaD are shown in *blue* and *green*, while *S. aureus* MoaE and MoaD are colored *cyan* and *yellow*. Note the rotation of the MoaD subunits relative to MoaE. Significant conformational changes are also shown in the β7-β8 hairpin formed by MoaE residues 121 to 133 (*black* arrows indicate this shift while residues of the active site loop are displayed in *red*).

to *S. aureus* MoaD Phe55 at a nearby position, thus preserving the structural framework of the interface as seen in figure 2.8.

Lastly, the *S. aureus* MoaE β strands formed by residues 45 to 52, 81 to 90 and 121 to 136 (β3, β5, β7, respectively) are all in the vicinity of the ordered loop 36 to 44 and exhibit shifts of up to 6 Å when compared to the *E. coli* structure. It is unclear whether these shifts are due to residues 36 to 44 becoming ordered, or if they reflect true structural differences between *S. aureus* and *E. coli* MPT synthase. Although there are hydrophobic interactions between the side chains of residues located in these strands and their symmetry mates (with Trp38, Lys43 contacting Ile75, Tyr24 and Phe19), crystal packing effects can be excluded as the source of the structural changes in this region since a similar conformation is also observed in the complex of *S. aureus* MPT synthase and precursor Z where the packing is quite different.

C. Structure of *S. aureus* MPT synthase in complex with precursor Z

The crystals of the MPT synthase-precursor Z complex diffracted up to 2.5 Å resolution and belong to the orthorhombic space group $P222_1$ with unit cell dimensions of a = 56.6 Å, b = 58.1 Å, and c = 331.8 Å containing two MoaD-MoaE heterotetramers in the asymmetric unit. The structure of the complex was refined to an R-factor of 0.206 and R_{free} of 0.255 resulting in a model with good stereochemistry; 97.8% of all non-Pro and non-Gly residues in the most favored regions of the Ramachandran diagram (Fig 2.9) [77], 2.2% in generously allowed regions and no residues in disallowed regions (Table 2.2). Manual positioning of precursor Z into the unbiased difference density maps

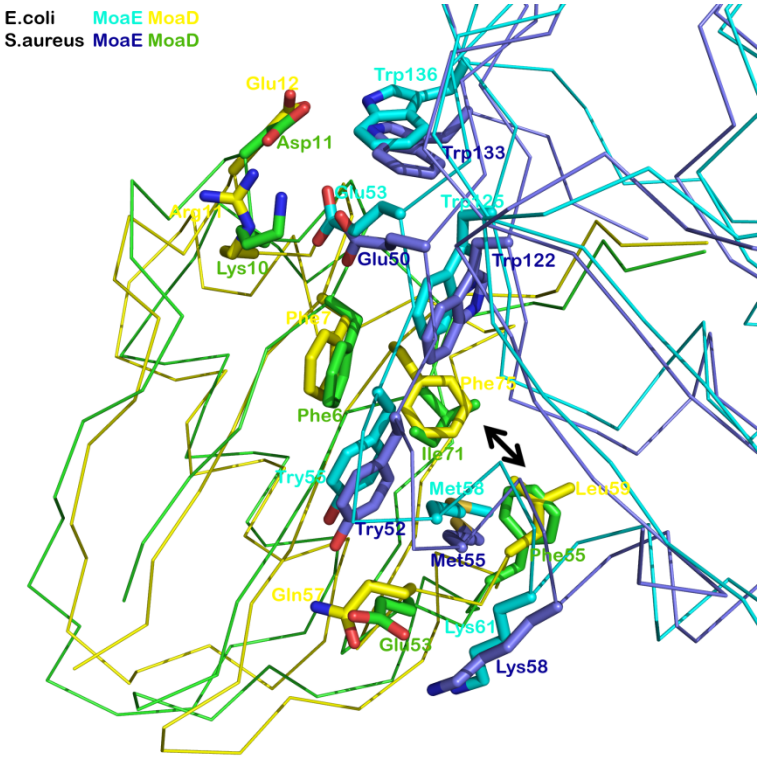

Figure 2.8: Superposition and conservation of the MoaE-MoaD interface in *E. coli* and *S. aureus* MPT synthase. The superposition is based on the entire heterotetramer in contrast to figure 2.7. The α-carbons are colored as follows: *S. aureus* MoaD *green* and MoaE in *blue*; *E. coli* MoaD in *yellow* and MoaE in *cyan*. The interface side chain residues are depicted in all-bonds representation. A conserved exchange between residues of *E. coli* and *S. aureus* MoaD is highlighted by the *black* arrow.

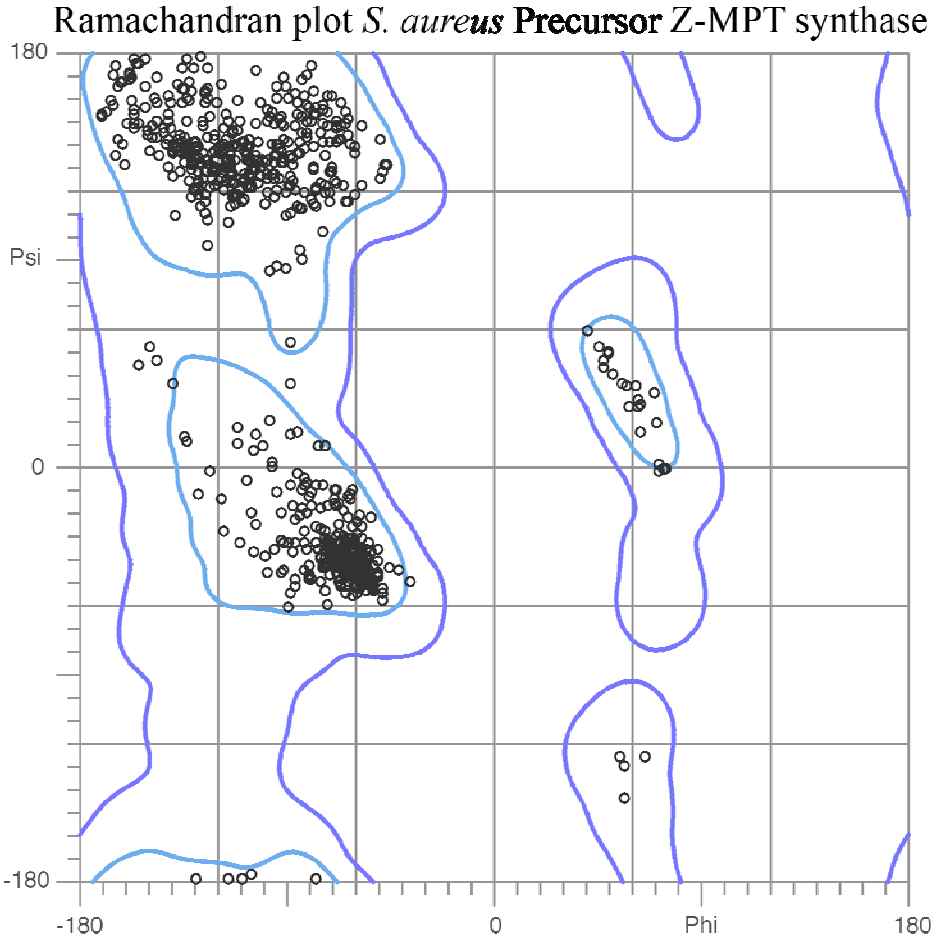

Figure 2.9: Ramachandran diagram (non-Gly residues) of the *S. aureus* precursor Z-MPT synthase complex. The model has good stereochemistry with 97.8% of all non-Pro and non-Gly residues in the most favored region of the Ramachandran diagram, 2.2% in generously allowed regions, and no residues in the disallowed regions, as defined by MOLPROBITY.

resulted in excellent fits for the substrate in three of the four heterodimers present in the asymmetric unit. As seen in figure 2.10a and 2.10b, precursor Z is bound in the postulated substrate-binding site, in close vicinity to the MoaD C-terminus and the MoaE dimer interface [36,39,61].

When the four MoaD/MoaE heterodimers in each asymmetric unit of the complex structure are compared to each other, there are small structural differences as reflected by an average pairwise rms deviation of about 0.5 Å. The most pronounced structural differences between the heterodimers are seen in the loop encompassing residues 39 to 45. Interestingly, there is a correlation between the average B-factor of the precursor Z bound in the structure and the conformation of this loop. The three heterodimers (A-B, H-G, K-J) in which the bound precursor Z has an average B-factor less than 100 $Å^2$ (indicating a higher occupancy of precursor Z) adopt nearly identical loop conformations, whereas the heterodimer (E-D) in which the bound substrate has an average B-factor greater than 100 $Å^2$ (indicating a lower occupancy of precursor Z) displays a conformational change resulting in a shift of the loop by approximately 5 Å. In this heterodimer, the loop adopts a conformation similar to the apo-structure. Consequently, the overall rms deviation following superposition of C-alpha atoms between this heterodimer and the apo-structure is smaller (0.6 Å) compared to the average rms deviation between the apo-structure and the heterodimers which display lower B-factors for the substrate (average rms deviation of ~0.7 Å). These observations suggest that the loop conformation is coupled to the presence or absence of substrate in the active site. The electrostatic surface representation of *S. aureus* MPT synthase heterotetramer reveals

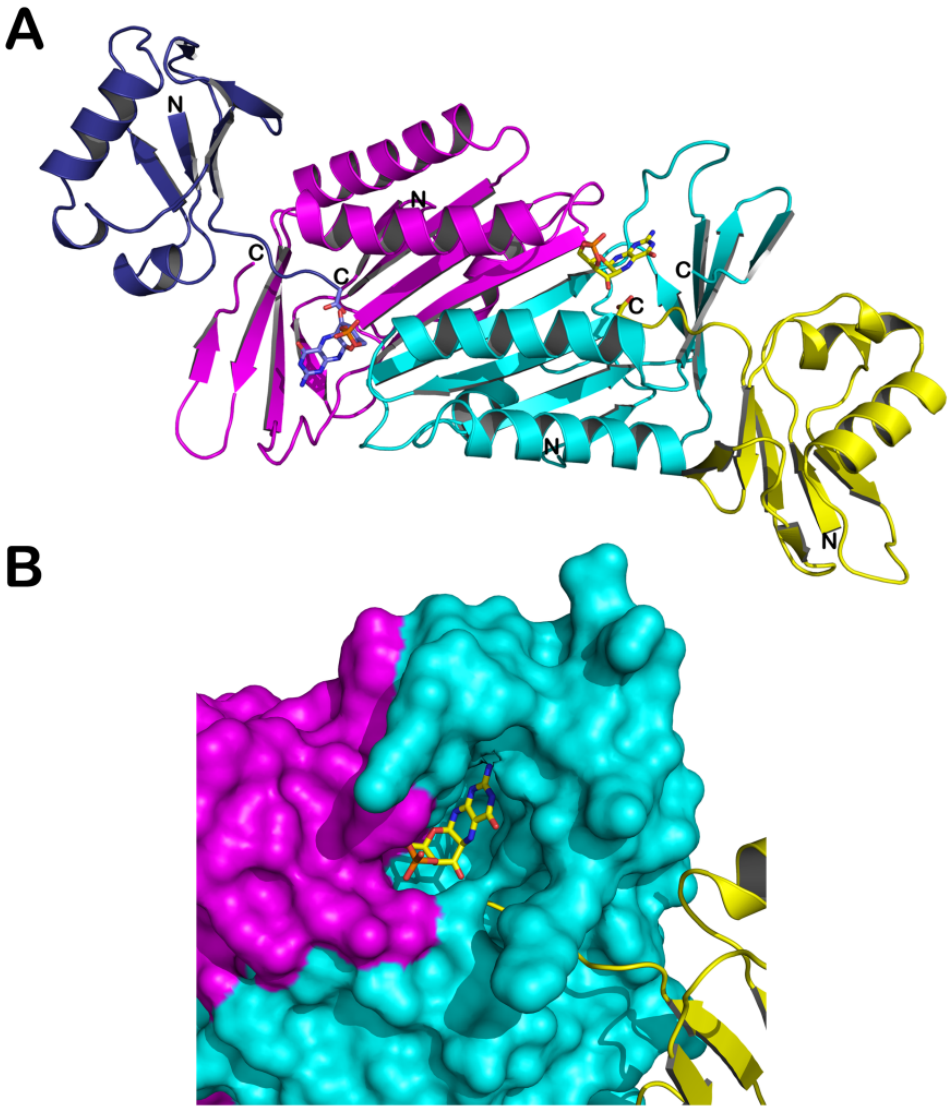

Figure 2.10: Structure of *S. aureus* MPT synthase in complex with precursor Z. (**a**) Ribbon diagram of the *S. aureus* MPT synthase heterotetramer with MoaE (*magenta* and *cyan*) and MoaD (*dark blue* and *yellow*). The C-terminal carboxylates and precursor Z are shown in all bonds representation. The precursor Z carbon atoms are colored according to the adjacent MoaD subunit (*dark blue* and *yellow*). (**b**) Surface representation of the proximal MoaE (*cyan*) and distal MoaE (*magenta*) subunits with precursor Z in all bonds representation (*yellow*) and the adjacent MoaD subunit (*yellow*).

a distinct concentration of positively charged residues, which was also found in *E. coli* MPT synthase (Fig 2.11).

D. Chemical structure of precursor Z

The chemical structure of precursor Z was originally determined by Wuebbens, Rajagopalan and Johnson is shown in figure 2.12 [64,78]. However, a subsequent paper by Santamaria et al., describing precursor Z overproduction followed by 1H-NMR analysis reported a slightly different structure with a geminal diol at the C-1' position instead of a keto group [32]. For the precursor Z structure in the cocrystals, both possible structures were considered. While both fit an omit difference density map equally well (Fig. 2.12a), the distances between the C-terminal glycine of MoaD and the geminal diol are short (Fig. 2.12b) resulting in greater steric hindrance than in the carbonyl model. Therefore, the original precursor Z structure containing the C-1' keto group was used as the model for the cocrystal structure. Since geminal diols readily dehydrate to form a carbonyl, both models are chemically similar, and it is possible that precursor Z can exist in either or both forms depending on solvent and protein environment.

E. MPT synthase active site

The structure of MPT synthase in complex with precursor Z defines the active site of the enzyme in significantly more detail than in the previously published *E. coli* MPT synthase structures where the assignment was based on the presence of highly conserved, surface-exposed residues [36,39]. These conserved residues included Phe34, Arg39, His103, Arg104, Met115, Lys119 and Lys126 of *E. coli* MoaE, which correspond to *S.*

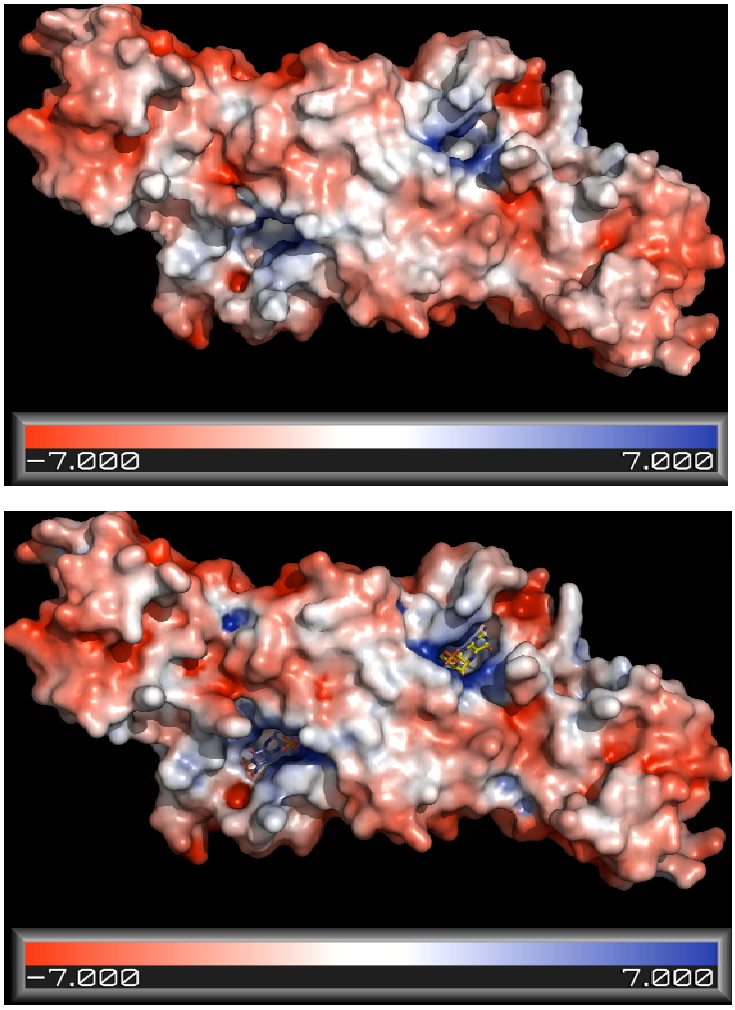

Figure 2.11: Electrostatic potential of the *S. aureus* MPT synthase heterotetramer. Blue and red regions indicate electropositive (>7k_BT) and electronegative (<-7k_BT) regions. The calculations were performed assuming an ionic strength of 100 mM. Top- apo MPT synthase; Bottom- MPT synthase precursor Z complex. A distinct positively charged surface area is located at the active site where the negatively charged precursor Z binds.

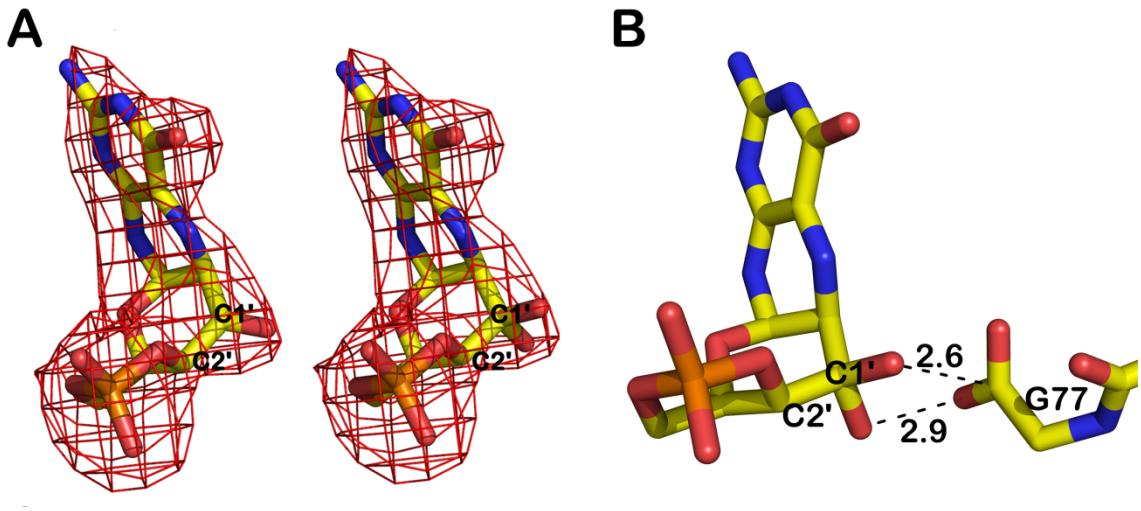

Figure 2.12: Precursor Z identification. (**a**) Unbiased difference density maps (contoured at 3.0 times the rms devation) of the keto (left) and geminal diol (right) forms of precursor Z (C-atoms in *yellow*, N-atoms in *blue*, O-atoms in *red* and P-atom in *orange*). The C-1' and C-2' positions are labeled. (**b**) The close distances between the geminal diol and C-terminal glycine are highlighted.

aureus residues Phe31, Arg36, His100, Arg101, Ile112, Lys116, and Lys123. The His/Arg pair in both structures (*E. coli* MoaE residues 103/104 and *S. aureus* residues 100/101) is located in the distal MoaE subunit and has been shown to coordinate a sulfate-ion in one of the crystal forms of *E. coli* MPT synthase [39]. As described for the *S. aureus* apo-structure, the precursor Z binding pocket is located at the conjunction of the MoaE dimer interface and the MoaD C-terminus in each half of the heterotetramer. The MoaD C-terminus gains access to the active site by threading through the MoaE subunit from the opposite side, and the active site pocket has a predominately positively charged molecular surface that embraces the negatively charged C-terminus of MoaD. In the complex structure, the substrate fits nicely into the MoaE cavity containing the highly conserved residues (Fig. 2.13a). The strictly conserved Phe31 residue is part of a small hydrophobic patch adjacent to the substrate, which also includes the type-conserved residues Val92 and Ile112 (Fig. 2.13b). Arg36 stacks via a cation-π interaction with the precursor Z pterin ring system, this interaction has also been found in many well documented cases contributing to small molecule recognition at protein binding sites [79-81]. The positively charged residues His100 and Arg101 coordinate the cyclic phosphate of precursor Z, a role postulated previously on the basis of the structure of *E. coli* MPT synthase in complex with sulfate [39]. Finally, the amino groups of Lys116 and Lys123 form hydrogen bonds with both the MoaD C-terminal carboxylate and the C-1' oxygen of precursor Z with distances ranging from 2.5-3.1 Å (Fig. 2.13c). These distances have also been confirmed when the active site is drawn with LIGPLOT, a program that presents all the interaction between precursor Z and nearby side chain residues (Fig. 2.14). As

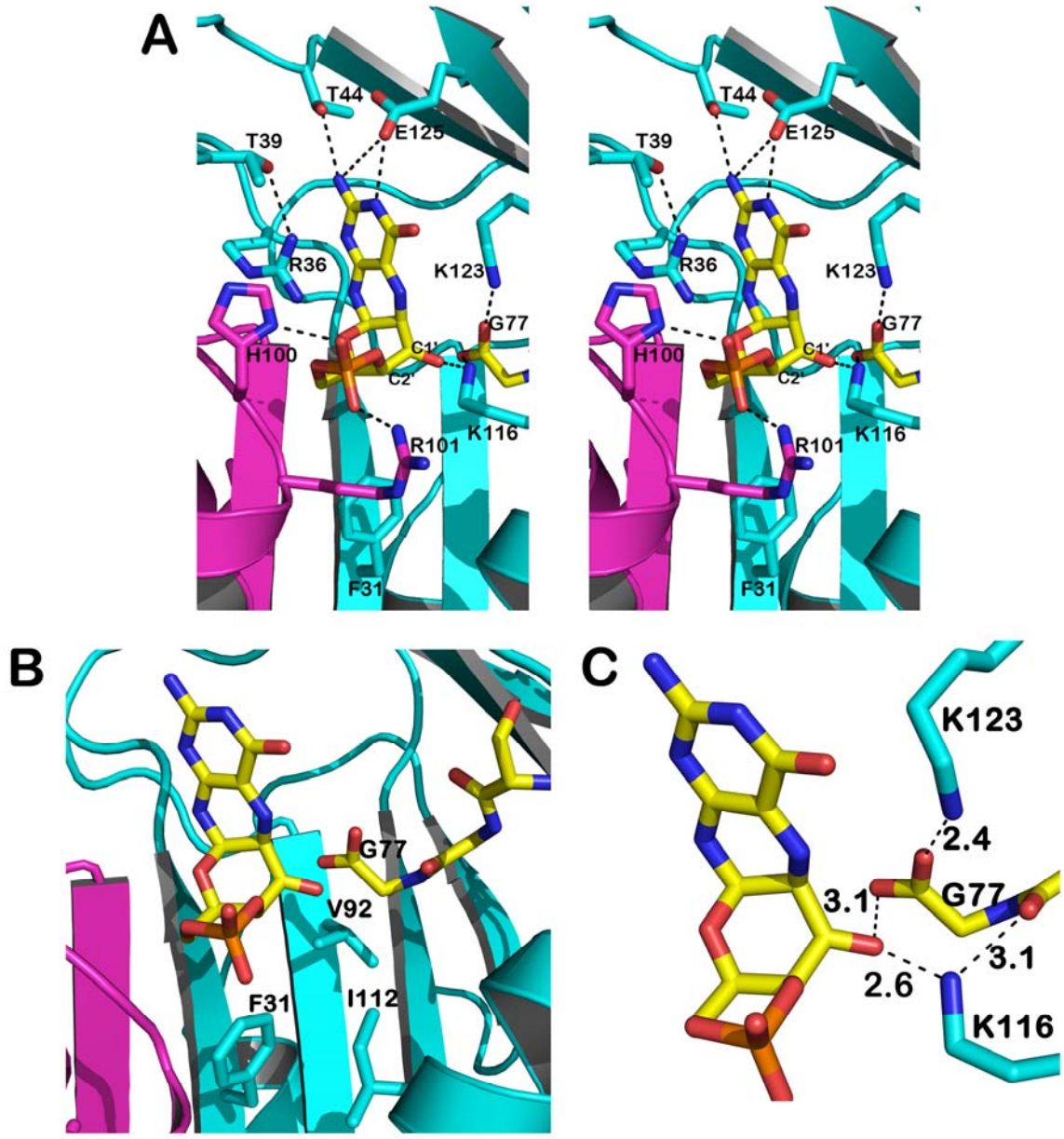

Figure 2.13: Substrate-binding in the active site. (**a**) Close-up stereo view of the precursor Z binding pocket. Polar residues interacting with the substrate are shown with their side chains and the hydrogen bonds between the enzyme and its substrate as dashed lines. (**b**) Hydrophobic patch adjacent to active site showing the strictly conserved Phe31 and type-conserved Val92 and Ile112. (**c**) Enlarged view of the C-terminal glycine of MoaD together with its surrounding residues with the distances between the polar atoms.

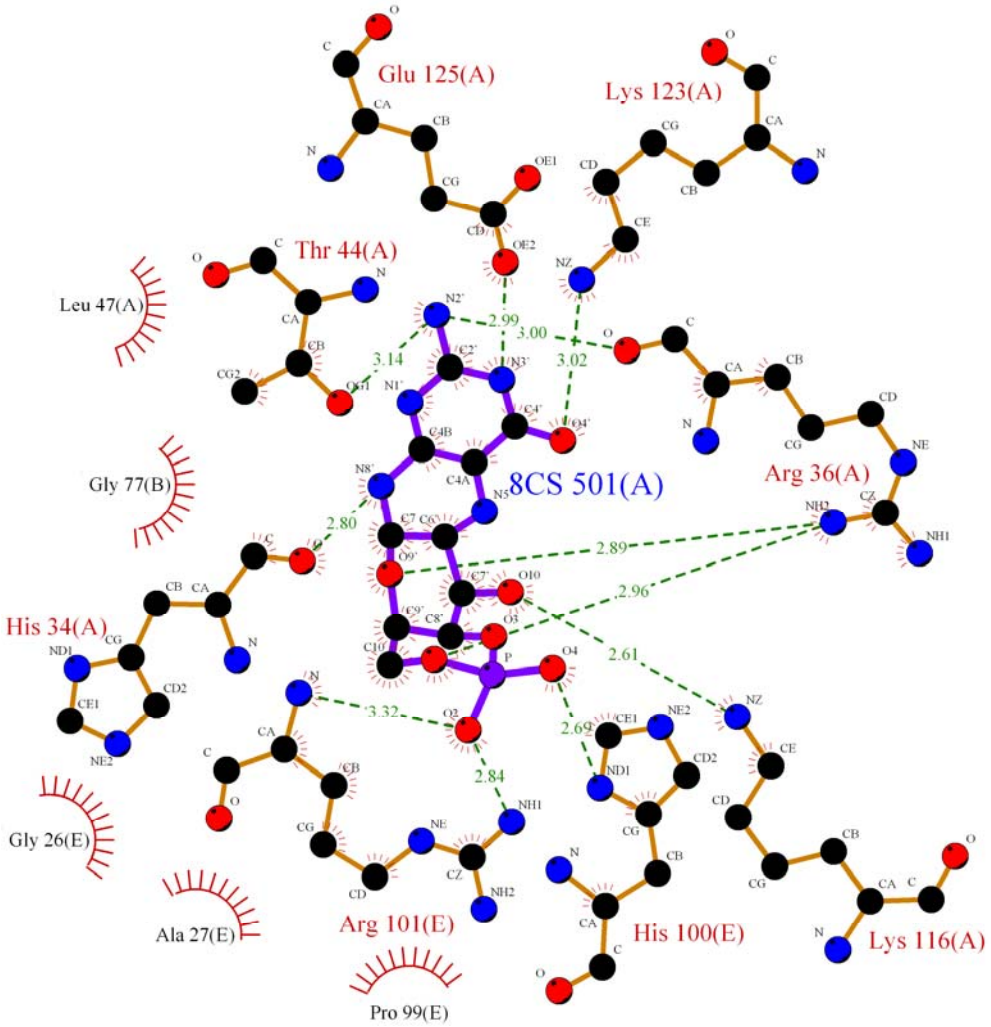

Figure 2.14: LIGPLOT representation of substrate-binding interactions in the active site. Hydrogen bonds are shown as *green* dashed lines with distances in Å, while residues engaged in hydrophobic contacts with the substrate are marked by circular fragments with short radially arranged lines in red. Precursor Z and all polar residues found near it are drawn in ball-and-stick representation, for non-polar residues only the names are indicated. Residues are labeled with the appropriate subunit letter in parentheses (proximal MoaE- "A", Distal MoaE- "E", and MoaD- "B"). Precursor Z is labeled as 8CS, its residue name in the PDB file.

mentioned before, conformational changes between the apo- and complex-structures occur in the loop formed by residues Thr39-Glu45. Several amino acids present in this loop interact with Arg36 and the pterin NH_2 group of precursor Z, which apparently stabilize the loop compared to the apo-structure. A comparison of the *S. aureus* apo-MPT synthase structure and the substrate complex indicates few conformational changes in the active site except for the side chain of Arg36 which points away from the active site in the apo-structure (Fig 2.15).

F. Implications for the catalytic mechanism of MPT synthase

As mentioned before, the conversion of precursor Z to MPT requires the addition of sulfur atoms at adjacent side chain carbons and the concomitant linearization of the precursor Z cyclic phosphate. Previous work with *E. coli* MPT synthase variants identified a pair of MoaE lysine residues at the active site proposed to be involved directly in the two sulfur transfer steps. *E. coli* Lys119 (*S. aureus* Lys116) has been implicated in the first sulfur transfer since the K119A variant is completely inactive [61]. Lys126 (*S. aureus* Lys123) has been implicated in the second transfer since MPT synthase reactions containing the K126A MoaE variant accumulate large quantities of a reaction intermediate that in the wild-type is only present in small amounts. This intermediate is mono-sulfurated and tightly bound to the MPT synthase complex indicating that each precursor Z molecule binds to a single active site where it remains bound until completely converted to MPT [61]. Although initial biochemical results

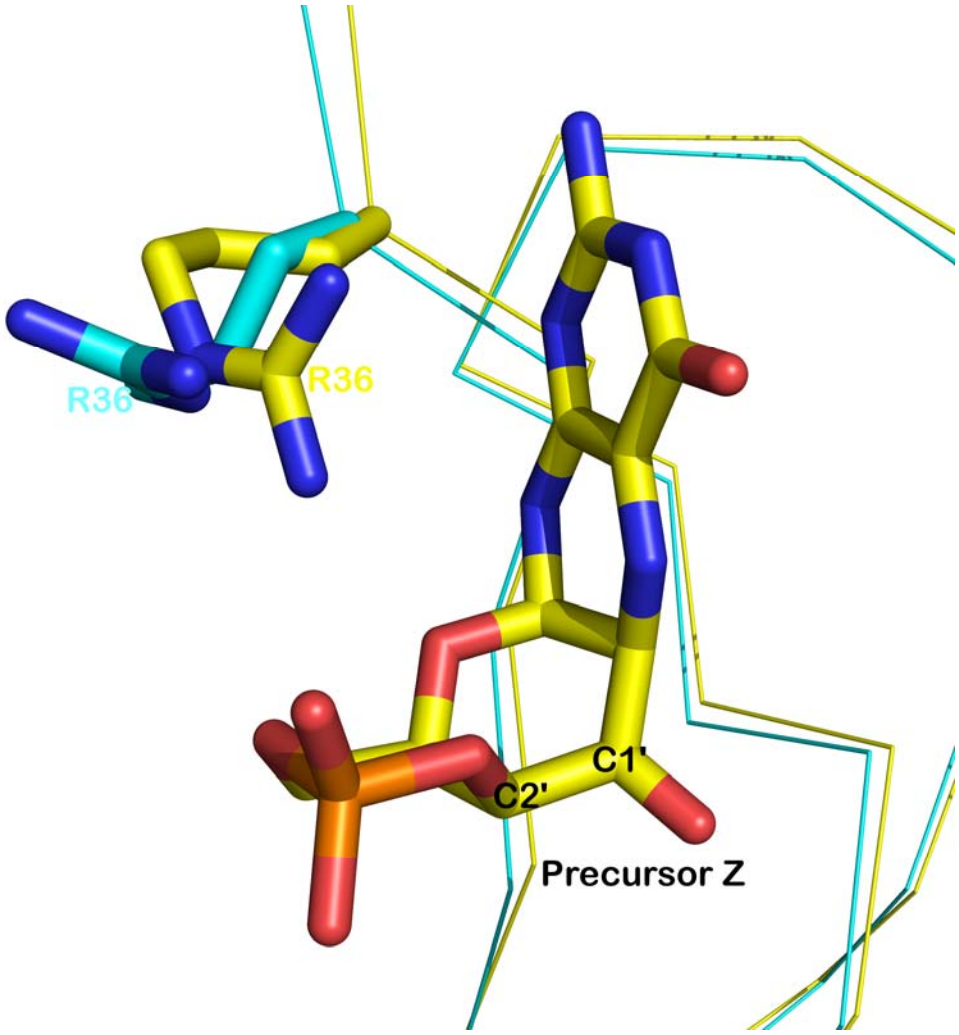

Figure 2.15: Conformational change of Arg 36 in active site of *S. aureus* MPT synthase. Active site showing precursor Z and the Arg36 residue in all bonds representation, apo- (*cyan*) and precursor Z-MPT synthase complex (*yellow*). Arg36 interacts with the aromatic pterin moiety of precursor Z via a cation-π interaction.

indicated that the intermediate contained a linear phosphate, it was not possible to determine whether its single sulfur atom was located at C-1' or C-2'. At first glance, the close proximity between the MoaD C-terminal glycine and the precursor Z C-1' carbon in the co-crystal structure suggests that the first sulfur atom transferred from a MoaD thiocarboxylate is incorporated at the precursor Z C-1' position. However, since these crystals were formed from inactive MPT synthase that does not contain the thiocarboxylate group at the MoaD C-terminus, this structure represents a non-catalytic enzyme-substrate complex. In this inactive co-crystal, the side chains of Lys123 and Lys116, the MoaD C-terminal carboxylate of Gly77 and the C-1'-oxygen of precursor Z are all approximately 3 Å away from each other (Fig. 2.13c). In active MPT synthase, the presence of the bulkier thiocarboxylate at Gly77 would necessitate conformational changes in the active site. The most plausible scenario would be a shift of the MoaD C-terminus to the C-2' position where there is less steric crowding. Superposition of the MoaD C-terminal residues from the structure of activated *E. coli* MPT synthase (PDB entry 3BII) [39] onto the *S. aureus* MPT synthase/precursor Z complex as seen in figure 2.16 reveals that, when activated, the MoaD C-terminal glycine could adopt a favorable conformation for attack at the C-2' position of precursor Z.

Biochemical evidence for the addition of the first dithiolene sulfur to the C-2' position was obtained by our collaborators, Drs. Margot Wuebbens and K.V. Rajagopalan (Department of Biochemistry, Duke University) through further structural characterization of the mono-sulfurated intermediate previously identified in *E. coli* MPT

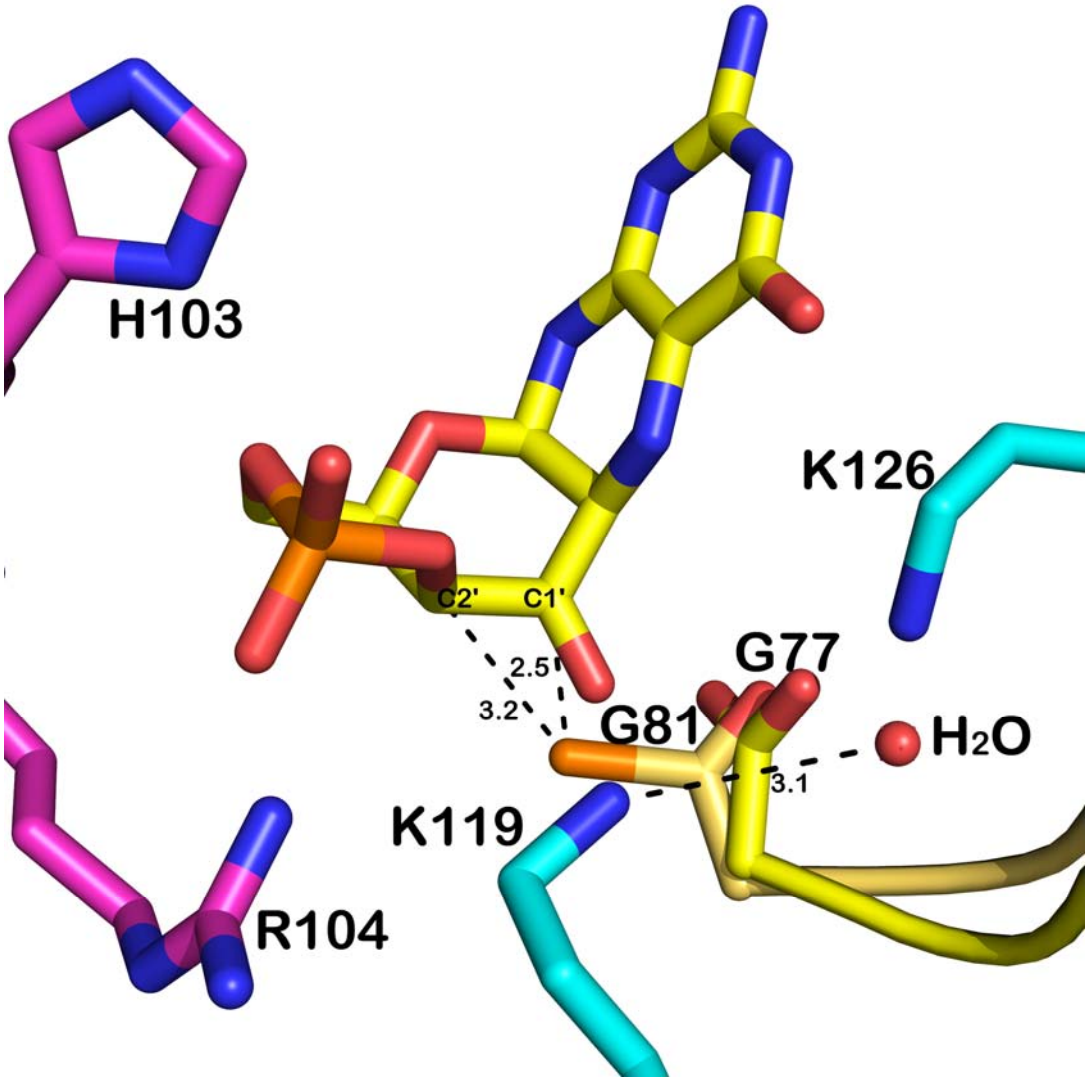

Figure 2.16: Possible points for the initial S-transfer in the MPT synthase catalyzed mechanism. Superposition of *S. aureus* MoaD and precursor Z onto residues of activated *E. coli* MPT synthase (PDB entry, 3BII) in which the MoaD C-terminus is present as a thiocarboxylate. Proximal MoaE (*cyan*), distal MoaE (*magenta*) and the C-terminus of MoaD (*yellow* and *tan*, sulfur in *orange*), dashed lines show distances. When the positions of the terminal glycines are compared, the thiocarboxylated terminus adopts a favorable conformation for attack at both the C-1' and C-2' position.

synthase reactions with the K126A variant [61].

Due to the extreme lability of Moco when released from molybdoenzymes, its structure was originally determined indirectly through the characterization of stable, oxidized derivatives of MPT. One of these derivatives, Form B, is generated when MPT is aerobically acidified at pH 2-3 and heated [75,76]. As seen in figure 2.1, this derivative retains the MPT C-2' dithiolene sulfur atom in the form of a thiophene ring. Form B is structurally identical to the Moco catabolic end product, urothione [75,76], except for the methyl sulfide at the C1' position. To determine the side chain location of the single intermediate sulfur, an expression vector for the *S. aureus* K123A MoaE variant was created, and the protein was purified. MPT synthase reaction mixtures containing either *E. coli* K126A MoaE or *S. aureus* K123A MoaE along with precursor Z and their respective MoaD-SH partners were acidified to pH 2 and then analyzed by reversed phase HPLC for the presence of fluorescent Form B. Figure 2.17, panel I, shows the elution position of control, dephosphorylated Form B generated from the Moco-containing protein sulfite oxidase. As seen in panel II, when the HPLC chromatograms of the two MPT synthase reactions are overlaid, a fluorescent peak eluting at a position similar to the Form B control was observed in both reactions suggesting that the K123A *S. aureus* MPT synthase reaction produces the same intermediate as the *E. coli* K126A reaction and that Form B can be generated from that intermediate. Co-elutions of the fluorescence peaks in panel II with each other (solid trace in panel III) as well as with the Form B control (dashed trace of panel III) support these conclusions. Since the thiophene sulfur atom at the C2' position of Form B cannot be derived from a C-1' sulfur, the

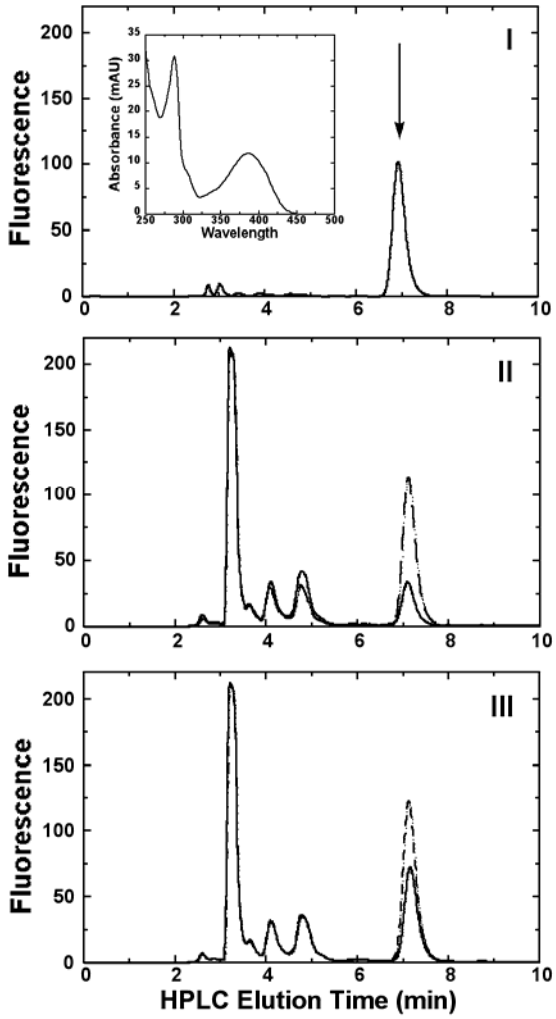

Figure 2.17: Generation of Form B from MPT synthase reactions. (Panel I) HPLC analysis of a 16 µl-aliquot of the Form B control reaction. The arrow indicates the elution position of Form B, and the insert shows the online-spectrum of Form B. (Panel II) Overlay of the HPLC chromatograms obtained from 200 µl-injections of the *S. aureus* K123A reaction (—) or the *E. coli* K126A reaction (- - -). (Panel III) Overlay of the co-injection of 100 µl aliquots of the K123A and K126A reactions (—) with a coinjection of 8 µl of the Form B control reaction with 100 µl each of the K123A and K126A reactions (- - -).

generation of Form B from the intermediate indicates that its sulfur is located at C-2' as shown in figure 2.1. Therefore, the initial sulfur transfer during Moco biosynthesis occurs at this position.

Using this knowledge as well as evidence that MPT synthase is able to catalyze an identical reaction at two adjacent carbon atoms while the substrate remains bound at the same active site [61], the mechanistic proposal outlined in figure 2.18 was formulated for MPT synthase. In this scheme, the initial attack and transfer of the MoaD-SH sulfur atom occurs at the C2' position coupled to the hydrolysis of the cyclic phosphate. This involves the direct attack of the thiocarboxylate sulfur on the C2' carbon resulting in an intermediate in which the MoaD C-terminus is covalently linked to the substrate via a thioester bond. This adduct is subsequently hydrolyzed by a water molecule, and the essential role of Lys116/119 (*S. aureus*/*E. coli* numbering) could be due to its participation in this reaction. Consistent with this idea there is a bound water molecule at a distance of 3.1 Å from the amino group of this lysine and 3.5 Å from the carbonyl carbon of terminal glycine in the position observed in activated *E. coli* MPT synthase (Fig. 2.16). Another possible role for this lysine would be to act as the general base in the second half reaction (see below). The opening of the cyclic phosphate in the intermediate will cause it to bind in a slightly different conformation in which the C-1' atom is possibly being pushed towards Lys123/126 (*S. aureus*/*E. coli* numbering). However, the linearized phosphate is still ligated by the strictly conserved His/Arg pair from the distal MoaE subunit. In the second step, a new MoaD thiocarboxylate attacks the C1' carbon, resulting in a covalent intermediate. Elimination of a water molecule converts it to

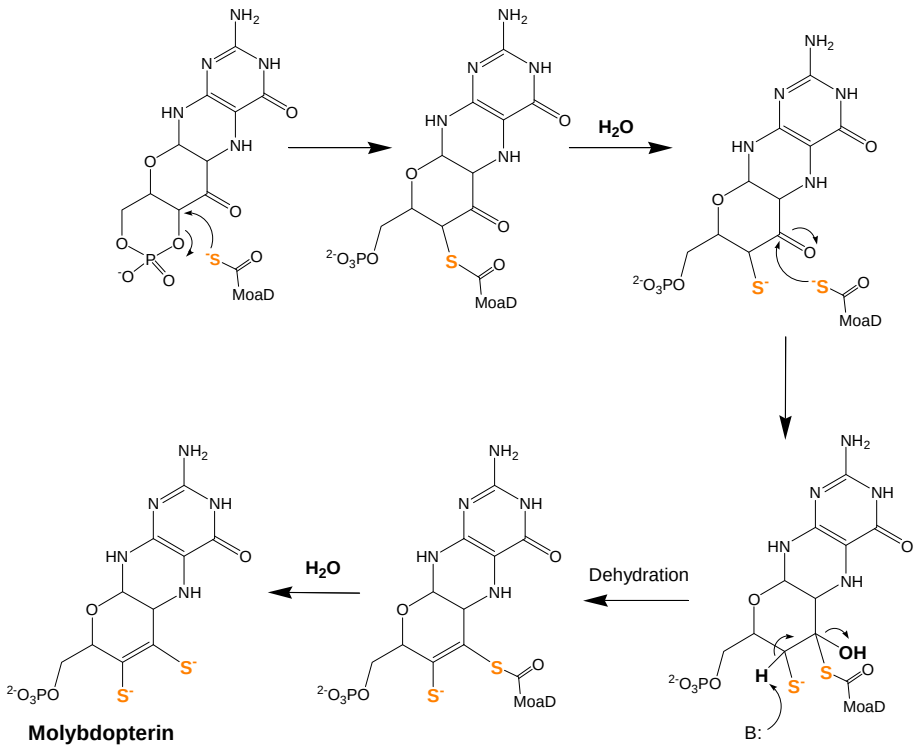

Figure 2.18: Outline of a possible reaction mechanism of MPT synthase.

molybdopterin by forming a C1'-C2' double bond, and subsequent hydrolysis of the thioester intermediate.The inability of the *E. coli* MoaE mutant corresponding to *S. aureus* K123A to further convert the mono-sulfurated intermediate to MPT may be due to either a role as general base which abstracts the proton from the C2' position (if this reaction is not carried out by the other lysine residue), or a structural change in the active site resulting from the smaller Ala side chain which leads to non-productive binding of the intermediate.

Overall, this mechanism is similar to the sulfur transfer reaction during thiamine biosynthesis [82]. In this pathway the ThiS-ThiG heterodimer is involved in sulfur transfer via the C-terminally thiocarboxylated ThiS. ThiS shares the ubiquitin-like fold present in MoaD [83], while its binding partner ThiG, like MoaE, also contains a critical lysine residue (Lys 96) in the active site, which, however, has been shown to form a covalently linked imine intermediate to its substrate, 1-deoxy-D-xylulose-5-phosphate (DXP) [84]. In contrast to MPT biosynthesis, only a single S-atom is transferred during thiamine biosynthesis and ThiG therefore does not need to bind the substrate and a hemisulfurated intermediate in two distinct yet similar ways. Lastly, our crystal structure shows that the *S. aureus* MoaE Lys116 (*E. coli* Lys119) does not engage in a covalently linked imine intermediate with the substrate, as does Lys96 of ThiG and its substrate. However, the structure of MPT synthase complex with precursor Z contains an inactivated MoaD C-terminal glycine and Lys119 may be protonated in the inactive form; it could be possible that upon introduction of a thiocarboxylated MoaD C-terminal glycine the environment inside the active site promotes a Lys119 covalent imine

intermediate with precursor Z. In this case the thiocarboxylated MoaD C-terminus is probably negative because the MoaD polypeptide, like all other polypeptides is a zwitterion, $^{+}NH_3$--MoaD--COO^{-}, or in this case $^{+}NH_3$--MoaD--COS^{-} which may be sufficient to deprotonate the Lys119 residue and trigger the formation of a covalent intermediate or act as a general base during the first sulfur transfer reaction. A covalent intermediate may explain its apparent high binding ability in MPT formation assays with *E. coli* MoaE K126A and its propensity to accumulate it [61]. Although no studies have shown that MPT synthase forms this type of covalent intermediate *in vivo*, a systematic search for this particular detail has not been published. An intermediate-MPT synthase complex would certainly not only provide great insight into how the second sulfur transfer occurs, but would also confirm or reject the mechanism determined in this chapter for the first sulfur transfer, and whether there is truly any covalent intermediate similar to that observed during thiamin biosynthesis.

G. MPT synthase mutants leading to Moco deficiency

Almost all of the mutations that cause Moco deficiency belong to either of two groups, group A or group B, depending on whether the first or second steps during Moco biosynthesis are affected. Nevertheless the resulting Moco deficiency typically manifests itself with an indistinguishable phenotype. The less common of the two, group B, exhibit mutations in MOCS2A/B, the equivalent of MPT synthase in humans. These mutations correspond to the *S. aureus* MoaE E125K point mutation [31,58]. Biochemical studies of group B mutations revealed that the corresponding *E. coli* E128K mutation decreases the

activity of MPT synthase by a factor of 17. Substitution of Glu125 with a lysine in the complex structure (see model in Fig. 2.19) results in a loss of hydrogen bonds between the glutamate side chain and the N1 and N2 atoms of the pterin and close unfavorable contacts between the N1 and N2 atoms and the lysine side chain, thus inhibiting binding of precursor Z.

In addition to the point mutant premature terminations of MoaD after the residue corresponding to Cys5 of MOCS2A and MoaE after the residues corresponding to Pro115 of MOCS2B were also observed [31,58]. While the MoaD truncation is so severe that a complete inactivation is certain, a recent study has also shown that MPT synthase activity is very sensitive to subtle deletions and mutations at the C-terminus of MoaD [85]. Although this study only revealed minor effects when the penultimate Gly was changed to Ala or Ser, substitution of a Glu at this position was severe. The deletion of the *E. coli* MoaD G81, or additions of an additional Gly at position 82 totally inhibited MPT formation. Additionally the G81A mutant severely reduced activity. These results were expected considering that the terminal Gly of *E. coli* MoaD is the primary source of the ene-dithiolate S-atoms. In case of the MOCS2B truncation the observed effect is surprising since the residues corresponding to this truncation are disordered in both the apo-form and precursor Z-complex of *S. aureus* MPT synthase. It therefore appears as if these residues are neither needed for a general stabilization of the enzyme nor for substrate-binding. They could, however, be required to stabilize the mono-sulfurated intermediate in the active site by preventing its dissociation from the MoaE subunit, especially during the time frame from the dissociation of the first MoaD subunit

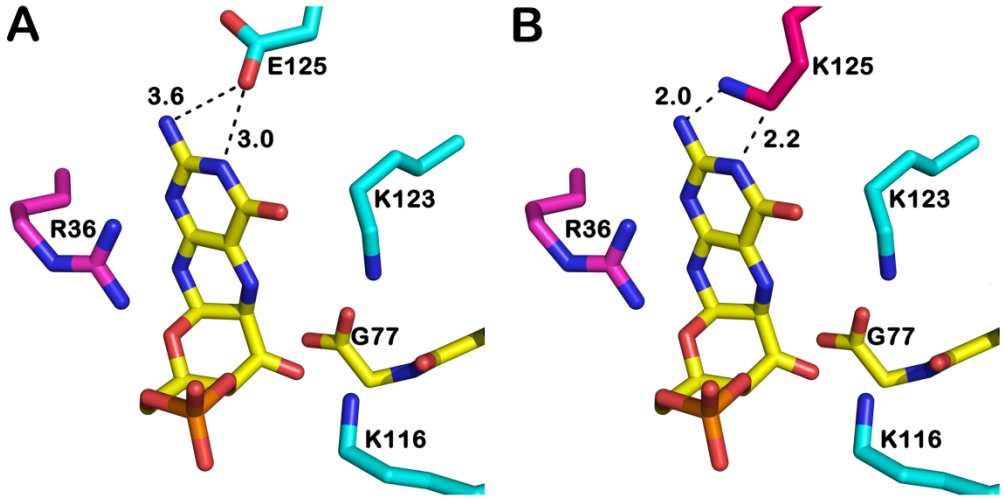

Figure 2.19: Structural basis of Moco deficiency. (**a**) Close-up view of the interaction between *S. aureus* Glu125 and the N1 and N2 atoms of precursor Z. (**b**) A hypothetical model of the E125K mutation found in Moco deficient patients, assuming no conformational changes in either the protein or bound precursor Z, leads to very close steric contacts and loss of the hydrogen bonds.

following the initial S-transfer until a new thiocarboxylated MoaD subunit binds to deliver the second S-atom.

H. Conclusion

The co-crystal structure of MPT synthase with precursor Z not only confirms the general location of the active site, but also defines the substrate-binding and catalytically important residues in significantly more detail. In conjunction with biochemical experiments which demonstrate that the first S-atom is incorporated at the C2' position this allows us to describe the catalytic mechanism in significantly more detail. The structure also provides a rationale for understanding the effects of mutations in human MPT synthase which leads to Moco deficiency. Since there are still questions remaining concerning the exact role of Lys119 and Lys126 (Lys 116 and Lys123 in *S. aureus*) in the sulfur transfer mechanism, whether it occurs via a covalent imine intermediate involving Lys119, or a general base-catalyzed mechanism, a crystal structure of the intermediate in complex with MPT synthase is an important next step and hence was the original goal of the studies described in the next Chapter.

Chapter 2

Attempts to Crystallize a MPT Synthase-Hemisulfurated Intermediate Complex Leads to the Crystal Structure of a Unique Domain Swapped MPT Synthase

I. Introduction

The transition metal, molybdenum, is the 42nd element and is found in trace amounts in almost all biological life forms, mainly in the form of the molybdenum cofactor. Moco is required for a variety of redox reactions in prokaryotes, archaea and eukaryotes in which its biosynthesis is very well conserved. Moco is an essential component of all molybdoenzymes [2-5] with the exception of nitrogenase, and the maturation of these proteins depends on a variety of enzymes involved in the biosynthesis of Moco. Mutations in the genes encoding the enzymes involved in Moco biosynthesis in humans lead to Moco deficiency, a rare but severe disease [56,57] which eventually causes death in early infancy. Many of the mutations found in Moco deficiency have been classified as either group A or group B Moco deficiency. Group A mutations interfere with the formation of a key intermediate in the pathway, while group B mutations disrupt the formation of the 1,2 dithiolene of molybdopterin.

Following the crystal structure analysis of an MPT synthase-precursor Z complex (as described in Chapter 1) the structural characterization of a complex of the enzyme with the hemisulfurated intermediate would represent another significant advance towards understanding the catalytic mechanism of the enzyme. Since extensive attempts to crystallize the *E. coli* K126A variant, which accumulates the intermediate have been unsuccessful, MPT synthase from a variety of bacteria were cloned, purified and screened under a variety of crystallization conditions. Our attempts to obtain the co-crystal structure of the active site mutant of MPT synthase, which accumulates the hemisulfurated intermediate, has led to the discovery of a domain swapped oligomeric form of the *V. cholerae* MPT synthase which consists of a trimer of heterotetramers.

Domain swapping is a structural phenomenon that plays an important role in the mechanism of oligomerization of proteins. In very simple terms domain swapping can be

described as a process in which the monomeric units in the oligomeric structure become entangled with each other (Fig. 3.1). This "entangling" occurs when equivalent regions of two or more monomers, typically the N- or C-terminus, extend and interact with the main domain of another monomer. The flexibility of the hinge loop connecting the main domain with the mobile region is a key feature to facilitate this swapping phenomenon. Engineering the hinge loop by lengthening or shortening it has been shown to affect domain swapping and can change the equilibrium between the monomer and the domain swapped-oligomer [86-89]. Domain swapping in various proteins has been discovered, such as the human prions and human cystatin C that form domain swapped structures that could be the building blocks for amyloid fibers found in Alzheimers disease [90-95]. RNase A has also been reported to form domain swapped dimers and trimers, however, in this case the conversion requires lyophilization in acetic acid [96,97]. Park et al [98] suggest that the domain swapped state of RNase A most likely exists *in vivo*, since the dissociation constant for dimerization occurring at physiological conditions is about 20-fold greater than concentrations of RNase A in the bovine pancrease. Diphtheria toxin, undergoes domain swapping when it is endocytosed and has been shown to exist in this state with its receptor [99].

All in all, domain swapping can occur in proteins to assist in physiologically relevant oligomerization processes. In the case for MPT synthase the formation of such an oligomerization is the first to be observed, however, its significance remains unclear.

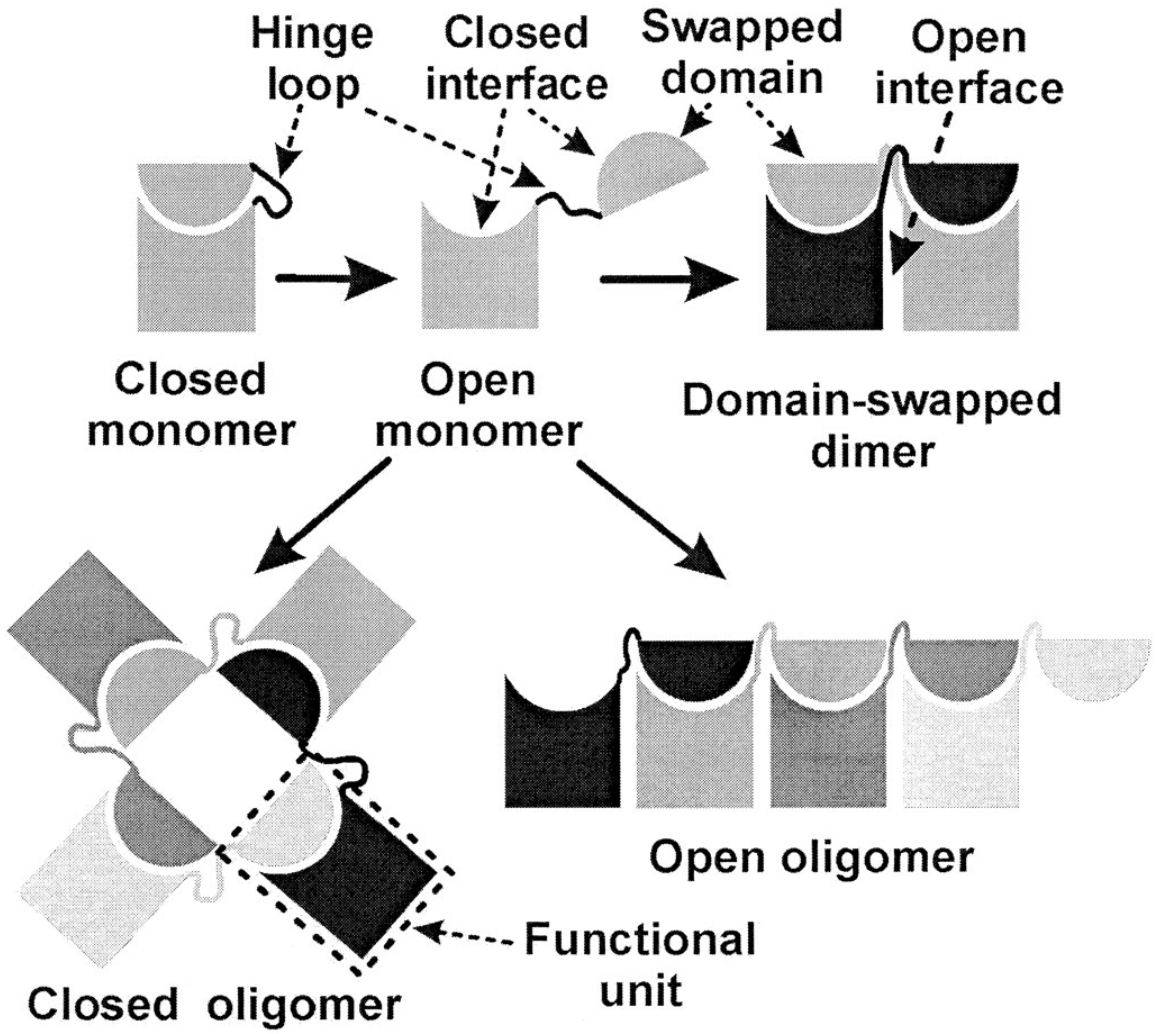

Figure 3.1: Domain swapping scheme (reproduced from Liu et al [100]). In their monomeric form domain swapping proteins are formed in either a closed or open state. The open conformation is the starting point for the formation of either a domain swapped dimer, which contains two monomers sharing equal N-terminal or C-terminal regions linked by a flexible hinge loop or an oligoner, which in turn can consist of a defined number of subunits (closed oligomers) or a quasi-infinite arrangment of subunits (open oligomer). The flexible loop adopts different conformations in the closed and domain-swapped state.

II. Materials and Methods

A. Cloning, expression and purification of the *V. cholerae* MPT synthase (His-tagged; pET-21b)

The sequence encoding the *moaD* and *moaE* genes from *V. cholerae* (VC) genomic DNA (ATCC, Manassas, VA) was subcloned as a contiguous sequence into the pET-21b vector (Novagen, San Diego, CA) which introduces a hexa-His tag at the C-terminus of MoaE. 300 nM of each of the *V. cholerae* pET-21b forward and reverse primers (Table 3.1) were added to the PCR reaction, containing 100 ng of *V. cholerae* genomic DNA and 200 μM NTPs, 1X Expand Buffer, and 1U High Fidelity Enzyme Mix (Expand High Fidelty PCR System, Roche Applied Science, Indianapolis, IN).

The His-tagged MPT synthase was transformed into Rosetta BL21 *E. coli* cells by heat shock [63] and subsequently cells were selected after overnight growth at 37ºC on LB plates containing 100 μg/mL ampicillin and 34 μg/mL chloramphenicol. Single colonies were picked and used to inoculate 25 mL LB/amp/cam media for overnight growth. The resulting culture was utilized to inoculate 1L of LB/amp/cam which was grown to an OD_{600} = 0.5 at 37ºC. At that time the cells were induced with 0.5 mM isopropyl-β-D-thiogalactopyranoside (IPTG) and grown at 30˚C for 3 hours. Cells were harvested by centrifugation at 8000 x g for 25 minutes at 4˚C and lysed in 50 mM Tris-HCl, pH 8.0, 300 mM NaCl and 10 mM imidazole by passing them twice through a French pressure cell at 1,500 psi followed by centrifugation at 16,000 x g. The protein was initially purified by Ni^{2+}affinity chromatography using 5 mL Ni^{2+} agarose beads

Table 3.1

V. cholerae pET-21b primers

F-NdeI VC MoaD	*GAA GGA GAT ATA CAT ATG ATT AAG GTG CTG TTT TTT GCC CAA*
R-XhoI VC MoaE	*G GTG GTG GTG GTG GTG GTG CTC GAG TTC CCA GCG CTG CGC GG*

V. cholerae pTYB1 primers

F-NdeI VC MoaD	*GAA GGA GAT ATA CAT ATG ATT AAG GTG CTG TTT TTT GCC CAA*
R-SapI VC MoaD	*G GTC CAT AGC TCT TCC GCA GCC TCC AGT CAC TGG*
F-NdeI VC MoaE	*GAA GGA GAT ATA CAT ATG GAC CAT CGC GTA TCG GTG*
R-SapI VC MoaE	*G GTG CTC GAG GC TCT TCC TGC TTC CCA GCG CTG C*

Primer sequences used in the PCR amplification of MoaE and MoaD subunits for cloning into pET-21b and pTYB1 expression vectors.

(Qiagen). The column was washed with lysis buffer containing 100 mM of imidazole, and subsequently the protein was eluted from the column by increasing the imidazole concentration to 250 mM. In the second and final chromatography step, the protein was run on a 26/60 Superdex 200 size exclusion column (GE Healthcare, Piscataway, NJ), where the only observed protein eluted at a volume of 210 mL, similar to the major peak of the *S. aureus* counterpart. The purity of *V. cholerae* MPT synthase was verified by SDS PAGE analysis (Fig. 3.2) and the protein was concentrated to 14 mg/mL calculated on the basis of a molar extinction coefficient of $\varepsilon = 32095\ M^{-1}cm^{-1}$ (PROTPARAM) using a Centricon-20 Centrifugal Filter Unit (Millipore, Billerica, MA) with a molecular weight cutoff of 10,000 Da.

B. Cloning, expression and purification of the active *V. cholerae* MPT synthase (untagged; pTYB1)

The sequence encoding the *moaD* and *moaE* genes from *V. cholerae* was subcloned into the pTYB1 vector using *V. cholerae* pTYB1 primers where the *moaD* and *moaE* sequences were subcloned separately (following the procedure described in section A) into a cleavable intein chitin binding domain fusion tag [61]. In order to produce a thiocarboxylated MoaD C-terminal glycine the method described in Wuebbens et al [61] was used. In this procedure the C-terminal fused intein on MoaD is cleaved by substituting $(NH_4)_2S$ for DTT, which is normally used for intein cleavage, resulting in a catalytically active thiocarboxylated MoaD C-terminus (Fig. 3.3). Activated wild-type MPT synthase protein was provided by Dr. Margot M. Wuebbens (Duke University).

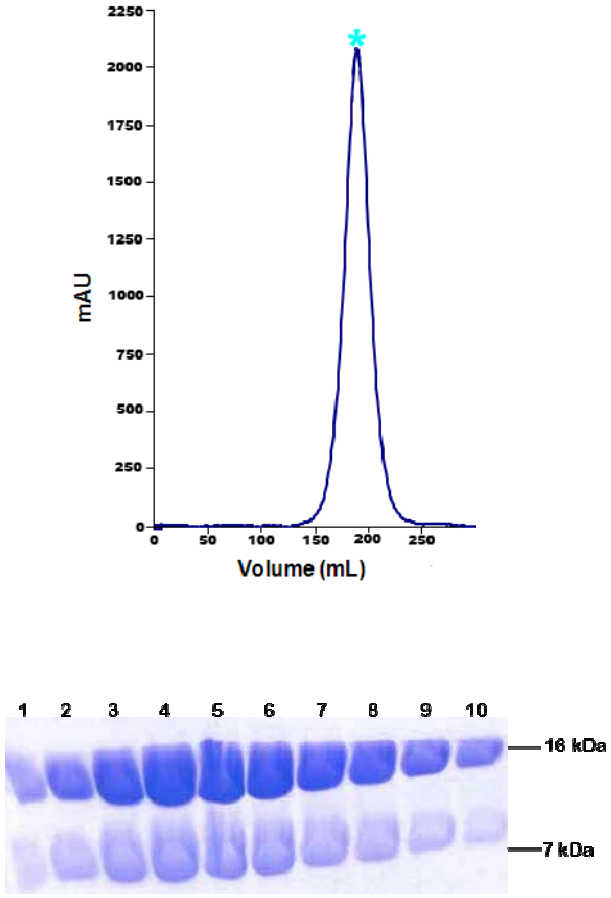

Figure 3.2: Size exclusion chromatography of His tagged *V. cholerae* MPT synthase. The enzyme eluted from the column at an elution volume around 210 mL. Each fraction contained about 3 mL and 12 µl were applied to the gel (Fractions #1-10 from peak indicated by asterisk).

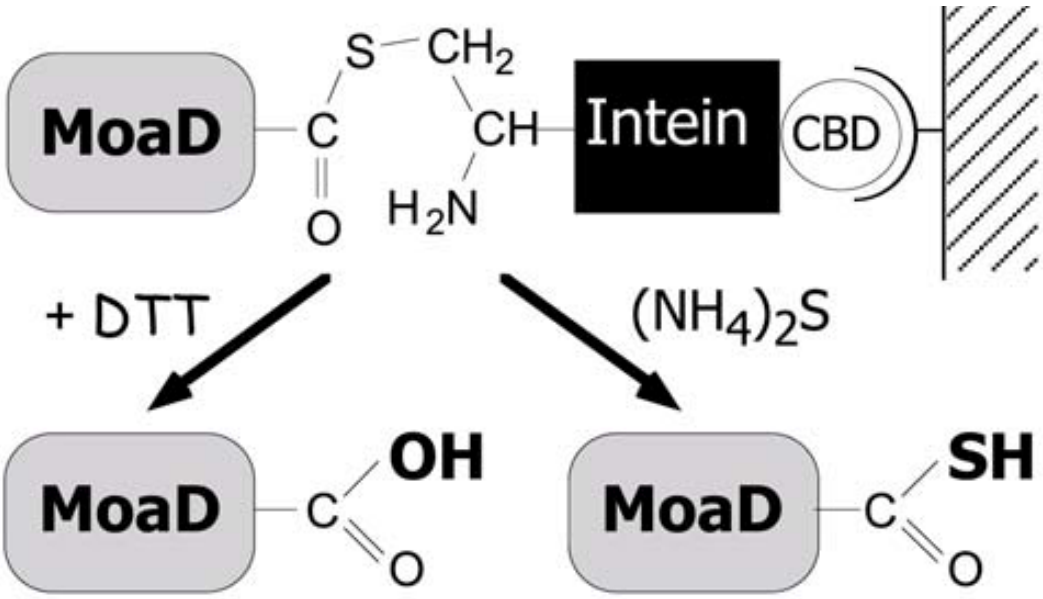

Figure 3.3: Formation of thiocarboxylated MoaD using the intein mediated method. The intein fused at the MoaD C-terminus is cleaved using DTT to produce an inactive untagged protein. A modified procedure using $(NH_4)_2S$ produces a thiocarboxylated MoaD, which is biologically active.

C. Site Directed Mutagenesis of the *V. cholerae* MoaE (untagged; pTYB1)

The pTYB1 MoaE K125A variant was made by using the Quick Change site directed mutagenesis kit (Roche Applied Science, Indianapolis, IN) with K125A mutation primers (Table 3.2). The corresponding protein was purified using the protocol described in section B. Activated MoaD and untagged K125A MoaE protein samples were provided by Dr. Margot M. Wuebbens (Duke University).

D. Formation of the intermediate loaded MPT synthase

The purified K125A MoaE and thiocarboxylated MoaD proteins were added to 15 mL of 50 mM Tris-HCl, 50 mM NaCl, pH 8.0, together with precursor Z, to allow for the accumulation of the intermediate. Precursor Z was purified using the procedure described in the Materials and Methods of Chapter 2, sections E and F.

E. Crystallization of *V. cholerae* MPT synthase variants

Suitable crystallization conditions for purified MPT synthase were screened using the Hampton Crystal Screens and Emerald Wizard Screens. A total of three MPT synthase variants were used (Table 3.2), the His-tagged (*h*) and untagged (*u*) MPT synthase (*h*VC-MPTS, *u*VC-MPTS) in the wild-type sequence context, as well as the mutated untagged MPT synthase containing the MoaE K125A mutant and thiocarboxylated MoaD (*a*K125A). The three samples (*h*VC-MPTS, *u*VC-MPTS, *a*K125A) were subjected to the hanging drop vapor diffusion technique, and crystals were produced mainly in conditions which contained either calcium or magnesium ions

Table 3.2

Sample name	
h*VC-MPTS	C-terminally His-tagged MoaE, inactive MoaD
***u*VC-MPTS**	untagged MoaE, inactive MoaD
a*K125A	untagged K125A MoaE, activated MoaD
a*K125Aint	untagged K125A MoaE, activated MoaD + precursor Z

Listing of protein sample names derived from *V. cholerae* MPT synthase.

Note: In all cases MoaD is untagged.
*denotes crystals were sufficient for data collection.

as an additive. The first condition which produced crystals was the protein sample *h*VC-MPTS. These crystals were produced from 1.4 M $MgSO_4$, 0.1 M HEPES, pH 7.5 at a concentration of 14 mg/mL (Fig. 3.4, left panel). Although the protein sample *u*VC-MPTS crystallized, the crystals did not produce any reflections when tested in the X-ray beam. The *a*K125A sample was crystallized against a reservoir containing 4% (w/v) PEG 8000, 0.1 M HEPES, pH 7.5, 0.2 M Ca-Acetate at a protein concentration of 10 mg/mL (Fig. 3.4, right panel). The PEG 8000 derived crystals grew to dimensions of 0.22 x 0.14 x 0.14 mm^3 after three to four days and the $MgSO_4$ derived crystals reached a final size of 0.30 x 0.22 x 0.04 in the same amount of time.

The PEG 8000 crystals belong to the trigonal space group P321 with unit cell dimensions of $a = b = 144.9$ Å and $c = 87.0$ Å and contain three MoaD-MoaE heterotetramers in the asymmetric unit. The $MgSO_4$ crystals belong to the orthorhombic space group $C222_1$ with unit cell dimensions of $a = 94.5$ Å, $b = 167.9$ Å and $c = 163.1$ Å and contain three heterodimers in the asymmetric unit. A total of 180° of diffraction data were recorded in 1° increments revealing 116,897 and 127,728 reflections of which 32,128 and 65,487 are unique reflections for the $MgSO_4$ and PEG derived crystals, respectively.

F. Crystallization attempts of the intermediate MPT synthase co-crystal complex

The same procedure described in section E was used in initial attempts to crystallize the intermediate-loaded protein (*a*K125A-int) using the PEG condition.

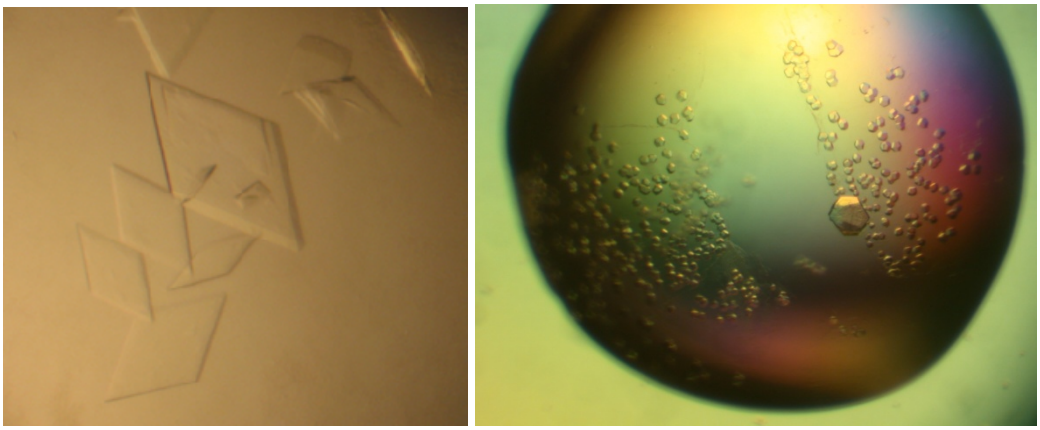

Figure 3.4: Crystals of domain swapped *V. cholerae* MPT synthase. Left panel - His tagged MPT synthase; Right panel - Untagged K125A MPT synthase.

However, these conditions were modified to improve the crystal morphology while at the same time trying not to impede the protein's ability to bind to the intermediate. Crystallization of the protein was possible in a simple condition containing only 0.1 M $CaCl_2$ after 2-3 weeks, but larger crystals were obtained from 0.6 M $CaCl_2$ and 0.4 M Na-formate in only 2-3 days at room temperature. To minimize oxidation of the intermediate some crystallization trays were set up in an anaerobic tent with an atmosphere consisting of 95-98% Argon and 2-5% Hydrogen, with less than 10 ppm of oxygen being present. Experiments with anaerobic crystallization trays necessitating temperatures different from those in the anaerobic chamber, were sealed in a plastic bag, taken out of the anaerobic tent and incubated at 22ºC, 10ºC and 4ºC.

G. Data collection of *V. cholerae* MPT synthase

All diffraction data were collected on beamline X26C at the National Synchrotron Light Source, Brookhaven National Laboratory at a wavelength of 1.1 Å. The PEG crystals (*a*K125A) were soaked immediately in mother liquor with 30% glycerol while the $MgSO_4$ crystals (*h*VC-MPTS) were soaked gradually in 5% increments of glycerol until reaching 30%, lastly the crystals were plunged into liquid nitrogen. Diffraction data were indexed, integrated and scaled using the HKL [66] suite.

H. Structure Determination and Refinement of the *V. cholerae* MPT synthase (*h*VC-MPTS, *a*K125A)

The structure of the orthorhombic *V. cholerae* MPT synthase (*h*VC-MPTS) was solved by molecular replacement with the program MOLREP [73] using the *E. coli* MPTS heterotetramer/heterodimer [39] as the search model. The rotational and translational searches were performed using data in the resolution range from 50 to 4 Å and identified one and a half MPT synthase heterotetramers or three heterodimers in the asymmetric unit. The structure of the trigonal *V. cholerae* MPT synthase (*a*K125A) was solved by molecular replacement with the model of the heterotetramer derived from the orthorhombic crystal form. In this case the rotational and translational searches were also performed using data in the resolution range from 50 to 4 Å, which identified three MPT synthase heterotetramers in the asymmetric unit.

The models were refined using the program REFMAC [69], initially using rigid body refinement and subsequently using TLS and restrained refinement. Model building was carried out using the program O [72]. Ca ions, sulfates and acetates were manually positioned appropriately and water molecules were added using the program ARP [74].

I. Structure Determination and Refinement of the intermediate loaded *V. cholerae* MPT synthase (*a*K125Aint)

Data collection and structure determination of the crystals grown from intermediate loaded MPT synthase (*a*K125A-int) followed the procedure outlined in sections G and H, above. However, the crystals underwent a complete change in crystal

packing from a trigonal space group to the monoclinc space group $P2_1$ for crystals grown aerobically as well as inside an anaerobic tent (*a*K125Aint-1) and back to the orthorhombic $C222_1$ for crystals set up in the anaerobic tent and grown inside airtight bags outside the tent (*a*K125Aint-2) which required new rounds of molecular replacement using MOLREP. The search model used for solving both structures was the heterotetramer from the P321 structure. The rotational and translational searches were performed using the same resolution range from 50 to 4 Å. These searches identified one MPT synthase heterotetramer and two MPT synthase heterotrimers in the $P2_1$ crystals having the same subunit arrangement as in the P321 structure, whereas the $C222_1$ crystals contained one heterotrimer and one heterodimer in the asymmetric unit in an overall arrangment which is related to the orthorhombic crystals described above. The refinement of both structures was performed using the steps described in the above section describing the structure determination and refinement.

J. Analytical size exclusion chromatography

The purified active K125A MPT synthase was diluted to a final concentration of 1-2 mg/mL and 500 µL of the protein was injected onto a Superdex 10/30 analytical size exclusion chromatography column (GE Healthcare, Piscataway, NJ) fully equilibrated with each of the following buffers:

A. 50 mM Tris/HCl pH 8.0 and 50 mM NaCl

B. 2 mM CaAcetate, 0.1 M HEPES pH 7.0

C. 50 mM CaAcetate, 0.1 HEPES pH 7.0

D. 0.2 M CaAcetate, 0.1 HEPES pH 7.0

Molecular weight standards (Sigma-Aldrich, Bellefonte, PA) consisting of cytochrome c (12 kDa), carbonic anhydrase (29 kDa), bovine albumin serum (66 kDa), β-amylase (200 kDa), alcohol dehydrogenase (35 kDa, 70 kDa, 135 kDa) and Blue Dextran (2,000 kDa, V_o) were used to calibrate the column and produce a molecular weight standard curve (Fig. 3.5) according to the equation:

$$\log(MW) = -1.702(Ve/Vo) + 8.02$$

K. Form A analysis using crystals derived from intermediate loaded crystals

The procedure described in Chapter 2 section J describing the generation of Form B, was used except that KI/I_2 was added during the reaction. Addition of KI/I_2 promotes the formation of Form A rather than Form B from molybdopterin and also produces this derivative from the intermediate. Crystals from twenty-four wells were collected by using a cryo loop and used as the source of any intermediate or molybdopterin in the analysis.

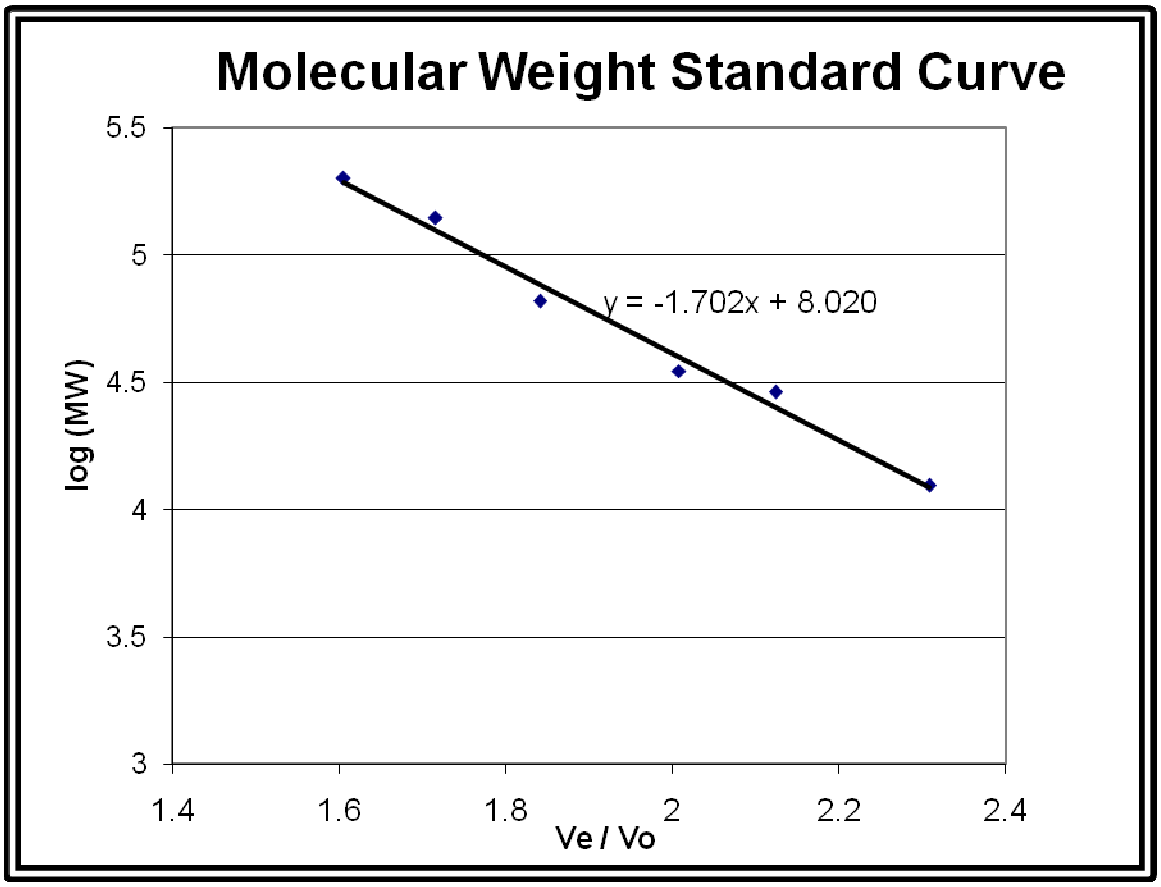

Figure 3.5: Calibration curve of molecular weight standards. The following protein standards were used: cytochrome c (12 kDa), carbonic anhydrase (29 kDa), bovine albumin serum (66 kDa), β-amylase (200 kDa), alcohol dehydrogenase (35 kDa, 70 kDa, 135 kDa) and Blue Dextran (2,000 kDa, V_o), Ve is the elution volume; V_o is the void volume determined by the elution volume of Blue Dextran which was 7.4 mL.

III. Results and Discussion

A. Orthorhombic crystal form of *V. cholerae* MPT synthase (*h*VC-MPTS)

The orthorhombic crystal form diffracted X-rays up to 2.8 Å resolution and the resulting data set has an overall completeness and R_{sym} of 98.7% and 6.8%, respectively (96.0% and 79.3% in the last shell), with an overall $\langle I/\sigma I \rangle$ of 14.4 (2.2 in the highest resolution shell) (Table 3.3). The structure was refined at 2.8 Å resolution (Table 3.3) to an R-factor of 0.193 (R_{free}= 0.228). The resulting model contained all residues in the MoaD subunit (1 to 81), as seen before in structures published from our lab [36,39]. However, for the first time all residues from the MoaE subunit are ordered, including residues corresponding to the disordered active site loop (residues 39 through 47) of *E. coli* MoaE and the disordered C-terminal helix (residues 137 to 148) of *S. aureus* MoaE. Surprisingly, a continuous difference density feature spanning adjacent MoaE subunits belonging to different heterotetramers was discovered. This indicated that domain swapping had occurred and the domain swapped region of MoaE consisting of the C-terminal region from residue 131 to 150 was manually built into the electron density maps. After model building and refinement, the final model of the orthorhombic form of MPT synthase contained 61 water molecules and 5,595 protein atoms all having good stereochemistry with 94.6% of all non-Pro and non-Gly residues in the favored regions of the Ramachandran diagram [101], and only 1.3% of residues in disallowed regions including Arg4, Asp39 and Arg130 in three MoaE subunits.

Table 3.3

	*h*VC-MPTS	*a*K125A	*a*K125Aint-1	*a*K125Aint-2
Space group	$C222_1$	P321	$P2_1$	$C222_1$
Resolution limits (Å)	50 - 2.8	50 - 2.5	50 - 3.3	50 - 2.4
Completeness	0.987	0.959	0.997	0.994
R_{sym}	0.068	0.068	0.28	0.097
$\langle I/\sigma I \rangle$	14.4	38.4	7.9	29.8
All reflections	116,897	127,728	103,767	136,942
Unique reflections	32,128	65,487	31,673	44,175
Number of reflections used	30,474	61,931	30,060	41,499
Subunit composition in the asymmetric unit	3 x MoaE 3 x MoaD	6 x MoaE 6 x MoaD	6 x MoaE 4 x MoaD	3 x MoaE 2 x MoaD
Number of protein atoms	5,595	11,119	8,857	4,983
R_{cryst}	0.193	0.197	0.249	0.188
R_{free}	0.228	0.245	0.289	0.229
rms deviation from ideal values in				
Bond distances (Å)	0.020	0.017	0.012	0.017
Bond angles (º)	1.875	1.623	1.784	1.693
Chiral centers ($Å^3$)	0.136	0.118	0.105	0.104
Ramachandran statistics	94.6/1.3	94.4/1.3	86.6/3.3	94.7/1.8

Listing of protein sample names derived from *V. cholerae* MPT synthase

*a*K125Aint-1 corresponds to a dataset collected with crystals grown in the anaerobic chamber, additionally, data were collected from crystals that were prepared and grown aerobically although is the corresponding statistics are not shown here. K125A-int2 is derived from a crystal which was set up in the anaerobic chamber, sealed in a plastic bag and subsequently transferred out of the chamber into an incubator, which was equilibrated at 22°C.

$R_{sym} = \sum_{hkl} \sum_i |I_i - \langle I \rangle| / \sum_{hkl} \sum_i I_i$ where I_i is the i^{th} measurement and $\langle I \rangle$ is the weighted mean of all measurements of I. $\langle I/\sigma I \rangle$ indicates the average of the intensity divided by its standard deviation. $R_{cryst} = \Sigma \, ||F_o| - |F_c|| / \Sigma \, |F_o|$ where F_o and F_c are the observed and calculated structure factor amplitudes. R_{free} same as R_{cryst} for 5% of the data randomly omitted from refinement. Numbers in parentheses apply to the respective highest resolution shell. Ramachandran statistics indicate the fraction of residues in the most favored and disallowed regions of the Ramachandran diagram as defined by the program MOLPROBITY.

B. Trigonal crystal form of *V. cholerae* MPT synthase (*a*K125A)

The trigonal crystals diffracted X-rays up to 2.5 Å resolution and the resulting data have an overall completeness and R_{sym} is 95.9% and 6.8%, respectively (85.4% and 62.7% in the last shell) (Table 3.3), the overall $<I/\sigma I>$ of the data was 38.4 (2.6 in the highest resolution shell). The structure of the trigonal crystal form was refined at 2.5 Å resolution (Table 3.3) to R-factors of 0.197 (R_{free}= 0.245). After model building and refinement, this structure contained 304 water molecules and 11,119 protein atoms (derived from three heterotetramers). The model displays good stereochemistry with 94.4% of all non-Pro and non-Gly residues in the favored regions of the Ramachandran diagram [101], and only 1.3% of residues in disallowed regions, these include Arg4, Asp39 and Arg130 from the six subunits of MoaE.

C. Primary sequence comparison of *V. cholerae* structures

The *V. cholerae* MoaE and MoaD subunits are more closely related to their *E. coli* counterparts than the *S. aureus* subunits; the primary sequence identity of the *V. cholerae* and *E. coli* MoaE subunits is 62% while that of the *V. cholerae* and *E. coli* MoaD subunits is 69% compared to 35.5% and 25.9% between the MoaE and MoaD subunits from *E. coli* and S. aureus, respectively. This identity reflects a closer evolutionary relationship between the *V. cholerae* and *E. coli*. The resulting proportions of charged and uncharged residues in the primary sequence are equivalent to that of *E. coli* MPT synthase; both *E. coli* and *V. cholerae* MoaE and MoaD contain 58% of the total residues that are uncharged. The number of negatively and positively charged residues is about the same, with *E. coli* and *V. cholerae* both having 23 positively and 34 to 36 negatively charged residues.

D. Structural comparisons of the orthorhombic and trigonal crystal forms of *V. cholerae* MPT synthase (*h*VC-MPTS, *a*K125A)

The overall structure of *V. cholerae* from the orthorhombic (Fig. 3.6) and trigonal (Fig. 3.7) derived structures are very similar. A comparison of the heterotetramers from the orthorhombic and trigonal crystal forms show a smaller degree of structural variance with an rms deviation of 0.8 Å over the entire structure consisting of 141 Cα atoms (Fig. 3.8a), excluding the loop region (residues 38 to 42), which undergoes conformational changes between the two crystal forms. In contrast comparison of the structures of *V. cholerae* MPT synthase (Fig. 3.6 and 3.7) reveals a few noteworthy differences to that of *E. coli* MPT synthase [36]. A superposition of all residues of the heterotetramer except for the C-terminal region of MoaE (127-149) from either the orthorhombic or trigonal structures reveals an rms deviation of 1.0 Å when compared with the $I2_12_12_1$ crystal form of *E. coli* MPT synthase (PDB entry 1NVI). Most notable among the differences is the association of adjacent MoaE/MoaD heterotetramers into a previously unobserved quaternary arrangement. In both the trigonal and orthorhombic structures the $(MoaD/MoaE)_2$ heterotetramers oligomerize with two adjacent heterotetramers, forming a heterododecamer. In the trigonal crystals the entire heterododecamer constitutes the content of the asymmetric unit, while the orthorhombic crystals contain half of the heterododecamer in the asymmetric unit with a crystallographic two fold axis generating the full heterodecamer. The C-terminal regions (MoaE residues 122-149) of adjacent MoaE subunits, which include the last helix are participating in inter-subunit interactions

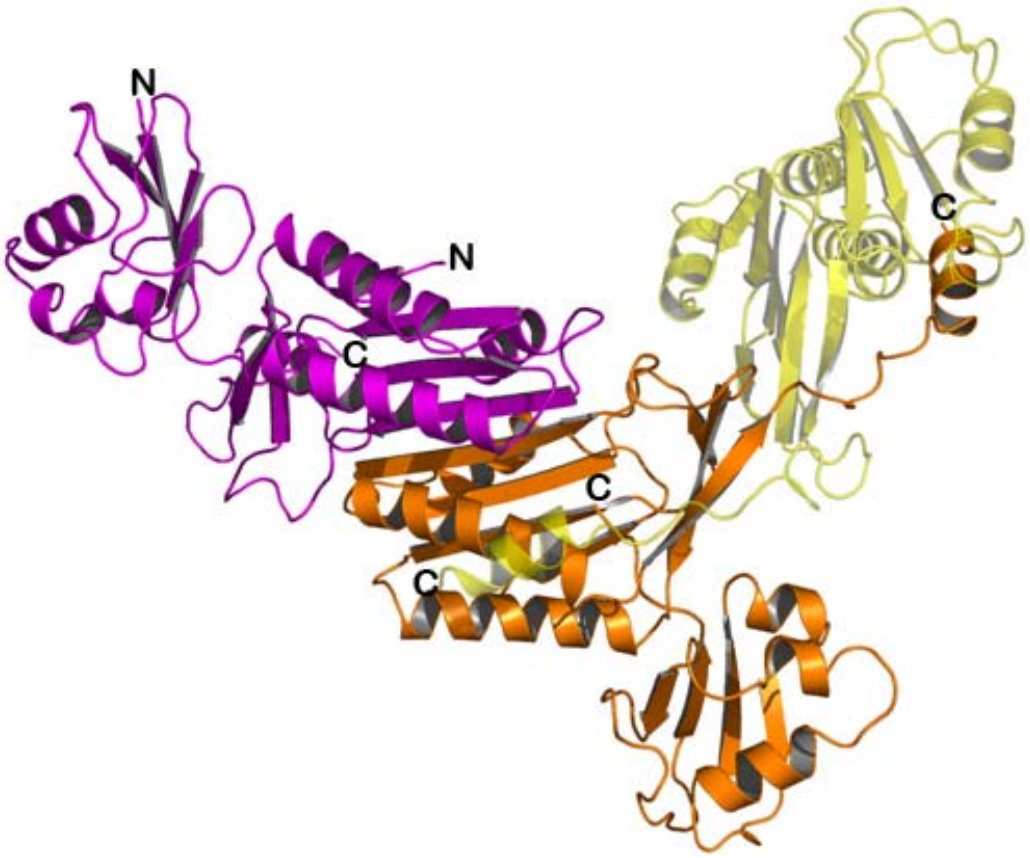

Figure 3.6: Ribbon representation of *V. cholerae* MPT synthase. Structure of MPT synthase in the $C222_1$ space group showing the three MoaD-MoaE heterodimers present in the asymmetric unit (colored in *magenta*, *orange* and *yellow*) which show domain swapping between the MoaE subunits (*orange* and *yellow*). The complete trimer of heterotetramers can be generated by applying the symmetry operations and forms the same trimer of heterotetramers depicted in figure 3.7.

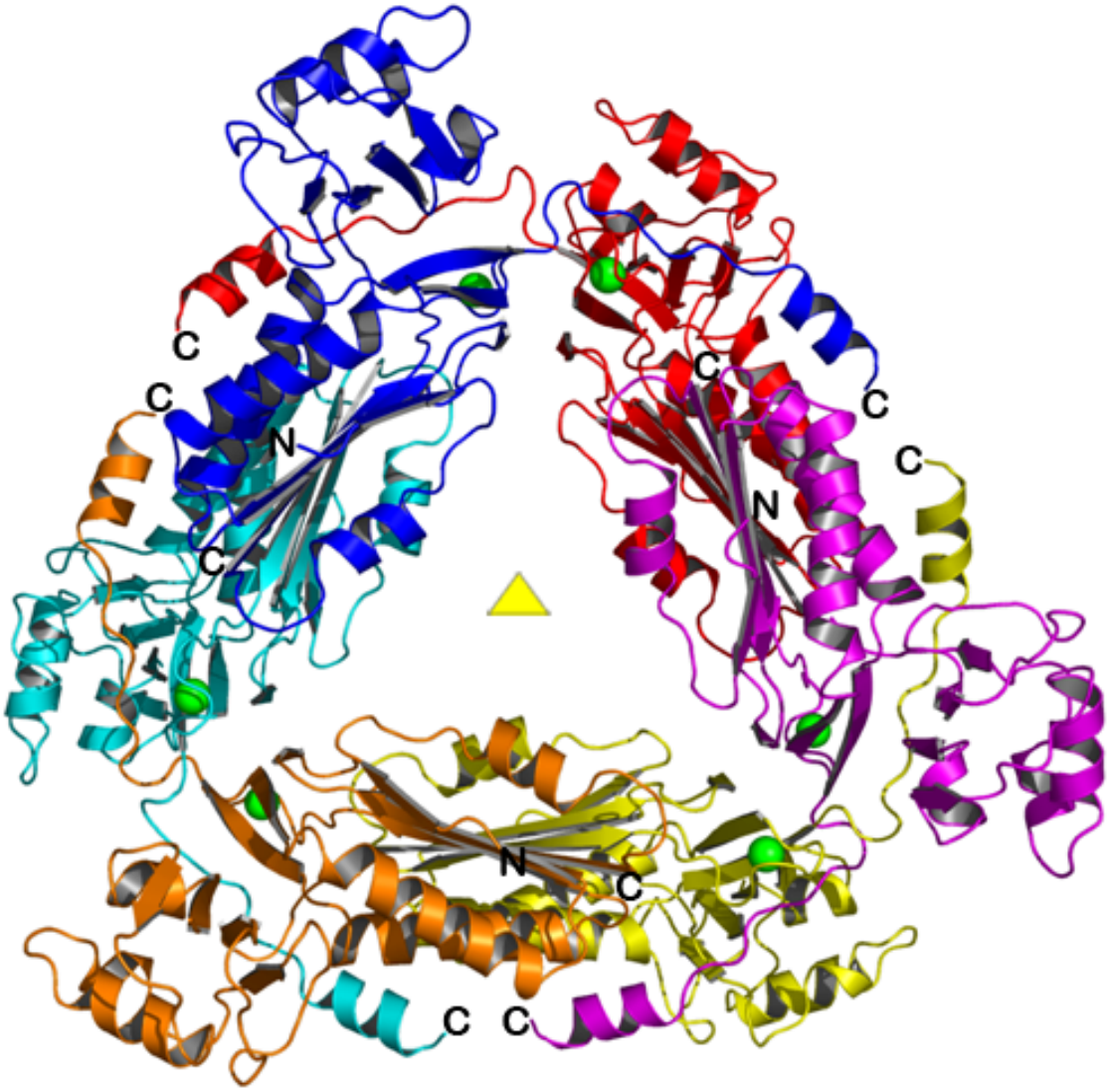

Figure 3.7: Ribbon representation of the structure of *V. cholerae* MPT synthase trimer of heterotetramers present in the asymmetric unit of the P321 crystals. The crystallographic threefold axis of symmetry is indicated by a *yellow* triangle. All MoaE subunits domain swap their C-termini with neighboring MoaE subunits. In this structure Ca^{2+} (*green* spheres) ions were identified in all MoaE β2-β3 loops. Each heterodimer is colored *orange*, *yellow*, *magenta*, *red*, *blue*, and *cyan*.

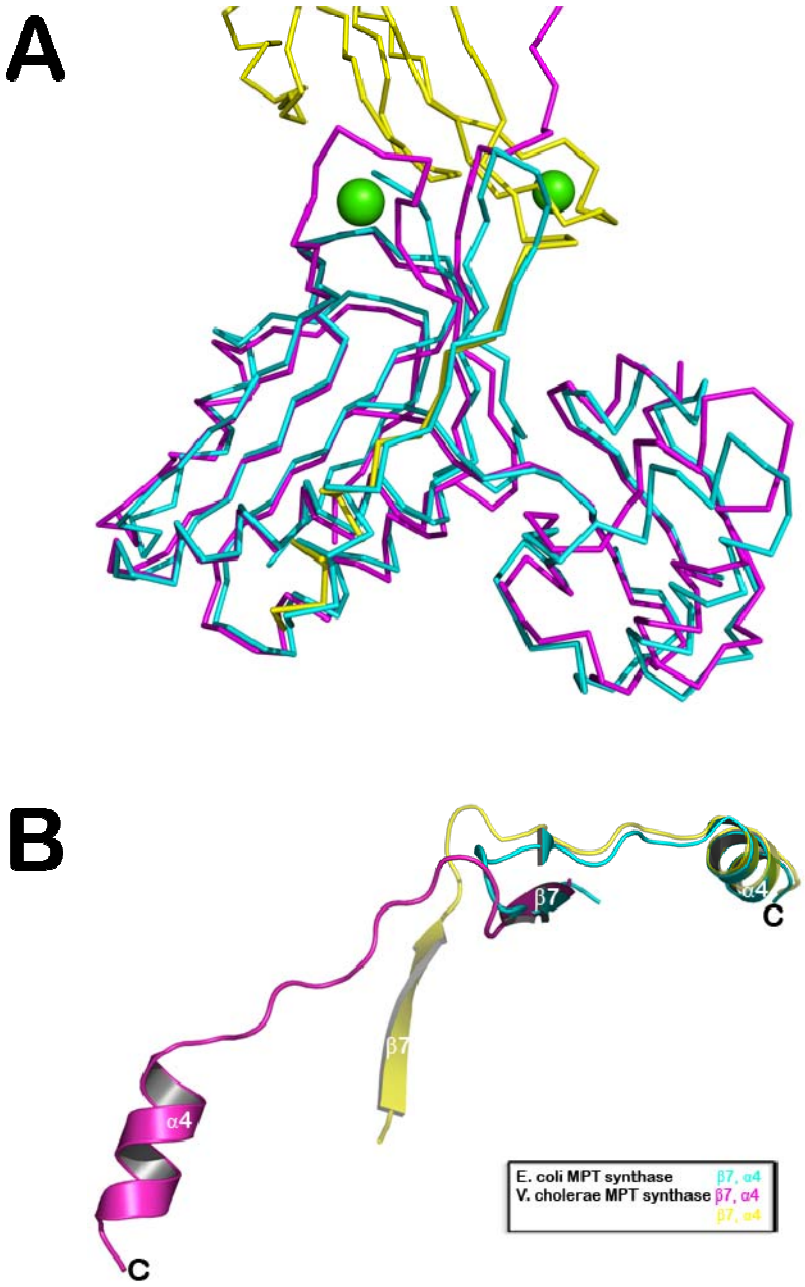

Figure 3.8: Comparison of the *V. cholerae* and *E. coli* MPT synthase. (**a**) Superposition of *E. coli* (cyan) and *V. cholerae* MPT synthases (magenta and yellow). (**b**) Conformational change in the C-terminal region of MoaE with the domain swapped conformation in *yellow* and *magenta* (for the two adjacent MoaE monomers) and the non-swapped conformation *E. coli* MPT synthase in *cyan*.

that consist of a mixture of hydrophobic and hydrophilic contacts that help to form the heterododecamer. These interactions are made possible by a rearrangement of the Glu127 – Trp149 residues, which cross over from their own subunit to an adjacent subunit. As a consequence, domain swapping of the C-terminal region occurs in all *V. cholerae* MPT synthase structures. The swap of the C-terminal residues could be unambiguously identified from an inspection of the unbiased electron density for residues of MoaE 131 to 138, which form the hinge loop prior to the last α-helix in the MoaE subunit. These residues adopt a different conformation compared to the *E. coli* enzyme (Fig. 3.8b) and allow the C-terminal helix to interact with the core of the MoaE subunit of the adjacent heterodimer in exactly the same orientation as in the non-domain swapped *E. coli* MPT synthase counterpart when they are compared.

E. Metal ion binding loop

In the P321 structure of *V. cholerae* MPT synthase, we identified a metal ion in the MoaE loop region between β2 and β3 (Val37-Asn45), shown in figure 3.9. The bound metal most likely is a Ca^{2+} ion, which is coordinated by the side chain carboxylate oxygens of Asp39 and Asp44, the main chain carbonyl group of Val46 and a water molecule. The average oxygen-metal distance is approximately 2.4 Å and the metal is coordinated with octahedral geometry. However, no electron denstiy was found near this loop in the $C222_1$ crystals of *V. cholerae* (*h*VCMPTS) MPT synthase, even though the crystallization conditions contained Mg^{2+} ions. Additionally, the loop conformation was not altered in comparison to the loop structure determined from crystals grown in the presence of calcium. In all previous structures of MPT synthase from *E. coli* (PDB entries 1NVI and 1FM0) this loop region is disordered, but it is also ordered in the apo-structure of *S. aureus* MPT synthase and in its complex with precursor Z. The *V. cholerae* MPT

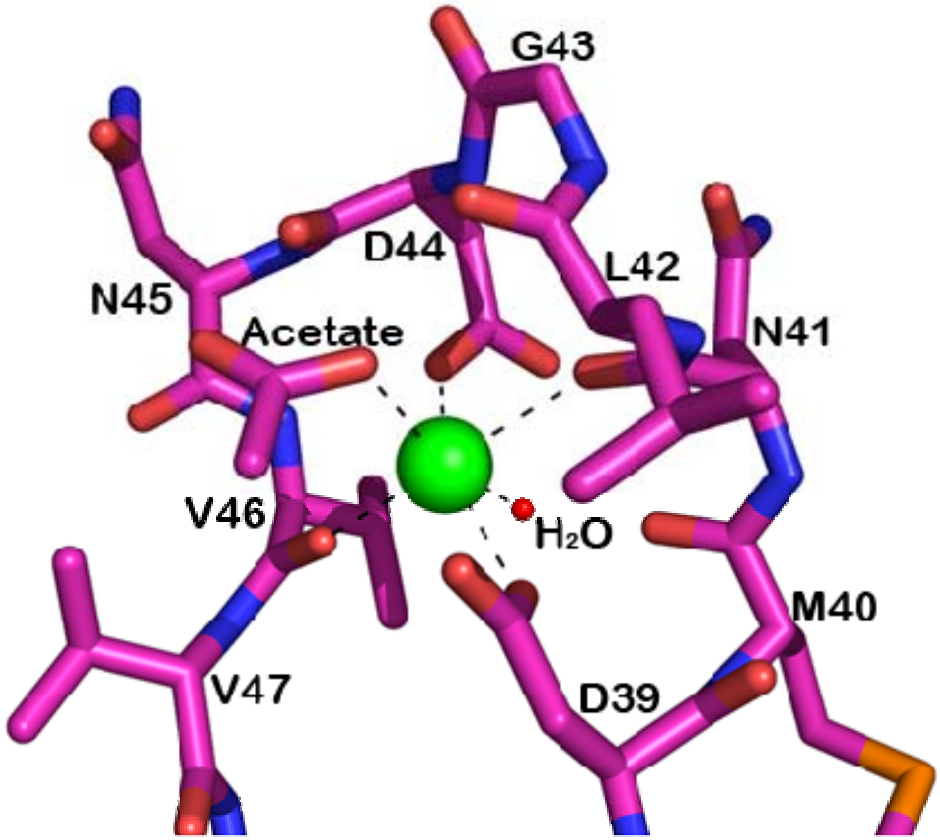

Figure 3.9: Close up view of the β2-β3 loop in one MoaE subunit. Dashed lines indicate the coordination of the bound Ca^{2+} (shown as a *green* sphere) by MoaE loop residues in all bonds representation (*magenta*).

synthase active site is further enclosed by Arg134 found on the C-terminus when it is compared to *E. coli* MPT synthase where the loop was disordered (Fig. 3.10) and *S. aurues* MPT synthase where the C-terminus was disordered (Fig. 2.6b).

F. Molecular weight determination using analytical size exclusion chromatography

To test whether *V. cholerae* MPT synthase exists in solution in the crystallographically observed heterododecameric state, its oligomerization state was studied using analytical size exclusion chromatography (Fig. 3.11). The protein sample *a*K125A was applied to a column equilibrated with 50 mM Tris/HCl, pH 8.0, and 50 mM NaCl from which it eluted in a single peak, 14 mL after injection. Surprisingly, after adjusting the pH to 7 in the presence of at least 50 mM Ca-acetate *V. cholerae* MPT synthase predominantly eluted after 12 mL with a smaller peak running at 14 mL; increasing the Ca-acetate concentration to 200 mM led to an increase of the peak at 12 mL. At a significantly smaller Ca-acetate concentration of 2 mM only the peak at 14 mL could be detected. If the pH was either increased to 8 or decreased to 6, the larger peak could not be observed. With the aid of molecular weight standards the peaks at 14 and 12 mL were determined to correspond to molecular weights of 50 kDa and 150 kDa, respectively, and hence either represent a heterotetrameric (50 kDa) or heterododecameric (150 kDa) oligomer of the enzyme.

G. Significance of the oligomer and the Ca^{2+} binding site in the β2-β3 loop

The oligomer discovered in our structures has not been reported in any of the other *E. coli* or *S. aureus* crystal structures of MPT synthase. In all published structures of *E. coli* MPT synthase, the β2-β3 loop, corresponding to residues 39 to 46 is disordered, whereas it is ordered in the apo-form of *S. aureus* MPT synthase and in its complex with

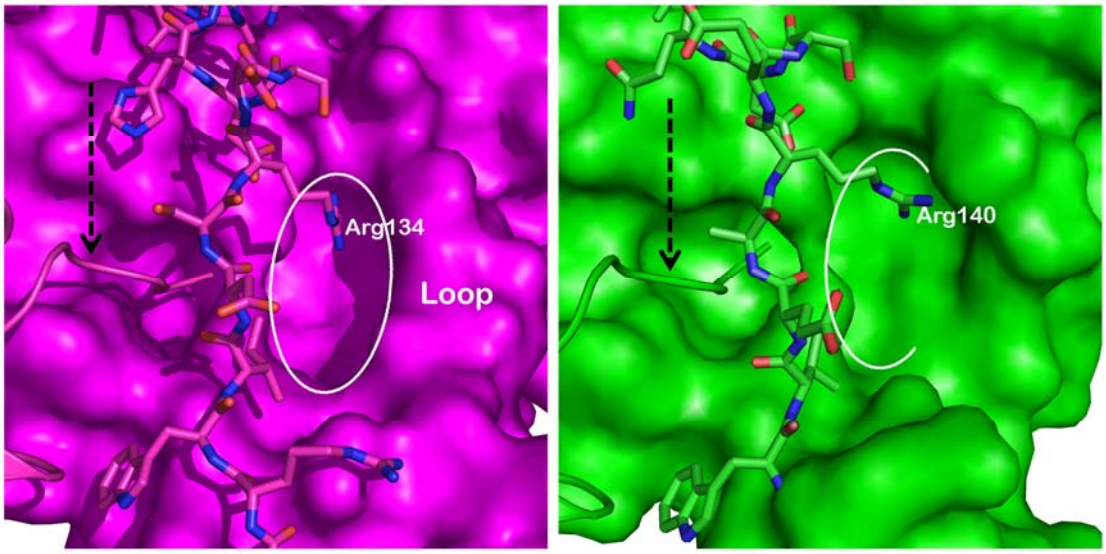

Figure 3.10: Comparison of the surface representations of *V. cholerae* and *E. coli* MoaE (*magenta* and *green*, respectively) adjacent to the active site loop region. The all bonds representation corresponds to the C-terminus of MoaE which undergoes the domain swap in *V. cholerae* MPT synthase. A defined pocket is present in the *V. cholerae* enzyme where the substrate precursor Z would bind (left panel). In the *E. coli* MoaE surface representation (right panel), the cavity is open and solvent accessible. The MoaE cavity is highlighted by a white circle and the MoaD C-terminus is highlighted by a dashed arrow.

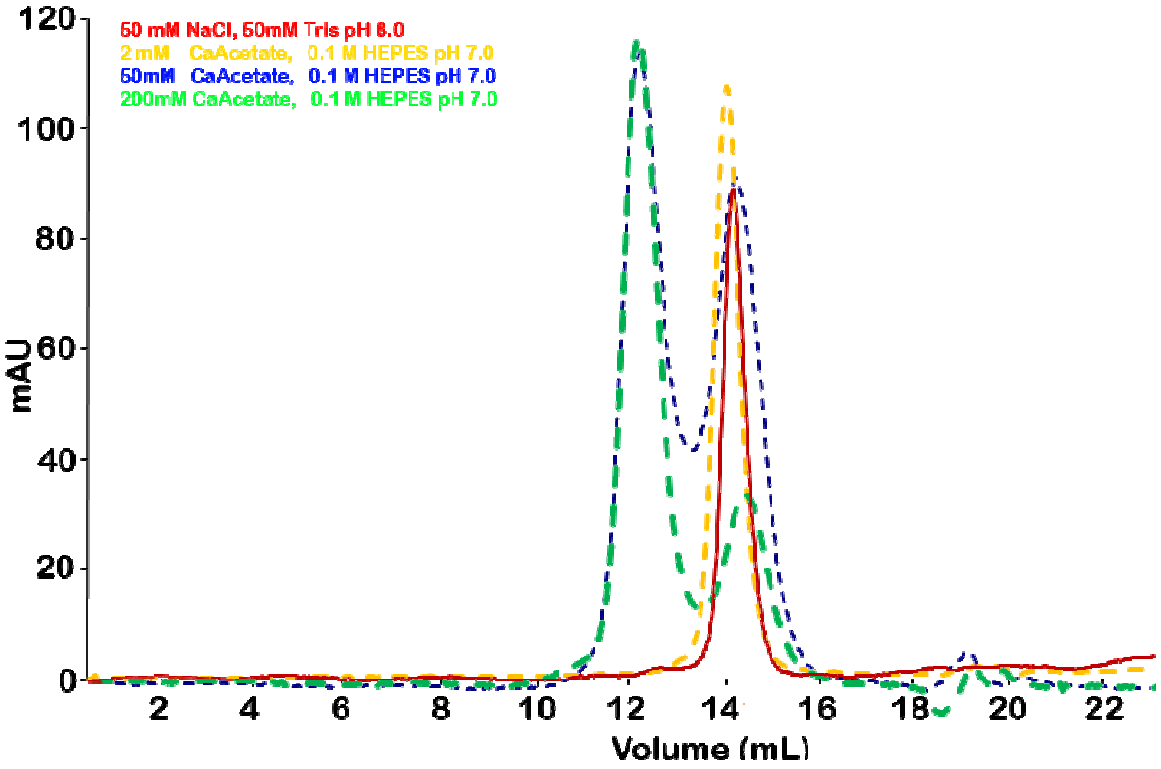

Figure 3.11: Analytical size exclusion chromatography of *V. cholerae* MPT synthase. The column was equilibrated with (**1**) 50 mM Tris/HCl, pH 8.0, 50 mM NaCl (*red*), (**2**) 50 mM HEPES, pH 7.0, 2 mM Ca-acetate (*yellow*), (**3**) 50 mM HEPES, pH 7.0, 50 mM Ca-acetate (*blue*) and (**4**) 50 mM HEPES, pH 7.0, 200 mM Ca-acetate (*green*) and MPT synthase samples in its original buffer were applied to each column.

precursor Z. The residues in this loop are partially conserved in various organisms with either of the residues glutamine, glutamate, aspartate and asparagine at position 39 of *E. coli* and *V. cholerae* MoaE. Other highly conserved residues in this loop include Arg38 and Gly43; Arg38 interacts with the pterin ring of precursor Z (as revealed by the co-crystal structure of the *S. aureus* enzyme with MPT) and Gly 43 based on the various structures (loop disorder in *E. coli*, *S. aureus* loop movement, *V. cholerae* expanded loop width) seems to provide structural flexibility.

Investigation of the residues near the C-terminal region of MPT synthase, the site where the actual domain swap occurs, showed that *E. coli* MPT synthase contains a proline at position 131 whereas there is a threonine at the corresponding position 130 of *V. cholerae* and a Glu at the corresponding position 128 of *S. aureus* MPT synthase (Fig. 3.12a). Pro131 is at the i+1 position of a β-turn linking β7 and β8 of *E. coli* MPT synthase, which adopts a trans-peptide. Interestingly, this proline is absent from the MoaE subunit of many other MPT synthase proteins, including *V. cholerae* MPT synthase and *S. aureus* MPT synthase. Consistent with this hypothesis, *S. aureus* MPT synthase, exhibits larger oligomeric states which eluted early from size exclusion chromatography columns (Fig. 2.3) presumably due to domain swapping. The lack of a domain swapped *S. aureus* MPT synthase may be due to the fact that the crystallization condition did not contain Ca^{2+} which seems to cause domain swapping. The rigid nature of the proline found in the *E. coli* MoaE hinge region may make it difficult for the C-terminal region of *E. coli* MPT synthase to form the domain swapped conformation. Upon binding of a divalent cation to the β2-β3 loop, its altered conformation may influence the position of the C-terminal α-helix due to steric hindrance, since the β2-β3 loop is very close to the residues of the C-terminus (Fig. 3.12b). The indicated 3 Å distance has been measured between Val36 carbonyl and the methyl group of Thr129.

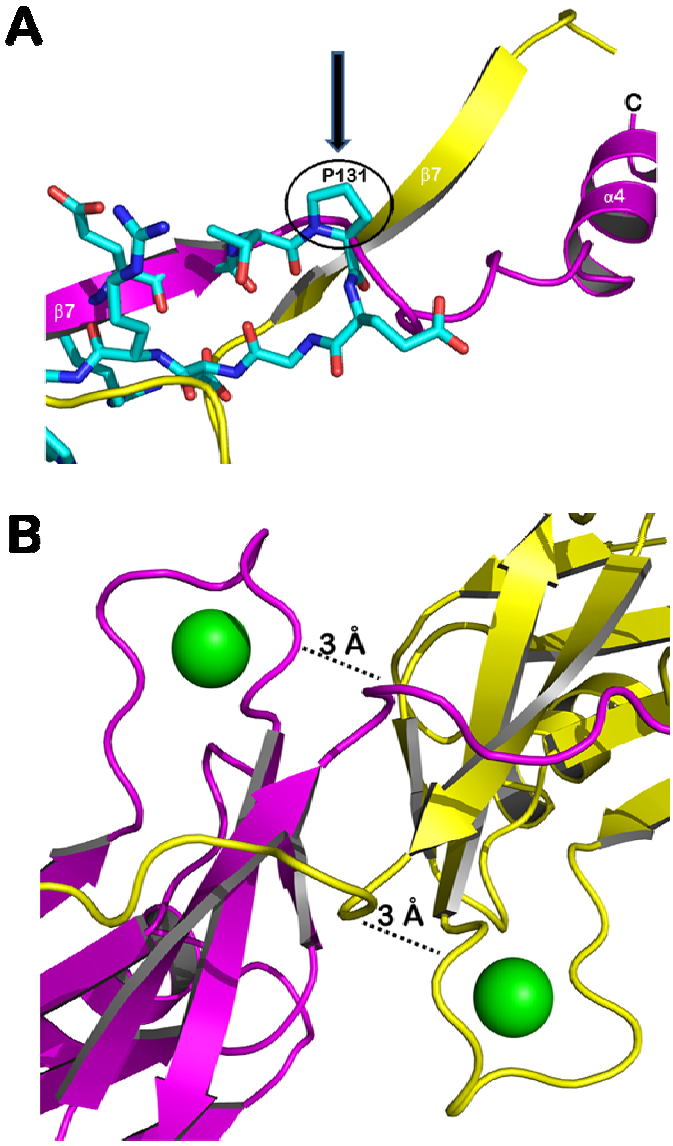

Figure 3.12: Factors promoting domain swapping in *V. cholerae* MPT synthase. (**a**) Superposition of the *E. coli* MoaE (*cyan*) and *V. cholerae* MoaE C-terminal regions (*yellow* and *magenta*). The proline at the i+1 position of the β-turn hinge region following β7 in the *E. coli* MoaE structure is highlighted. *E. coli* MoaE is one of few species exhibiting a proline at this position. (**b**) Ribbon diagram of Ca^{2+} binding region and C-terminal domain swapped region showing the close proximity of these two structural features

Binding of cations to this loop is pH dependent and thus is probably influenced by the protonation state of the charged residues coordinating the cation. Calcium binding to the 40-loop stabilizes the loop that may force the adjacent switch region loop to adopt a lesser sterically hindered conformation, therefore relieving the hinderance by adopting a C-terminal domain swap.

The calcium ion in all the *V. cholerae* K125A structures appears to help stabilize the β2-β3 loop through interactions with acidic residues and main chain atoms present in this loop. In the crystallization conditions of the *E. coli* MPT synthase and *S. aureus* MPT synthase the mother liquor did not contain any divalent cations in solution, such as Mg^{2+} or $Ca^{2+}$and hence the absence of a divalent cation in the structure is not surprising.

H. Attempts to visualize the hemisulfurated intermediate (*a*K125Aint-1)

The crystals derived from the intermediate loaded protein grew at all temperatures under aerobic conditions; however, the best crystals only diffracted X-rays up to ~2.9Å. These crystals belong to the monoclinic $P2_1$ space group with unit cell dimensions of a = 93.6 Å, b = 142.3 Å, c = 95.9 Å and β= 119.2° containing two heterotrimers and one heterotetramer in the asymmetric unit. Like the other *V. cholerae* MPT synthases, this structure also showed the domain swapped conformation, however, two of the six MoaD subunits did not exhibit electron density at all, while one MoaD subunit displayed only very weak electron density (Fig. 3.13). Most importantly, despite the presence of the intermediate in the protein sample used for crystallization the resulting structure showed no extra density in the active site which could be attributed to this intermediate.

The sub-stoichiometric complexes present in these crystals have never been observed, normally all subunits of the MPT synthase are found interacting in the manner

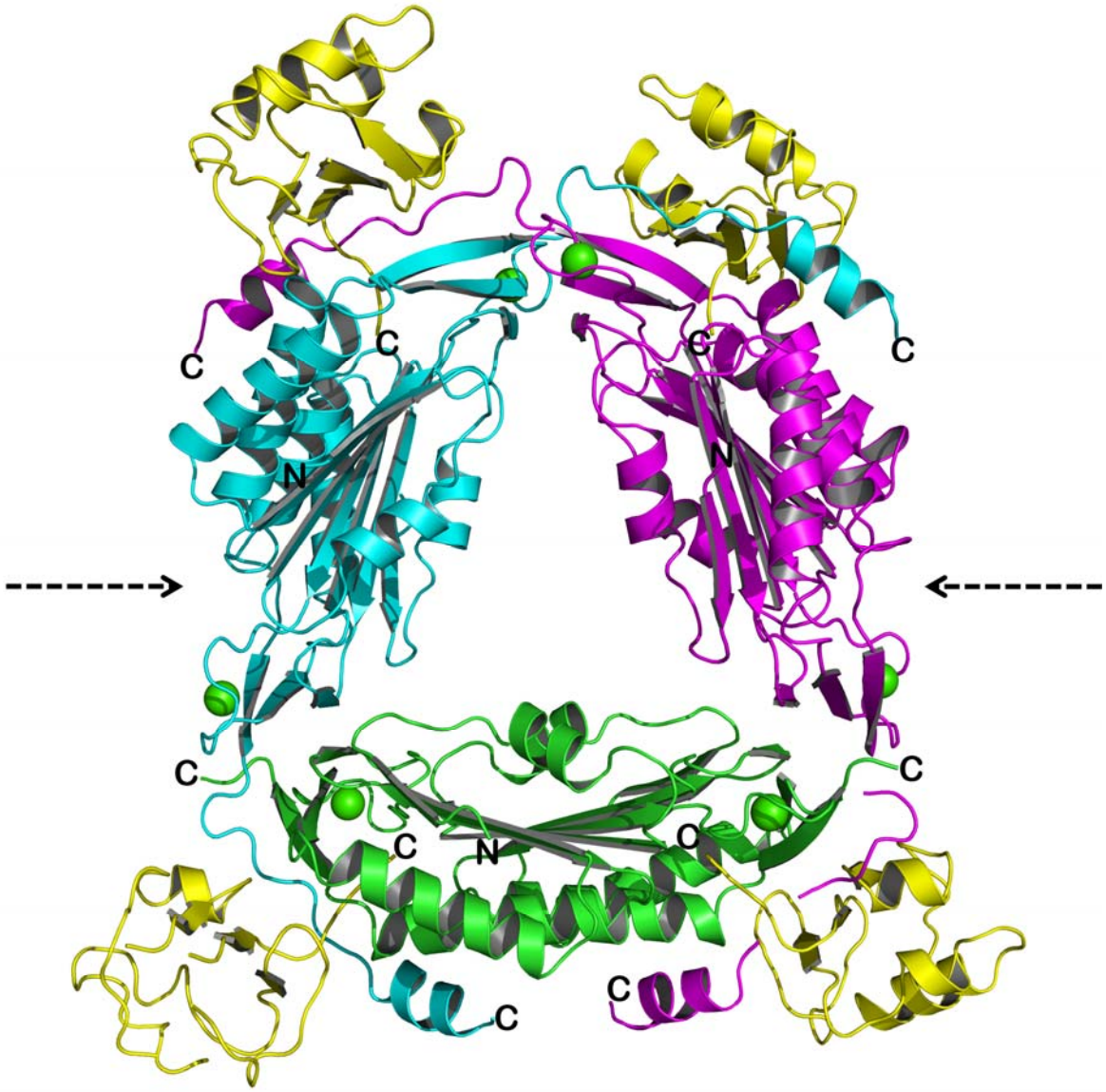

Figure 3.13: Ribbon representation of *V. cholerae* MPT synthase (*a*K125Aint-1) from crystals grown aerobically. MoaE subunits in *cyan*, *magenta* and *green*. MoaD subunits in *yellow*. Calcium atoms are depicted as *green* spheres. Dashed arrows indicate position of "missing" MoaD subunits from the normal MoaE-MoaD heterotetramer. The missing subunit results in the MoaE "only" part on a hetero*trimer*.

described in Chapter 1, in which a MoaE dimer interacts with two individual MoaD subunits. The structure of the K125A variant of *V. cholerae* MPT synthase revealed an unexpected subunit composition, in this case one MoaD and the central MoaE dimer could be located.

The absence of an intermediate from the active site led us to conclude that the MoaE K125A variant in combination with the thiocarboxylated MoaD is still able to act on the intermediate to form the product, molybdopterin, which then dissociates from the active site. Alternatively, the aerobic conditions combined with incubation at room temperature might have degraded the intermediate. To help minimize degradation of the hemisulfurated intermediate our next attempts were performed in an anaerobic tent (< 10 ppm O_2). In this environment the temperature cannot be controlled; it is slightly above room temperature but fluctuates depending on the surrounding laboratory temperature. The quality of crystals grown in this environment was generally rather poor with the best crystal diffracting only to 3.3 Å. This crystal had the same unit cell dimensions as the aerobic crystals. Assessment of this structure also showed weak or a total lack of density for three of the six MoaD subunits (Fig. 3.14). In addition density of the C-terminal helix of every MoaE subunit was significantly less well-defined. Inspection of all six active sites again did not reveal any new density, but unexpectedly an extra density was found near the interface of the heterotetramers. This feature is located in the interface between α-helix 3 of both MoaE subunits within each dimer, and was strongest in the I- and J-subunits of MoaE (*magenta* in Fig. 3.14). The position of this density is surprising; the

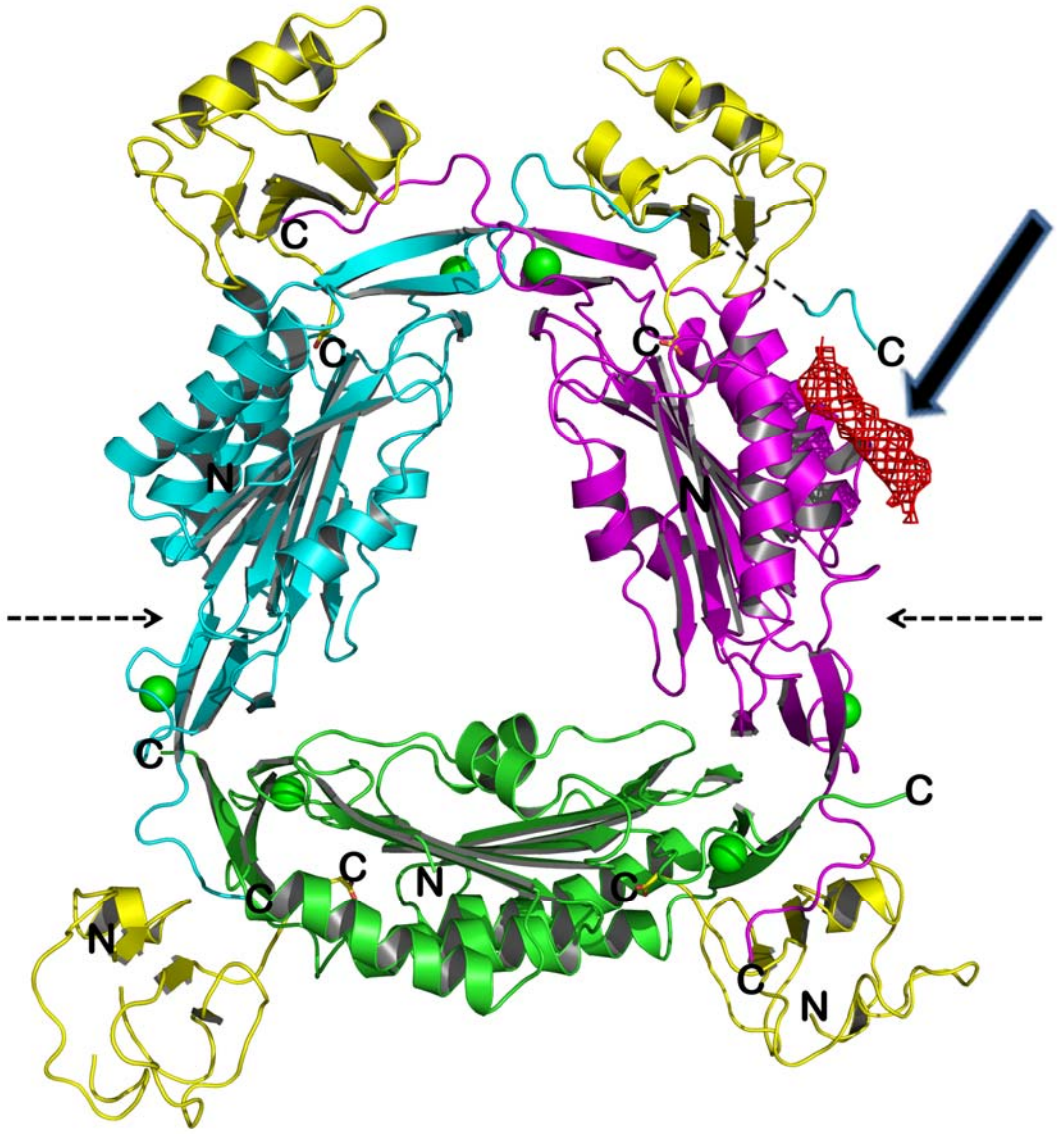

Figure 3.14: Ribbon representation of the 3.3 Å *V. cholerae* MPT synthase (*a*K125Aint-1) structure showing the unusual electron density. This difference density, indicated by large arrow, is shown here at a contour level of 2.5σ. All MoaD subunits are colored *yellow* and (dashed arrows indicate position of missing MoaD from the normal MoaE-MoaD heterotetramer, resulting in the MoaE "only" part on a hetero*trimer*) the three MoaE dimers are colored in *green*, *cyan* and *magenta*. The crystals used to determine this structure were grown under anaerobic conditions.

surrounding residues are primarily negatively charged, such as Glu111 and Asp115, but also include Asn104 (Fig. 3.15a, top). When the surrounding symmetry related molecules are generated, this density sits sandwiched between two hetero-trimers (Fig. 3.15a, bottom). The density is present on the surface of the heterotetramer and displays an elongated shape with a length of 14 Å.

Attempts to model this density feature with the intermediate or a related molecule were unsuccessful, primarily because of the elongated nature of the density (Fig. 3.15b, top and bottom), although the elongated oxidized form was the closest fit. The surrounding Glu, Asp and Asn residues individually could interact with the pterin moiety of the intermediate as demonstrated by the crystal structure with precursor Z and its interaction with Glu 125 of *S. aureus* MoaE, however, the overall negative charge would be counterproductive for binding the negatively charged intermediate. An inspection of the mother liquor composition reveals no molecules, which could explain this density, however, the fact that there is considerable disorder in the protein subunits leaves open the possibility that this feature corresponds to a region within a disordered segment of the polypeptide chain. As a biochemical approach to identify whether these crystals contain intermediate or molybdopterin, a Form A analysis was performed. The oxidative derivatives of the intermediate or molybdopterin generated by this assay can be identified after reverse-phase HPLC chromatography. Although multiple crystals were harvested and used in this test, no signal for the derivative of either the intermediate or molybdopterin could be detected (data not shown).

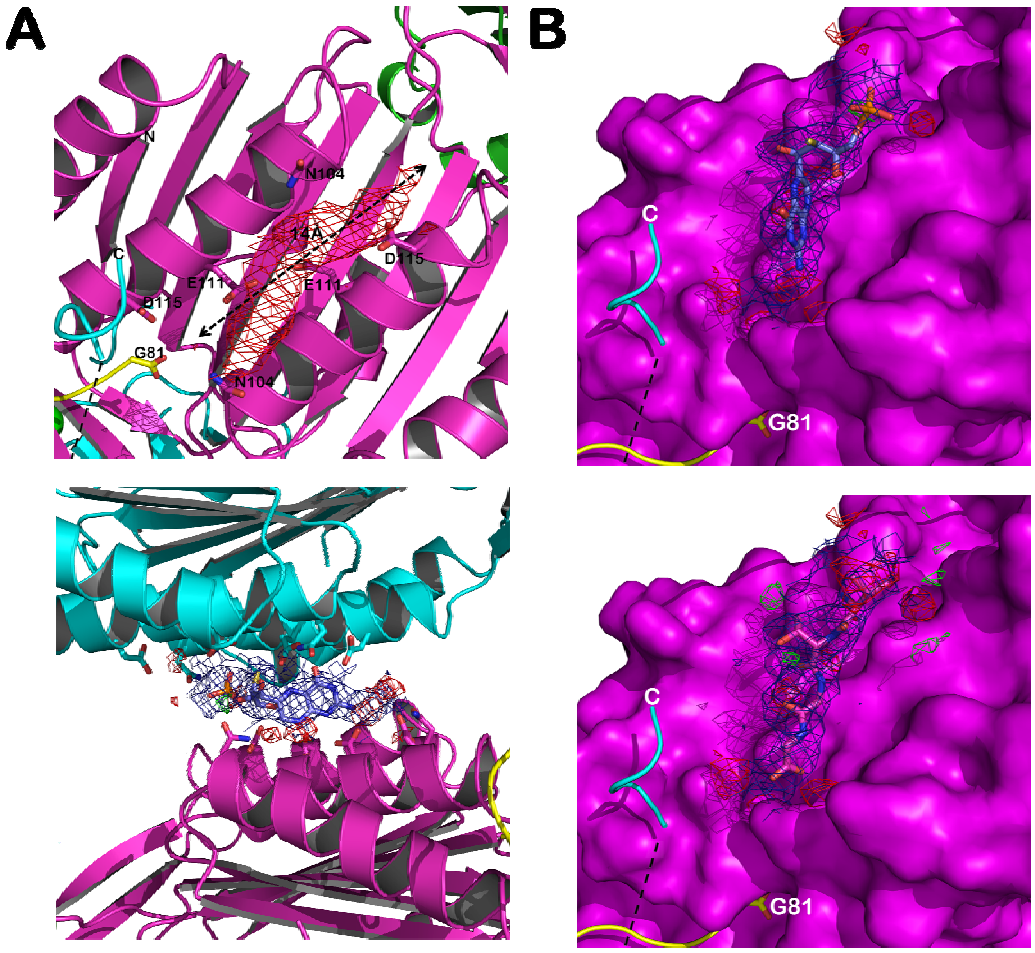

Figure 3.15: Close-up view of density at the surface of one of the heterotetramers found in the 3.3 Å MPT synthase structure (*a*K125Aint-1). (**a**) (Top) Close-up view of the density with the surrounding residues labeled. The length of this elongated density is approximately 14 Å. (Bottom) Generating the symmetry related subunits reveals the density sits sandwiched between two subunits. (**b**) 2Fo-Fc (*blue* mesh), positive Fo-Fc (contour level of 3.0σ, *red* mesh) and negative Fo-Fc electron density (contour level of 3.0σ, *green* mesh) are displayed. (Top) The electron densities from the linear oxidized version of MPT are compared with a tetrapeptide with the sequence of VTGG (Bottom).

Finally, crystallization attempts were setup anaerobically, in which the trays were sealed in airtight plastic bags and placed in incubators at defined temperatures. This technique improved the quality of crystals, yielding data to 2.4 Å (Table 3.3 for *a*K125Aint-2) the best resolution of all *V. cholerae* MPT synthase structures so far. These crystals belong to the orthorhombic $C2_12_1\,2_1$ space group with unit cell dimension of a = 93.3 Å, b = 168.0 Å, c = 142.2 Å and contain one heterotrimer ($MoaE_2$-MoaD) and one heterodimer (MoaE-MoaD) in the asymmetric unit. Also in this crystal form MPT synthase from *V. cholerae* displays the domain swapped form observed in all of its other crystal forms. Upon application of the relevant crystallographic symmetry operations it exhibits two heterotrimers and one heterotetramer similar to the $P2_1$ structure (Fig. 3.16). Unfortunately, further inspections failed to show additional electron density in the active site of any the MoaE subunits, and, in contrast to the *a*K125Aint-1 structure, it did not display the density feature found on the surface, which at the higher resolution of 2.4 Å might have been more easily interpreted.

A general observation that can be derived from all three structures derived from material that contained the intermediate is the sub-stoichiometric presence of MoaD subunits. This could indicate that the substrate was turned over and that its release is coupled to the dissociation of the discharged MoaD subunits after they transferred their thiocarboxylate sulfur onto the intermediate. In this respect the crystal structures reproduce what is biochemically expected to occur following completion of molybopterin synthesis.

I. Conclusion

Although the major goal of this chapter was to further understanding of the second sulfur transfer step by co-crystallizing a MPT synthase-intermediate complex, the venture has led to the discovery of a possible new oligomeric state of MPT synthase, although biochemical studies are needed for understanding the significance of divalent cation binding. A comparison between the MoaE and MoaD subunits provides some insight into the interplay between these subunits, which will be described in the next chapter. The crystallization of this protein is predictable and simple to perform due to the structural role the Ca^{2+} or Mg^{2+} seems to carry out. Since the crystallization step is a major bottleneck in general protein crystallography continued structural and biochemical studies should be performed to enhance the chances of a MPT synthase intermediate co-crystal complex. This should lead to a significantly more detailed understanding of this family of sulfur transferases.

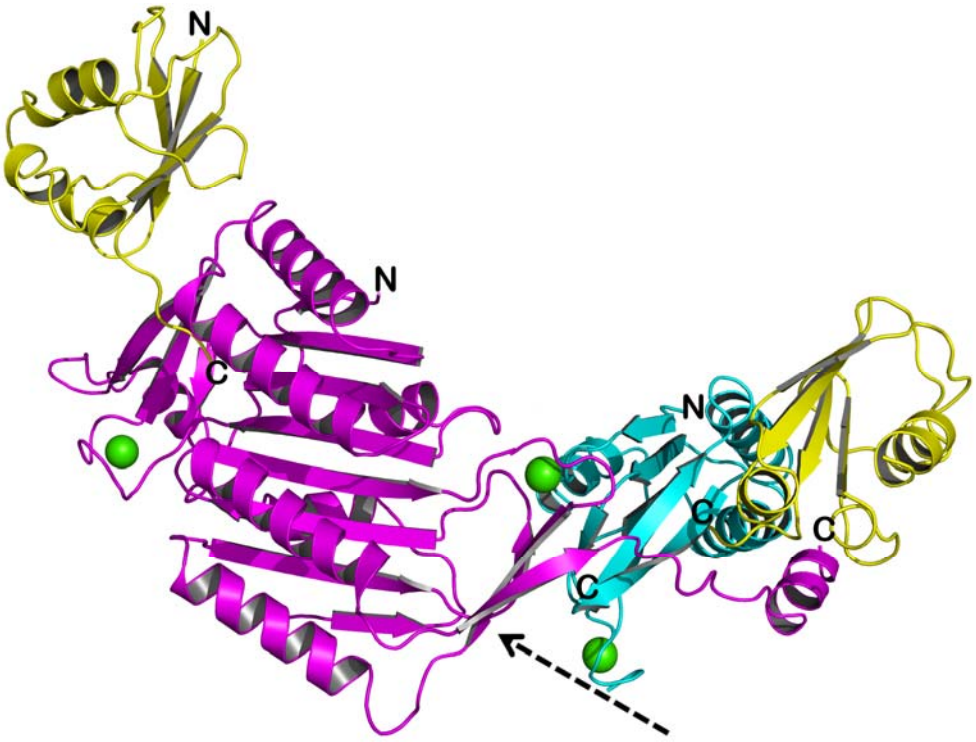

Figure 3.16: Ribbon representation of *V. cholerae* MPT synthase (*a*K125Aint-2) from crystals grown anaerobically in a sealed bag. MoaE subunits are shown in *cyan* (one subunit) and *magenta* (two subunits) with MoaD subunits in *yellow* (the dashed arrow indicates the position of the missing MoaD from the normal MoaE-MoaD heterotetramer resulting in a hetero*trimer*). Calcium ions are depicted as *green* spheres.

Chapter 3

Comparisons of the *S. aureus*, *V. cholerae* and *E. coli* MPT synthase Crystal Structures

I. Introduction

Since the first MPT synthase crystal structure was solved in 2001 by Rudolph et al [36], studies have continued to enhance our understanding of the role of MPT synthase in both its biosynthesis activity and the etiology of Moco deficiency. The structures of MPT synthase from *S. aureus* and *V. cholerae* described here significantly extend the set of available models of this enzyme and these data can be mined to further our understanding of this enzyme. The previous chapters describe six new and different structures, one structure in complex with substrate, and five apo-structures. Together they define the substrate-binding pocket in considerably more detail than what was visualized for the *E. coli* enzyme. The *V. cholerae* structures also reveal that the C-terminal helix and the preceding loop can participate in a domain-swapped oligomeric form of the enzyme. This oligomer is created by the arrangement of three $MoaD_2MoaE_2$ heterotetramers around a central three-fold axis of symmetry giving rise to a heterododecamer displaying D_3 symmetry. Finally, in all *V. cholerae* structures which were grown in the presence of the hemisulfurated intermediate, the standard 1:1 stoichiometry of MoaD and MoaE subunits is altered; within the heterododecamer two MoaD subunits do not show any density and a third is only very weakly defined.

To provide more structural understanding, a comparison of all structures following their superposition was undertaken and the results were analyzed in the context of multiple sequence alignments for the MoaD and MoaE subunits. From an analysis of the sequence alignments it is immediately apparent that selected residues in MoaD and MoaE show a high level of sequence conservation across various species (Fig. 4.1 and 4.2). The

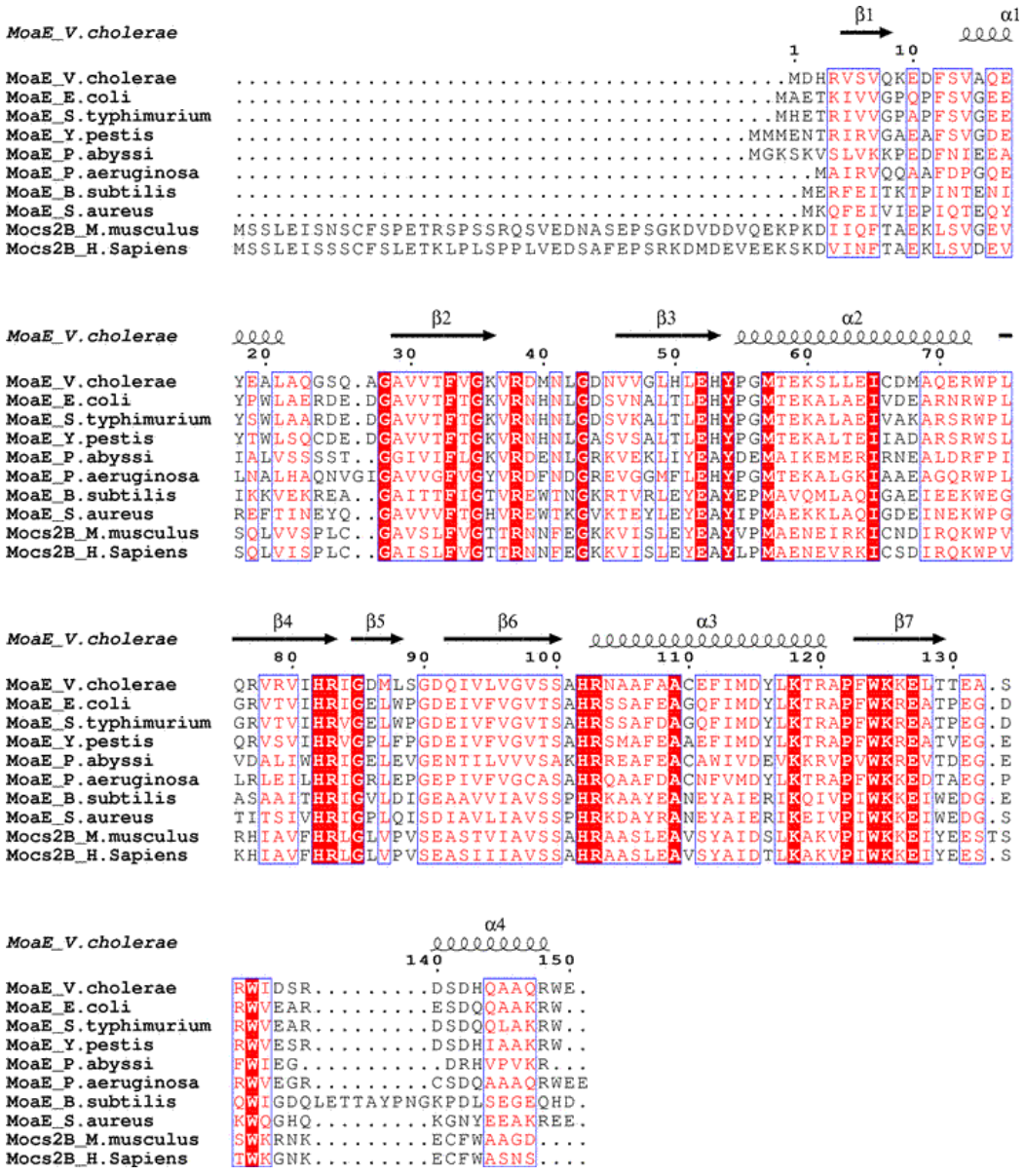

Figure 4.1: MoaE multiple sequence alignment. The top line features the secondary structure of the *V. cholerae* MoaE subunits. Residues highlighted in *red* are strictly conserved and those printed in *red* are partially conserved. *E. coli* numbering is ahead by one relative to the *V. cholerae* numbering and ahead by two relative to *S. aureus* numbering.

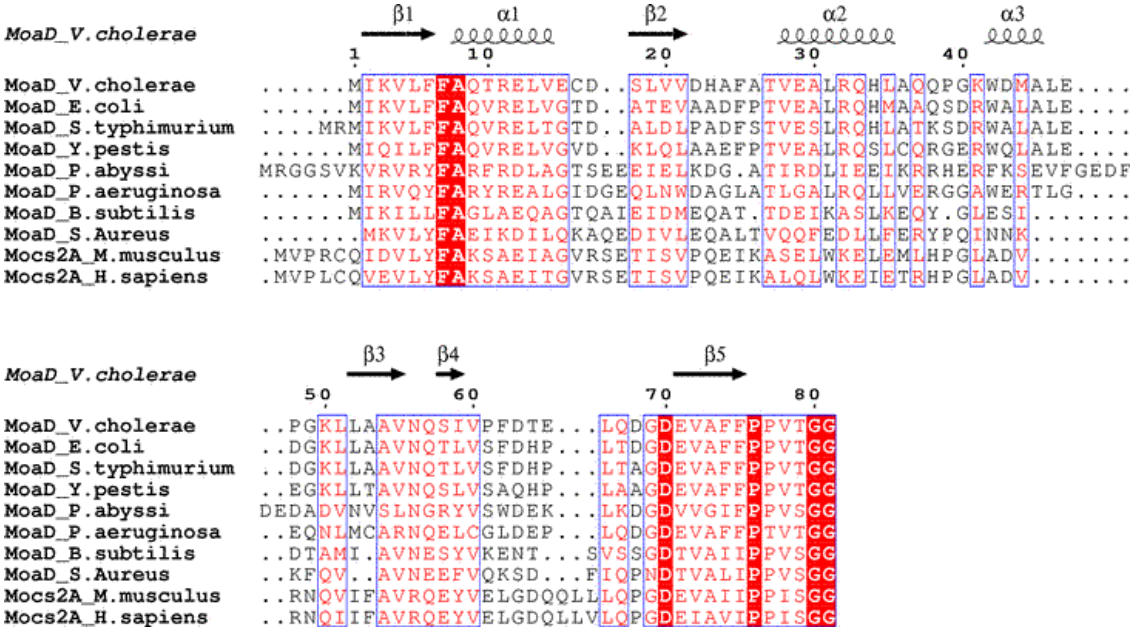

Figure 4.2: MoaD multiple sequence alignment. The top line features the secondary structure of the *V. cholerae* MoaD subunits. Residues highlighted in *red* are strictly conserved and those printed in *red* are partially conserved. *E. coli* numbering is the same as *V. cholerae* MoaD numbering while *S. aureus* numbering is three less than *E. coli* numbering.

MoaE subunit, is characterized by a higher level of conservation and identical residues are distributed across almost the entire length of the subunit with the exception of the ~30 N-terminal and ~15 C-terminal residues. Among the sequences included in the alignment there are 21 identical residues out of ~150 residues, so roughly one out of seven residues is invariant. In contrast MoaD contains only six invariant out of ~80 residues total, roughly one out of every 13 residues of which four are at the C-terminus including the Gly-Gly motif representing the last two residues. The remaining two conserved residues are near the N-terminus at the transition between the first β-strand and first α-helix and play important structural roles. In addition MoaD exhibits broad structural homology to proteins found in other biosynthetic pathways such as ThiS, the S-carrier involved in thiamin biosyntheis and ubiquitin as well as the related protein modifiers NEDD8 and SUMO. The C-terminal tail is essential in either of these two general functions: (1) During Moco and thiamine biosynthesis it gets activated in an ATP-dependent reaction followed by its conversion to a thiocarboxylate which then acts as the S-donor. (2) Ubiquitin and related protein modifiers are also activated in an ATP-dependent reaction and the activating enzymes are in fact related not only in structure but also in their primary sequence. Activated ubiquitin/SUMO/NEDD8 are then transferred onto target proteins where they elicit various biological responses [102,103].

Although the initial goal of the work described in Chapter 2 was to determine the co-crystal structure of MPT synthase in complex with the hemisulfurated intermediate, the resulting crystal structures containing MPT synthase hetero*trimers* and

heterotetramers, has unexpectedly provided details of the interplay between the MoaE and MoaD subunits.

II. Method

A. Structural comparison of MPT synthases by superposition using O

The PDB files for the structures solved in the previous chapters were read into the model building and analysis program O, and each structure was given an appropriate identifying molecule name. The structures were all superimposed onto the subunit of the complex with the lowest B factor for precursor Z (chain identifiers A for MoaE and B for MoaD). When necessary the biologically significant heterotetramer was generated and used in the superimposition. While leaving the structure for the MPT synthase precursor Z complex stationary, all other structures were manipulated using the commands LSQ-E, LSQ-I and LSQ-M to run the initial superimpositions calculations, then to improve these calculations by alignment and lastly to apply these calculations directly, which "moves" coordinates to their new position for visualization.

II. Discussion

A. Assessment of conserved residues found throughout MPT synthase structures

i. MoaE β2 strand

The β2 strand region, from Gly29-Gly44 (residue numbers refer to *E. coli* MPT synthase), contains four strictly conserved residues, Gly29, Phe34, Gly36, Arg39 and Gly44. This region harbors the active site loop, which is disordered in *E. coli* MPT synthase and undergoes conformational changes in the other structures. An initial inspection of this region in the *S. aureus* apo-structure could not explain the importance of Gly29 and Gly36. However, our precursor Z complex of the *S. aureus* MPT synthase shows that the Cα atom of Gly29 is 3.6 Å away from the substrate in *S. aureus* and would be at the same distance when the substrate is modeled into *E. coli* or *V. cholerae* MPT synthase. On the other end of the β2 strand, Gly36 is also in close proximity of precursor Z, in this case it is 4.4 Å away. If these residues were replaced with an alanine, the next biggest side chain, the distances between the substrate and the respective side chain Cβ atom were reduced to approximately 1.6 Å in case of residue 29, and to 2.4 Å at position 36. This analysis demonstrates that the strictly conserved glycines at these positions are the only residues able to accommodate the bound substrate (Fig. 4.3a). The β2-β3 or substrate-binding loop from all MoaE subunits in the *V. cholerae* and *S. aureus* structures show great flexibility in its conformation (Fig. 4.3b). The end of this loop includes the strictly resides conserved Gly44, which could be necessary to increase the flexibility of this loop; its main chain conformation is characterized by dihedral angles of ϕ=~-100°

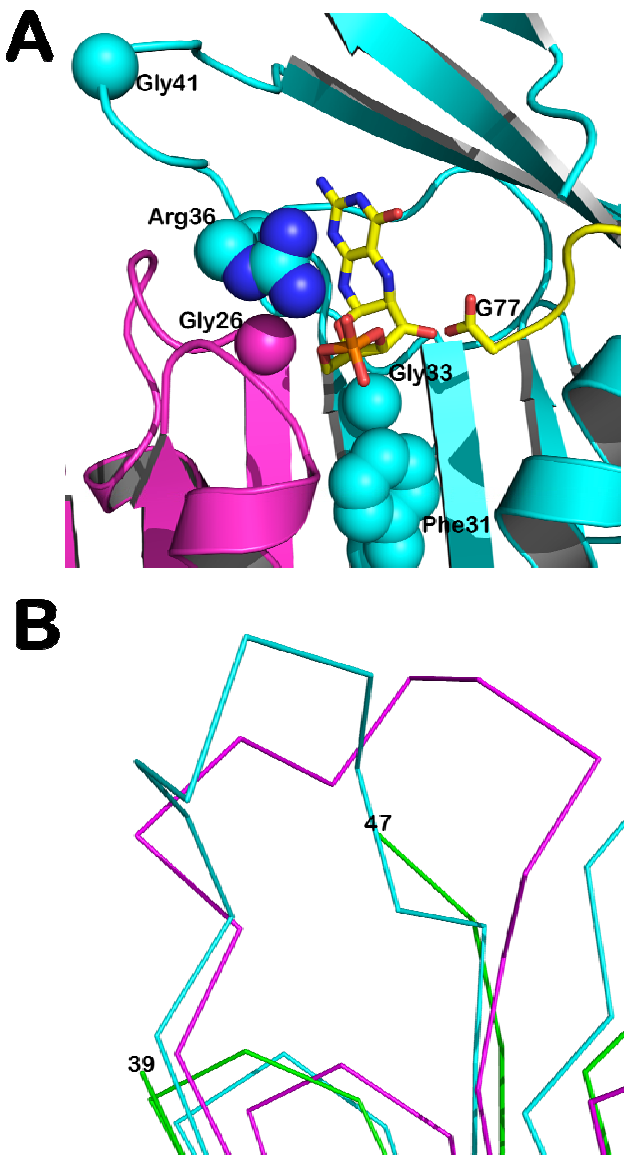

Figure 4.3: Features of the MPT synthase active site. (**a**) The strictly conserved residues in or near the active site loop, Gly26, Phe31, Gly33, Arg36 and Gly41 (the residue numbers refer to *S. aureus* MPT synthase) are shown in van der Waals representation. Note that Gly29 belongs to the distal MoaE. (**b**) Comparison of the loop region between β2 and β3 between *E. coli* (*green*, residues 40-46 are disordered), *S. aureus* (*cyan*) and *V. cholerae* (*magenta*) MPT synthase, the loops of *V. cholerae* and *S. aureus* were chosen to represent all loops in their respective structures.

and ψ=~11°, which, however, fall into a region that is accessible to all residues. Phe34 seems to be important for the structural integrity of the MoaE hydrophobic core immediately adjacent to the active site. Residues in this core include Ala29, Val32, Val97, Tyr108 and Met115 which are contributed from β1, α3, and β4. The remaining strictly conserved residue, Arg39, which corresponds to Arg36 of *S. aureus* MPT synthase originates from the β2 strand. In the precursor Z MPT synthase crystal complex the side chain of this residue was found above the plane of the pterin moiety engaging in cation-π interactions with precursor Z, and therefore was considered to be important for its binding and in line with this assumption substituting this residue with Ala reduces MPT production by 23 times compared to wild-type.

ii. MoaE β3-α2 region

The β3-α2 region, from Val47 to Arg73, includes three strictly conserved side residues, Glu53, Tyr55 and Met58, which participate with their side chains in the MoaE-MoaD interaction, Glu53 interacts via a salt-bridge with the positively charged MoaD surface residue Arg11, which is conserved in many MoaD species. MoaE Tyr55 and Met58 interact with the MoaD surface residues Phe7, Leu59 and Phe75, which are all type-conserved residues.

In the center of the α2 helix resides the strictly conserved Ile66. Inspection of this residue in all known MPT synthase structures strongly suggests a structural role for it in maintaining the MoaE structure. Ile66 is tucked inside the hydrophobic core between the β1 (Ile6) and β3 (Val79 and Val81) strands and the α3 helix (Ile114, Tyr117). The

distance between the closest neighboring side chain residues is about 3.1 Å. Due to its strict conservation and its position, a longer or shorter side chain may be enough to disrupt the core interactions contributed from the β1, β3 strands and the α3 helix.

iii. MoaE β4-β5 strands

The β4 and β5 strands encompassing the region from Gly77 to Trp89 and following the α2 helix contains three strictly conserved residues, His83, Arg84, and Gly86, which are all located below the buried MoaD C-terminal tail. The presumably uncharged side chain of His83 interacts via a hydrogen bond involving its Nε2 atom with the main chain N-H of MoaD Gly81 in all known structures of MPT synthase, which may be necessary for proper positioning of the MoaD C-terminal tail. At the same time the His83 H-bond also engages in a bifurcated H-bond between its Nδ1 atom and the MoaE main chain oxygens of Arg84 and Ile94. So far no biochemical studies have been carried out to confirm whether this interaction is indeed crucial for properly positioning the MoaD C-terminus. The MoaE strictly conserved residues Arg84 and Gly86 seem to only exhibit structural roles in the loop formed by the β4 and β6 strands. Arg84 helps to stabilize the loop between β4 and β6 strand by forming a salt bridge with the type-conserved Asp92 on the β6 strand, while Gly86 adopts a conformation that is only accessible for a glycine with main chain dihedral angles of ϕ=~100° and ψ=~-170°. Due to this special backbone conformation the side chain of a larger residue would be too close to the next residue as they essentially point in the same direction.

iv. MoaE α3 helix

The α3 helix, which consists of Arg104 to Arg121 contains four strictly conserved residue which are necessary for the binding of precursor Z and the catalytic activity of MPT synthase. The His/Arg pair corresponding to His103 and Arg104 in *V. cholerae* have been identified in the co-crystal complex of *S. aureus* MPT synthase with precursor Z as interacting with the cyclic phosphate group, demonstrating the importance of these residues in precursor Z binding. MoaE Ala107 is strictly conserved and may be important for the stabilizing interactions in the hydrophobic core between the α3 helix and central strand. Although the nearest residues, Val32 and Val99 are more than 4.2 Å away, there does not appear to be enough room to acoomodate a valine, the next largest hydrophobic side chain. Lys119, the last strictly conserved residue in this helix has been shown by biochemical studies to be vital for the sulfur transfer from the thiocarboxylated MoaD C-terminus to the C2' of precursor Z [39].

v. MoaE β7 strand region

The β7 strand region, from Pro123 to Trp136, contains three strictly conserved residues of the MoaE subunit. Lys126 and Glu128 have both been shown by biochemical studies [61] and by the precursor Z-MPT synthase structure to be important for the MPT synthase catalytic mechanism and proper binding of precursor Z, respectively. Trp136 is another MoaE residue residing in the interface between the MoaD and MoaE subunits,

and thus contributes to the recognition of MoaD and the stability of the MoaE-MoaD interaction. Since this region contains residues involved in binding and conversion of precursor Z and also binding of the MoaD subunit, proper positioning of these conserved residues inside the active site and within the MoaE-MoaD interface is of vital importance. The *E. coli* MoaEΔ141 deletion mutant in which the C-terminal helix has been removed, causes much greater disorder in the rest of the subunit from the β7 to β8 strand, and causes a shift of about 5 Å of the β3 strand, when compared to the native *E. coli* structure (Fig. 4.4). Additionally, the *E. coli* MoaEΔ141 deletion shows a 12-fold reduction in MPT formation [61]. This comparison suggests that Pro123 together with interactions of the C-terminus and MoaD helps in the proper alignment of residues from β7 that are located in the active site and on the surface of MoaE.

vi. MoaD β1-α1

The MoaD subunit when compared between all six structures and other MoaD species exhibits only limited sequence identity, however, it has high structural conservation. In between the β1 strand and α1 helix, from Ile2 to Val14, exist two strictly conserved residues whose side chains participate in the MoaE-MoaD hydrophobic interface. Phe7 resides approximately 3.4 Å away from the MoaE Tyr55, and 3.5 Å away from MoaE Trp125, together with MoaD Phe74 and Ala8, these five residues form a hydrophobic nucleus in the interface between the MoaE-MoaD subunits.

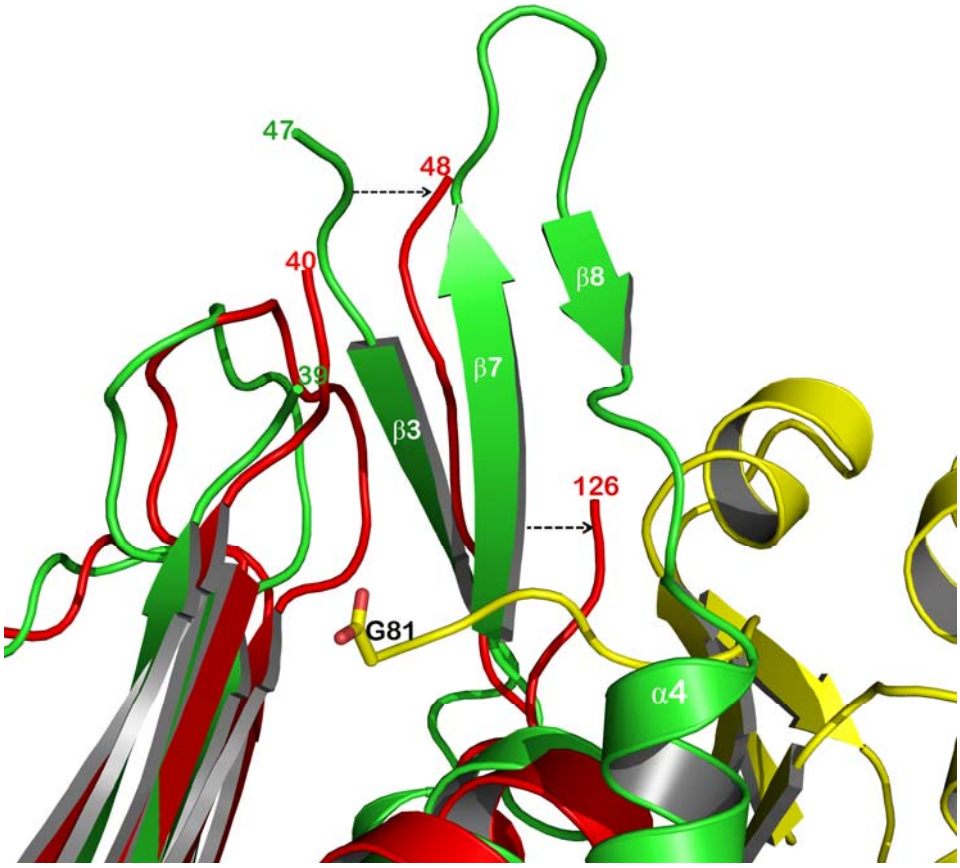

Figure 4.4: Comparison of *E. coli* MPT synthase from the wild-type (*green*, MoaE; *yellow* MoaD) and the MoaEΔ141 (PDB entry 1NVJ, *red*) structures in ribbon representation. MoaE Δ141 exhibits increased flexibility in the β7-β8 hairpin since residues past position 125 are disordered. The arrows indicate a concerted shift (to the right in this orientation) in the position of residues 48 and 126. The increase in flexibility of these residues could disrupt the interactions between them and the MoaD subunit.

vii. Consensus sequence in the MoaD β5 region

The β5 strand region is the last region, which contains strictly conserved residues in MoaD. The strictly conserved residue Asp70 is found at the beginning of β5 strand and interacts with the side chain nitrogen of Asn56 which is found 3 Å away. Inspection of sequence alignment shows that Asn56 is found in all species except for mouse and humans. The interactions between Asn56 and Asp70 seem to serve a structural role. The dual prolines at position 76 and 77 of which the first is strictly conserved and the second very highly conserved adopt a structure that allows the end of the β5 strand to turn sharply around the strictly conserved MoaE Trp125, while the Pro76 main chain carbonyl group acts as a hydrogen bond acceptor for the N-H of MoaE Trp125. The remaining strictly conserved double glycine motif at position 80 and 81, which are found at the C-terminal end, are required due to sterical limitations on their side chains which preclude the presence of larger residues and presumably also provides important flexibility to the C-terminal tail, which allows the terminal carboxylate to act on the correct position of the substrate. Lastly the terminal glycine is the important sulfur carrier, after thiocarboxylation by MoeB with the aid of a cysteine desulfurase. Subsequently, the thiocarboxylated terminal glycine attacks the C2' position of precursor Z and, after dissociation and re-association of MoaD, it then attacks the C1' position in the precursor Z substrate to ultimately yield molybdopterin.

B. Comparison of domain swapped MPT synthase enhances the understanding of the MoaE and MoaD interplay

When *V. cholerae* MPT synthase structures are compared, the domain swapped C-terminus reveals the necessity of an integral hydrophobic interface between the MoaE and MoaD subunits. As mentioned in the previous chapter all four crystal structures determined for *V. cholerae* MPT synthase contain an unusual oligomeric state, in which MPT synthase is present as a domain swapped oligomer. In two of these crystal structures, those from the MPT synthase-intermediate attempts, MPT synthase exists in the normal heterotetrameric form, but also in an unusual hetero*trimeric* state containing two MoaE subunits and only a single MoaD subunit. Inspection of the hetero*trimer* reveals no overall structural differences in the structure of the subunits, except for the MoaE subunit, which no longer has a MoaD interaction partner. The changes are confined to the C-terminal helix (Ala130 to Glu150), which shows moderate to no density in these structures. As a consequence the following pattern emerges: MoaE subunits missing a swapped-in C-terminal helix from the adjacent MoaE subunit do not interact with MoaD subunits. Upon closer inspection, the side chain of Tyr55 and Trp125 show a distinct conformational change between the activated *V. cholerae* structures derived from crystals prepared in the presence of the intermediate and other MPT synthase subunits (Fig. 4.5). Additionally, Trp135 is not participating in the hydrophobic interactions due to the fact that all residues from Ala130 to Glu150 are completely disordered indicating an increase in molecular flexibility. This C-terminal flexibility is not surprising since MPT synthase from *V. cholerae* can form the domain swapped

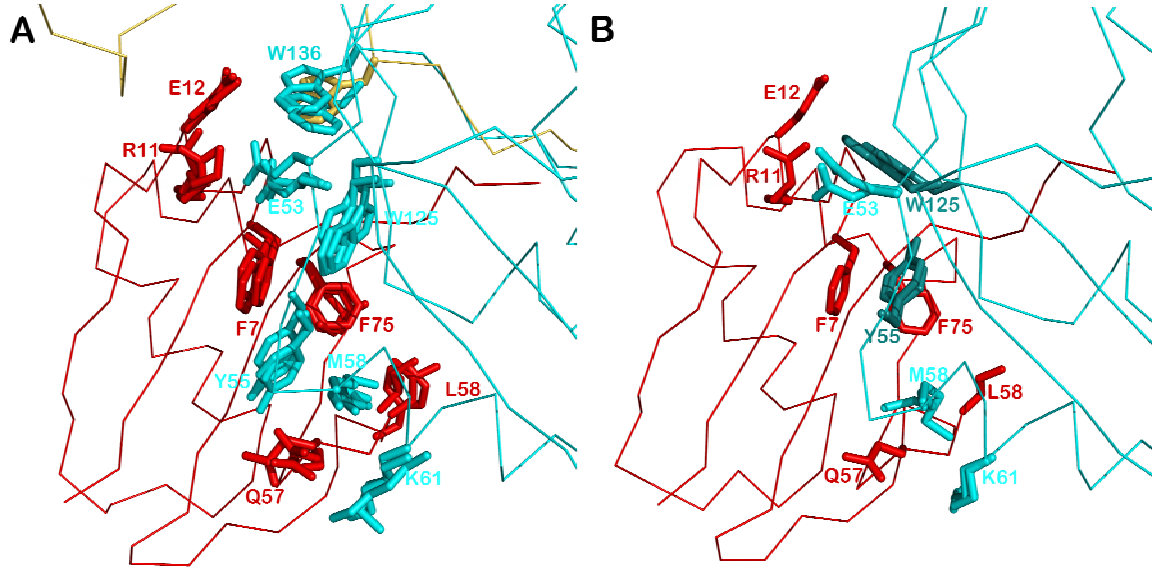

Figure 4.5: Comparison of the interface of MoaE-MoaD from *E. coli*, *S. aureus* and *V. cholerae*. (**a**) Superposition of interface side chains from MoaE (*cyan*) of the three species, the residue corresponding to *E. coli* Trp136 from the *V. cholerae* domain swapped MoaE in (*tan*) and MoaD (*red*). (**b**) *E. coli* MoaD superimposed onto the MoaE "only" part of the hetero*trimer* found in the *a*K125Aint *V. cholerae* 3.3 Å and 2.4 Å resolution structures. Please note the MoaD subunit (*red*) is shown here only as a reference, it is not interacting with this MoaE subunit (*cyan*). The residues exhibiting a comformational change, Tyr55 and Trp125, when (a) and (b) are compared are colored in *dark teal*. The loss of the residue corresponding to *E. coli* Trp136 (near the top in (a)) is apparently responsible for disrupting MoaE-MoaD interactions. In both panels the MoaD and MoaE side chains in the interface are in stick representation. For clarity, only the Cα trace of *E. coli* MPT synthase is shown in (a) and only the backbone of one of the *a*K125Aint *V. cholerae* structures is shown in (b).

conformation which critically depends on a different conformation of the C-terminus and it is also inherent in the *S. aureus* MPT synthase structures where the C-terminus is completely disordered. The superposition also suggests that the new conformations of Tyr55 and Trp125 would interfere with proper MoaE-MoaD interactions due to the clashes with MoaD residues Phe7 and Phe75. Tyr55 and Trp125 of MoaE may adopt this conformation, which is incompatible with MoaD binding when the C-terminal helix becomes more mobile, thereby moving Trp135 out of the interface. The loss of this residue could trigger the disruption of proper MoaE and MoaD interactions in the heterotrimeric states found in these structures. However, this is not the case in the *S. aureus* structures where the MoaE C-terminal helix contains charged residues and therefore cannot interact with the central MoaE residues via the hydrophobic interactions found in *E. coli* and *V. cholerae*, reflecting its intrinsic mobility demonstrated in our structures. Although the mobility of the C-terminus does not cause a disruption of MoaE-MoaD interactions in *S. aureus*, a conformational change of these residues may actually be caused by the sulfur transfer activity. Since Trp125 sits right above the active site and adjacent to Lys126, a residue that could sense the sulfur transfer, Lys126 could promote a new conformation in the nearby Trp125 which subsequently changes the conformation of Tyr55, and finally disrupt proper MoaE-MoaD interactions. This mechanism could be used in the normal interplay between MoaE and MoaD subunits which would allow MPT synthase to release discharged MoaD subunits.

Concluding Discussion

A. Co-crystal structure of MPT synthase with precursor Z

Our co-crystal structure of MPT synthase with precursor Z confirms the general location of the active site, defines atomic details of the substrate-binding mechanism and defines important residues for catalysis. It also provides a starting point for further analysis as to how the C-terminal thiocarboxylate can be used as the source of the dithiolene S-atoms during biosynthesis of the molybdopterin, although the details of how the enzyme carries out two identical S-transfer reactions at different acceptor sites within the substrate remain elusive. Due to the relationship between Moco and thiamin biosynthesis it is informative to compare the respective S-transfer reactions.

Similar to the molybdenum cofactor, thiamin is an essential cofactor in all living systems; it consists of a pyrimidine covalently linked to a thiazole. This cofactor is utilized for reactions which are central for amino acid metabolism, the pentose phosphate pathway and the citric acid cycle. In thiamin-deficient humans these processes do not function properly and result in disease states known as Beri Beri or Weminke-Korsakoff syndrome, both of which can be fatal [104,105]. The similarities between thiamine and Moco biosynthesis are restricted to the formation of the dithiolene group during Moco biosynthesis and the incorporation of a single S-atom during the formation of the thiazole moiety. In bacteria the thiazole is synthesized by six different proteins, ThiF, ThiG, ThiH, ThiI, ThiS, and a cysteine desulfurase, of which ThiF, ThiS and the cysteine desulfurase have clear counterparts during Moco biosynthesis. In addition, ThiG and MoaE carry out analogous function, yet they are unrelated in their primary sequence or three-dimensional structures.

The sulfur carrier protein adenylyl transferase (ThiF) catalyzes the adenylation of the carboxy terminus of the sulfur carrier proteins (ThiS), and the cysteine desulfurase catalyzes the transfer of the sulfur from cysteine to the ThiS-acyl adenylate to yield the ThiS thiocarboxylate [106]. This mechanism follows the same activation mechanism employed by the MoeB protein which catalyzes the adenylation of the MoaD protein and together with a sulfurase forms the thiocarboxylated form of MoaD. How this S is incorporated into the respective intermediates in each pathway is better established for thiamin biosynthesis. Studies about the early steps of thiazole formation have elucidated that imine formation between Lys96 on ThiG, also referred to as thiazole synthase, and its substrate DXP (1-deoxy-D-xylulose-5-phosphate) is followed by tautomerization forming an amino ketone, which is proposed to react with the ThiS thiocarboxylate and dehydroglycine to give thiazole phosphate (Fig. 5.1).

In all studies with MPT synthase thus far the MoaE subunit has not been found to form a covalent intermediate with the substrate. The co-crystal structure of *S. aureus* MPT synthase with precursor Z shows that MoaE does not form a covalent linkage with the substrate when MoaD is present in its inactive COO^--form. However, this does not eliminate the possibility that the thiocarboxylated MoaD promotes imine formation with the substrate by changes in the local electrostatics near the active site. Additionally, MPT synthase catalyzes two sulfur transfers in contrast to only a single S-transfer during thiamin biosynthesis, and experiments suggest that the first sulfur transfer occurs at the C2' position. Site directed mutagenesis studies demonstrated that the K119A mutation totally eliminates MPT synthase activity, a finding, which is similar to the K96A

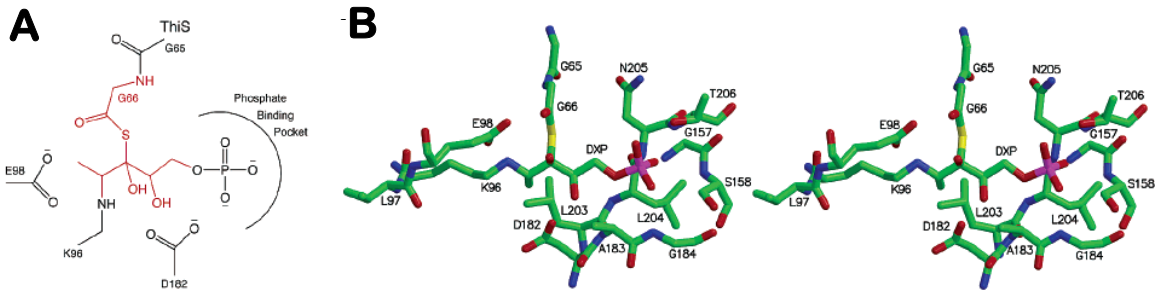

Figure 5.1: Model of DXP bound to the thiazole synthase active site. (**a**) Schematic representation showing DXP (*red*) and key amino acid side chains. Atoms shown in red were modeled using structural and mechanistic information. (**b**) Stereo view of a model of DXP bound to the thiazole synthase/ThiS complex (reproduced from Settembre et al. [83]).

mutation in thiazole synthase. Interestingly, MoaE Lys119 has been shown to form an unwanted covalent isopeptide side product with the C-terminus of a thiocarboxylated MoaD, which only forms when the active MPT synthase protein sits at 4ºC over a long period of time [36], this demonstrates that the lone pairs of nitrogen Lys119 are available. Lys119 is thus the most likely candidate for the formation of a posible imine intermediate, however, the only available carbonyl group on the substrate would be at the C2' carbon. It is unlikely that imine formation would change the conformation of the substrate because doing so would likely interfere with the proper transfer of the first sulfur from the MoaD C-terminus and interrupt the close binding interactions from the surrounding MoaE residues. The detailed characterization of the hemisulfurated intermediate found in the K126A mutant of the MoaE subunit should help to clarify these final details. So far it has not been possible to co-crystallize thiazole synthase with DXP, however, to help demonstrate the existence of a covalent intermediate mass spectrometry was used to capture it. This result helped in the construction of a model to show the possible positioning of DXP in the thiazole synthase active site [83]. Mass spectrometry might also be utilized to search for covalent intermediates which might need to be stabilized prior to such an analysis, such as reduction of the imine using $NaBH_4$. Although our biochemical experiments which demonstrate that the first S-atom is incorporated at the C2' position allow us to describe the catalytic mechanism in significantly more detail, it could not be used to predict the existence of a covalent intermediate.

The various MPT synthase structures, in particular the complex of the *S. aurues* enzyme with precursor Z, also provide a rationale for understanding the effects of mutations in human MPT synthase which lead to Moco deficiency. So far only one of the known mutations found in the active site of the MPT synthase has been identified in patients with molybdenum cofactor deficiency. The active site residue, Glu125, when mutated to a Lys abrogates MPT synthase activity. In our structure this can be explained by the loss of a hydrogen bond acceptor and the introduction of more steric hinderance against the NH_2 group of the pterin, which would clearly disrupt binding of precursor Z to the active site. Two point mutations found in the human version of MoaD, introduce larger side chains, Val7 to Phe and Ser14 to Arg, the only effect this causes is the disruption of the internal hydrophobic structure, possibly interfering with MoaE-MoaD interactions. The remaining human mutations leading to Moco deficiency in MPT synthase are nonsense mutations. These mutations cause incomplete translation of either the MoaE subunit or MoaD subunit or extend the wild-type sequence with a series of non-native residues, all causing severe disruption in native structure and activity.

B. Crystallization attempts with the hemisulfurated intermediate

The crystallization of the *V. cholerae* MPT synthase identified a Ca^{2+} ion dependent crystallization which promotes domain swapping of the C-terminal helix. All structures of *V. cholerae* MPT synthase show this unusual conformation, although biochemical experiments indicate that high concentrations of calcium ions are required to induce the domain-swapped conformation. However, the significance of the calcium ion

or any divalent ion requires further studies, the consistent domain swapping and oligomerization of three heterotetramers into a larger (150 kDa), heterododemaric complex cannot be more surprising. The domain swapping demonstrates that the C-terminus of *V. cholerae* MoaE can adopt an open and closed conformation. This flexibility is possibly coupled to the dissociation and re-association of the MoaD subunit, a process which is required for the two sulfur transfer reactions. These conformations can allow for the close association of other MPT synthase subunits and may act as a scaffold onto which other biosynthesis proteins bind to form a mega-complex.

Attempts to co-crystallize the hemi-sulfurated intermediate provided other crystal packings which all demonstrated the existence of oligomerization mediated by domain swapping, however, these attempts could not visualize the intermediate in the active site. The protein loaded with the intermediate contained thiocarboxylated MoaD protein which is necessary to produce a hemisulfurated intermediate in *E. coli* MPT synthase mutation studies, however, the lack of electron density for three of six MoaD subunits in these structures is a clear indication that MPT synthase even in the presence of a K125A mutant can catalyze complete conversion, which is then followed by MoaD dissociation. Recent studies comparing the intermediate accumulating mutants made in *E. coli* and *V. cholerae* MPT synthase show that the *V. cholerae* variant does not accumulate as much intermediate as initially thought, instead it produces a substantial amount of product (Dr. Margot Wuebbens, personal communication).

C. Future studies

The notion that MPT synthase sulfur transfer mechanism occurs via a covalent attachment similar to the sulfur transfer mechanism occurring in thiazole synthase, elevates the need for further studies of an intermediate co-crystal complex. Continuation of these co-crystallization experiments with *E. coli*, *S. aureus* and *V. cholerae*, and other species are needed to answer the remaining question. The main bottleneck in this process is protein crystallization.

Since the crystallization of the *V. cholerae* MPT synthase allows a convenient and predictable avenue, exploiting the calcium dependent crystallization described in this thesis may make the *V. cholerae* MPT synthase a good protein for future studies, but two hurdles need to be overcome. Optimization of the crystallization conditions containing polyethylene glycol (PEG) and calcium needs to be performed. PEG is a preferred precipitant to use for co-crystallization attempts, since high salt precipitants can interfere with protein ligand interactions. Previous attempts have shown some promising conditions (Fig. 5.2). K125A MPT synthase loaded with intermediate was initially tested for crystallization in a PEG condition containing $CaCl_2$ which formed pseudo-crystalline structures in the drop. When a range of PEG precipitants was used across a crystallization tray, these structures seemed to become more crystalline although they also became much smaller. Secondly, the amount of hemisulfurated intermediate must be increased to exhaust the remaining thiocarboxylated MoaD present and increase the occupancy of the intermediate at the active site. By focusing on these two aspects in future crystallization attempts one will improve the chances for a well diffracting MPT synthase-

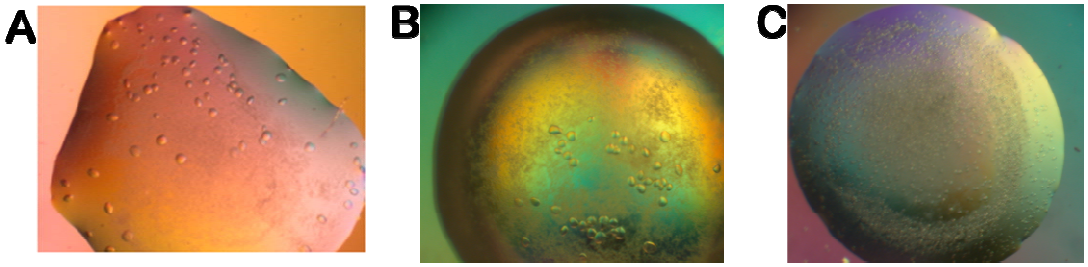

Figure 5.2: Promising conditions from crystallization attempts of the *a*K125Aint with PEG. (**a**) 0.5% PEG 8000, 0.1M HEPES, 0.1 M $CaCl_2$, pH 7.0 (**b**) 1.0% PEG 8000, 0.1 M HEPES, 0.1 M $CaCl_2$, pH 7.0 (**c**) 1.5% PEG 8000, 0.1 M HEPES, 0.1 M $CaCl_2$, pH 7.0.

intermediate co-crystals, hopefully resulting in a well defined identification of the intermediate and any surrounding structural modifications.

References

1. Rajagopalan K: *Escherichia coli and Salmonella typhimurium*, vol 1. Washington D.C.: American Society for Microbiology; 1996.

2. Hille R: **The Mononuclear Molybdenum Enzymes**. *Chem Rev* 1996, **96**:2757-2816.

3. Johnson JL, Wadman SK: *The metabolic basis of inherited disease*. New York: McGraw-Hill; 1989.

4. Johnson JL, Rajagopalan KV, Mukund S, Adams MW: **Identification of molybdopterin as the organic component of the tungsten cofactor in four enzymes from hyperthermophilic Archaea**. *J Biol Chem* 1993, **268**:4848-4852.

5. Koshiba T, Saito E, Ono N, Yamamoto N, Sato M: **Purification and Properties of Flavin- and Molybdenum-Containing Aldehyde Oxidase from Coleoptiles of Maize**. *Plant Physiol* 1996, **110**:781-789.

6. Lin JT, Stewart V: **Nitrate assimilation by bacteria**. *Adv Microb Physiol* 1998, **39**:1-30, 379.

7. Campbell WH: **Nitrate Reductase Biochemistry Comes of Age**. *Plant Physiol* 1996, **111**:355-361.

8. Meneshian A, Bulkley GB: **The physiology of endothelial xanthine oxidase: from urate catabolism to reperfusion injury to inflammatory signal transduction**. *Microcirculation* 2002, **9**:161-175.

9. Stevens CR, Millar TM, Clinch JG, Kanczler JM, Bodamyali T, Blake DR: **Antibacterial properties of xanthine oxidase in human milk**. *Lancet* 2000, **356**:829-830.

10. Vorbach C, Harrison R, Capecchi MR: **Xanthine oxidoreductase is central to the evolution and function of the innate immune system**. *Trends Immunol* 2003, **24**:512-517.

11. Mulder GJaJW: *Sulfation in Conjugation Reactions in Drug Metabolism: An Integrated Approach: Substrates, Co-substrates, Enzymes and Their Interactions In Vivo and In Vitro*. Edited by Mulder GJ. London: Taylor and Francis; 1990.

12. Dietrich CP, Sampaio LO, Toledo OM, Cassaro CM: **Cell recognition and adhesiveness: a possible biological role for the sulfated mucopolysaccharides**. *Biochem Biophys Res Commun* 1977, **75**:329-336.

13. Dietrich CP, Sampaio LO, Toledo OM: **Characteristic distribution of sulfated mucopolysaccharides in different tissues and in their respective mitochondria**. *Biochem Biophys Res Commun* 1976, **71**:1-10.

14. Johnson JL, Coyne KE, Garrett RM, Zabot MT, Dorche C, Kisker C, Rajagopalan KV: **Isolated sulfite oxidase deficiency: identification of 12 novel SUOX mutations in 10 patients**. *Hum Mutat* 2002, **20**:74.

15. Karakas E, Wilson HL, Graf TN, Xiang S, Jaramillo-Busquets S, Rajagopalan KV, Kisker C: **Structural insights into sulfite oxidase deficiency**. *J Biol Chem* 2005, **280**:33506-33515.

16. Bertero MG, Rothery RA, Palak M, Hou C, Lim D, Blasco F, Weiner JH, Strynadka NC: **Insights into the respiratory electron transfer pathway from the structure of nitrate reductase A**. *Nat Struct Biol* 2003, **10**:681-687.

17. Rothery RA, Blasco F, Magalon A, Weiner JH: **The diheme cytochrome b subunit (Narl) of Escherichia coli nitrate reductase A (NarGHI): structure, function, and interaction with quinols**. *J Mol Microbiol Biotechnol* 2001, **3**:273-283.

18. Blasco F, Guigliarelli B, Magalon A, Asso M, Giordano G, Rothery RA: **The coordination and function of the redox centres of the membrane-bound nitrate reductases**. *Cell Mol Life Sci* 2001, **58**:179-193.

19. Jormakka M, Tornroth S, Byrne B, Iwata S: **Molecular basis of proton motive force generation: structure of formate dehydrogenase-N**. *Science* 2002, **295**:1863-1868.

20. Pateman JA, Cove DJ, Rever BM, Roberts DB: **A Common Co-Factor for Nitrate Reductase and Xanthine Dehydrogenase Which Also Regulates the Synthesis of Nitrate Reductase**. *Nature* 1964, **201**:58-60.

21. Ketchum PA, Cambier HY, Frazier WA, 3rd, Madansky CH, Nason A: **In vitro assembly of Neurospora assimilatory nitrate reductase from protein subunits of a Neurospora mutant and the xanthine oxidizing or aldehyde oxidase systems of higher animals**. *Proc Natl Acad Sci U S A* 1970, **66**:1016-1023.

22. Nason A, Antoine AD, Ketchum PA, Frazier WA, 3rd, Lee DK: **Formation of assimilatory nitrate reductase by in vitro inter-cistronic complementation in Neurospora crassa**. *Proc Natl Acad Sci U S A* 1970, **65**:137-144.

23. Johnson JL, Jones HP, Rajagopalan KV: **In vitro reconstitution of demolybdosulfite oxidase by a molybdenum cofactor from rat liver and other sources**. *J Biol Chem* 1977, **252**:4994-5003.

24. Ketchum PA, Swarin RS: **In vitro formation of assimilatory nitrate reductase: presence of the constitutive component in bacteria**. *Biochem Biophys Res Commun* 1973, **52**:1450-1456.

25. Pienkos PT, Shah VK, Brill WJ: **Molybdenum cofactors from molybdoenzymes and in vitro reconstitution of nitrogenase and nitrate reductase**. *Proc Natl Acad Sci U S A* 1977, **74**:5468-5471.

26. Johnson JL, Hainline BE, Rajagopalan KV: **Characterization of the molybdenum cofactor of sulfite oxidase, xanthine, oxidase, and nitrate reductase. Identification of a pteridine as a structural component**. *J Biol Chem* 1980, **255**:1783-1786.

27. Menendez C, Siebert D, Brandsch R: **MoaA of Arthrobacter nicotinovorans pAO1 involved in Mo-pterin cofactor synthesis is an Fe-S protein**. *FEBS Lett* 1996, **391**:101-103.

28. Hanzelmann P, Schindelin H: **Crystal structure of the S-adenosylmethionine-dependent enzyme MoaA and its implications for molybdenum cofactor deficiency in humans**. *Proc Natl Acad Sci U S A* 2004, **101**:12870-12875.

29. Wuebbens MM, Liu MT, Rajagopalan K, Schindelin H: **Insights into molybdenum cofactor deficiency provided by the crystal structure of the molybdenum cofactor biosynthesis protein MoaC**. *Structure Fold Des* 2000, **8**:709-718.

30. Reiss J, Christensen E, Kurlemann G, Zabot MT, Dorche C: **Genomic structure and mutational spectrum of the bicistronic MOCS1 gene defective in molybdenum cofactor deficiency type A**. *Hum Genet* 1998, **103**:639-644.

31. Leimkuhler S, Charcosset M, Latour P, Dorche C, Kleppe S, Scaglia F, Szymczak I, Schupp P, Hahnewald R, Reiss J: **Ten novel mutations in the molybdenum cofactor genes MOCS1 and MOCS2 and in vitro characterization of a MOCS2 mutation that abolishes the binding ability of molybdopterin synthase**. *Hum Genet* 2005, **117**:565-570.

32. Santamaria-Araujo JA, Fischer B, Otte T, Nimtz M, Mendel RR, Wray V, Schwarz G: **The tetrahydropyranopterin structure of the sulfur-free and metal-free molybdenum cofactor precursor**. *J Biol Chem* 2004, **279**:15994-15999.

33. Schwarz G, Santamaria-Araujo JA, Wolf S, Lee HJ, Adham IM, Grone HJ, Schwegler H, Sass JO, Otte T, Hanzelmann P, et al.: **Rescue of lethal molybdenum cofactor deficiency by a biosynthetic precursor from Escherichia coli**. *Hum Mol Genet* 2004, **13**:1249-1255.

34. Westcott BL, Gruhn NE, Enemark JH: **Evaluation of Molybdenum-Sulfur Interactions in Molybdoenzyme Model Complexes by Gas-Phase Photoelectron Spectroscopy. The "Electronic Buffer" Effect**. *J. Am. Chem. Soc.* 1998, **120**:3382-3386.

35. Hahnewald R, Leimkuhler S, Vilaseca A, Acquaviva-Bourdain C, Lenz U, Reiss J: **A novel MOCS2 mutation reveals coordinated expression of the small and large subunit of molybdopterin synthase**. *Mol Genet Metab* 2006, **89**:210-213.

36. Rudolph MJ, Wuebbens MM, Rajagopalan KV, Schindelin H: **Crystal structure of molybdopterin synthase and its evolutionary relationship to ubiquitin activation**. *Nat Struct Biol* 2001, **8**:42-46.

37. Pitterle DM, Johnson JL, Rajagopalan KV: **In vitro synthesis of molybdopterin from precursor Z using purified converting factor. Role of protein-bound sulfur in formation of the dithiolene**. *J Biol Chem* 1993, **268**:13506-13509.

38. Pitterle DM, Rajagopalan KV: **The biosynthesis of molybdopterin in Escherichia coli. Purification and characterization of the converting factor**. *J Biol Chem* 1993, **268**:13499-13505.

39. Rudolph MJ, Wuebbens MM, Turque O, Rajagopalan KV, Schindelin H: **Structural studies of molybdopterin synthase provide insights into its catalytic mechanism**. *J Biol Chem* 2003, **278**:14514-14522.

40. Lake MW, Wuebbens MM, Rajagopalan KV, Schindelin H: **Mechanism of ubiquitin activation revealed by the structure of a bacterial MoeB-MoaD complex**. *Nature* 2001, **414**:325-329.

41. Leimkuhler S, Wuebbens MM, Rajagopalan KV: **Characterization of Escherichia coli MoeB and its involvement in the activation of molybdopterin synthase for the biosynthesis of the molybdenum cofactor**. *J Biol Chem* 2001, **276**:34695-34701.

42. Xiang S, Nichols J, Rajagopalan KV, Schindelin H: **The crystal structure of Escherichia coli MoeA and its relationship to the multifunctional protein gephyrin**. *Structure (Camb)* 2001, **9**:299-310.

43. Sandu C, Brandsch R: **Evidence for MoeA-dependent formation of the molybdenum cofactor from molybdate and molybdopterin in Escherichia coli**. *Arch Microbiol* 2002, **178**:465-470.

44. Liu MT, Wuebbens MM, Rajagopalan KV, Schindelin H: **Crystal structure of the gephyrin-related molybdenum cofactor biosynthesis protein MogA from Escherichia coli**. *J Biol Chem* 2000, **275**:1814-1822.

45. Schwarz G, Schrader N, Mendel RR, Hecht HJ, Schindelin H: **Crystal structures of human gephyrin and plant Cnx1 G domains: comparative analysis and functional implications**. *J Mol Biol* 2001, **312**:405-418.

46. Llamas A, Otte T, Multhaup G, Mendel RR, Schwarz G: **The Mechanism of nucleotide-assisted molybdenum insertion into molybdopterin. A novel route toward metal cofactor assembly**. *J Biol Chem* 2006, **281**:18343-18350.

47. Kuper J, Llamas A, Hecht HJ, Mendel RR, Schwarz G: **Structure of the molybdopterin-bound Cnx1G domain links molybdenum and copper metabolism**. *Nature* 2004, **430**:803-806.

48. Golden ML, Whaley CM, Rampersad MV, Reibenspies JH, Hancock RD, Darensbourg MY: **N2S2Ni metallodithiolate complexes as ligands: structural and aqueous solution quantitative studies of the ability of metal ions to form M-S-Ni bridges to mercapto groups coordinated to nickel(II). implications for acetyl coenzyme A synthase**. *Inorg Chem* 2005, **44**:875-883.

49. Hegg EL: **Unraveling the structure and mechanism of acetyl-coenzyme A synthase**. *Acc Chem Res* 2004, **37**:775-783.

50. Morrison MS, Cobine PA, Hegg EL: **Probing the role of copper in the biosynthesis of the molybdenum cofactor in Escherichia coli and Rhodobacter sphaeroides**. *J Biol Inorg Chem* 2007, **12**:1129-1139.

51. Johnson JL, Bastian NR, Rajagopalan KV: **Molybdopterin guanine dinucleotide: a modified form of molybdopterin identified in the molybdenum cofactor of dimethyl sulfoxide reductase from Rhodobacter sphaeroides forma specialis denitrificans**. *Proc Natl Acad Sci U S A* 1990, **87**:3190-3194.

52. Johnson JL, Indermaur LW, Rajagopalan KV: **Molybdenum cofactor biosynthesis in Escherichia coli. Requirement of the chlB gene product for the formation of molybdopterin guanine dinucleotide**. *J Biol Chem* 1991, **266**:12140-12145.

53. Dobbek H, Gremer L, Meyer O, Huber R: **Crystal structure and mechanism of CO dehydrogenase, a molybdo iron-sulfur flavoprotein containing S-selanylcysteine**. *Proc Natl Acad Sci U S A* 1999, **96**:8884-8889.

54. Vergnes A, Pommier J, Toci R, Blasco F, Giordano G, Magalon A: **NarJ chaperone binds on two distinct sites of the aponitrate reductase of Escherichia coli to coordinate molybdenum cofactor insertion and assembly**. *J Biol Chem* 2005.

55. Neumann M, Stocklein W, Leimkuhler S: **Transfer of the molybdenum cofactor synthesized by Rhodobacter capsulatus MoeA to XdhC and MobA**. *J Biol Chem* 2007, **282**:28493-28500.

56. Reiss J: **Genetics of molybdenum cofactor deficiency**. *Hum Genet* 2000, **106**:157-163.

57. Reiss J, Johnson JL: **Mutations in the molybdenum cofactor biosynthetic genes MOCS1, MOCS2, and GEPH**. *Hum Mutat* 2003, **21**:569-576.

58. Reiss J, Dorche C, Stallmeyer B, Mendel RR, Cohen N, Zabot MT: **Human molybdopterin synthase gene: genomic structure and mutations in molybdenum cofactor deficiency type B**. *Am J Hum Genet* 1999, **64**:706-711.

59. Kim EY, Schrader N, Smolinsky B, Bedet C, Vannier C, Schwarz G, Schindelin H: **Deciphering the structural framework of glycine receptor anchoring by gephyrin**. *Embo J* 2006, **25**:1385-1395.

60. Reiss J, Gross-Hardt S, Christensen E, Schmidt P, Mendel RR, Schwarz G: **A mutation in the gene for the neurotransmitter receptor-clustering protein gephyrin causes a novel form of molybdenum cofactor deficiency**. *Am J Hum Genet* 2001, **68**:208-213.

61. Wuebbens MM, Rajagopalan KV: **Mechanistic and mutational studies of Escherichia coli molybdopterin synthase clarify the final step of molybdopterin biosynthesis**. *J Biol Chem* 2003, **278**:14523-14532.

62. Gutzke G, Fischer B, Mendel RR, Schwarz G: **Thiocarboxylation of molybdopterin synthase provides evidence for the mechanism of dithiolene formation in metal-binding pterins**. *J Biol Chem* 2001, **276**:36268-36274.

63. Sambrook J, Russell DW: *Molecular cloning: a laboratory manual* edn 3rd. Cold Spring Harbor, NY: Cold Spring Harbor Laboratory Press; 2001.

64. Wuebbens MM, Rajagopalan KV: **Structural characterization of a molybdopterin precursor**. *J Biol Chem* 1993, **268**:13493-13498.

65. Jancarik J, Kim SH: **Sparse matrix sampling: a screening method for crystallization of proteins**. *J. Appl. Cryst.* 1991, **24**:409-411.

66. Otwinowski A, Minor W: *Methods in Enzymology- Macromolecular Crystallography*, vol 276 A: Academic Press; 1997.

67. Vagin AA, Isupov MN: **Spherically averaged phased translation function and its application to the search for molecules and fragments in electron-density maps**. *Acta Crystallogr D Biol Crystallogr* 2001, **57**:1451-1456.

68. Vagin A, Teplyakov A: **An approach to multi-copy search in molecular replacement**. *Acta Crystallogr D Biol Crystallogr* 2000, **56**:1622-1624.

69. Murshudov GN, Vagin AA, Dodson EJ: **Refinement of macromolecular structures by the maximum-likelihood method**. *Acta Crystallogr D Biol Crystallogr* 1997, **53**:240-255.

70. Winn MD, Isupov MN, Murshudov GN: **Use of TLS parameters to model anisotropic displacements in macromolecular refinement**. *Acta Crystallogr D Biol Crystallogr* 2001, **57**:122-133.

71. Winn MD, Murshudov GN, Papiz MZ: **Macromolecular TLS refinement in REFMAC at moderate resolutions**. *Methods Enzymol* 2003, **374**:300-321.

72. Jones TA, Zou JY, Cowan SW, Kjeldgaard: **Improved methods for building protein models in electron density maps and the location of errors in these models**. *Acta Crystallogr A* 1991, **47 (Pt 2)**:110-119.

73. Bailey S: **The CCP4 suite: programs for protein crystallography**. *Acta Crystallogr D Biol Crystallogr* 1994, **50**:760-763.

74. Perrakis A, Morris R, Lamzin VS: **Automated protein model building combined with iterative structure refinement**. *Nat Struct Biol* 1999, **6**:458-463.

75. Johnson JL, Rajagopalan KV: **Structural and metabolic relationship between the molybdenum cofactor and urothione**. *Proc Natl Acad Sci U S A* 1982, **79**:6856-6860.

76. Johnson JL, Hainline BE, Rajagopalan KV, Arison BH: **The pterin component of the molybdenum cofactor. Structural characterization of two fluorescent derivatives**. *J Biol Chem* 1984, **259**:5414-5422.

77. Lovell SC, Davis IW, Arendall WB, 3rd, de Bakker PI, Word JM, Prisant MG, Richardson JS, Richardson DC: **Structure validation by Calpha geometry: phi,psi and Cbeta deviation**. *Proteins* 2003, **50**:437-450.

78. Johnson JL, Wuebbens MM, Rajagopalan KV: **The structure of a molybdopterin precursor. Characterization of a stable, oxidized derivative**. *J Biol Chem* 1989, **264**:13440-13447.

79. Zacharias N, Dougherty DA: **Cation-pi interactions in ligand recognition and catalysis**. *Trends Pharmacol Sci* 2002, **23**:281-287.

80. Beene DL, Brandt GS, Zhong W, Zacharias NM, Lester HA, Dougherty DA: **Cation-pi interactions in ligand recognition by serotonergic (5-HT3A) and nicotinic acetylcholine receptors: the anomalous binding properties of nicotine**. *Biochemistry* 2002, **41**:10262-10269.

81. Gallivan JP, Dougherty DA: **Cation-pi interactions in structural biology**. *Proc Natl Acad Sci U S A* 1999, **96**:9459-9464.

82. Vander Horn PB, Backstrom AD, Stewart V, Begley TP: **Structural genes for thiamine biosynthetic enzymes (thiCEFGH) in Escherichia coli K-12**. *J Bacteriol* 1993, **175**:982-992.

83. Settembre EC, Dorrestein PC, Zhai H, Chatterjee A, McLafferty FW, Begley TP, Ealick SE: **Thiamin biosynthesis in Bacillus subtilis: structure of the thiazole synthase/sulfur carrier protein complex**. *Biochemistry* 2004, **43**:11647-11657.

84. Dorrestein PC, Huili Zhai H, Taylor SV, McLafferty FW, Begley TP: **The biosynthesis of the thiazole phosphate moiety of thiamin (vitamin B1): the early steps catalyzed by thiazole synthase**. *J Am Chem Soc* 2004, **126**:3091-3096.

85. Schmitz J, Wuebbens MM, Rajagopalan KV, Leimkuhler S: **Role of the C-terminal Gly-Gly motif of Escherichia coli MoaD, a molybdenum cofactor biosynthesis protein with a ubiquitin fold**. *Biochemistry* 2007, **46**:909-916.

86. Albright RA, Mossing MC, Matthews BW: **High-resolution structure of an engineered Cro monomer shows changes in conformation relative to the native dimer**. *Biochemistry* 1996, **35**:735-742.

87. Murray AJ, Lewis SJ, Barclay AN, Brady RL: **One sequence, two folds: a metastable structure of CD2**. *Proc Natl Acad Sci U S A* 1995, **92**:7337-7341.

88. Green SM, Gittis AG, Meeker AK, Lattman EE: **One-step evolution of a dimer from a monomeric protein**. *Nat Struct Biol* 1995, **2**:746-751.

89. Kortt AA, Malby RL, Caldwell JB, Gruen LC, Ivancic N, Lawrence MC, Howlett GJ, Webster RG, Hudson PJ, Colman PM: **Recombinant anti-sialidase single-chain**

variable fragment antibody. Characterization, formation of dimer and higher-molecular-mass multimers and the solution of the crystal structure of the single-chain variable fragment/sialidase complex. *Eur J Biochem* 1994, **221**:151-157.

90. Janowski R, Kozak M, Abrahamson M, Grubb A, Jaskolski M: **3D domain-swapped human cystatin C with amyloidlike intermolecular beta-sheets**. *Proteins* 2005, **61**:570-578.

91. Janowski R, Kozak M, Jankowska E, Grzonka Z, Grubb A, Abrahamson M, Jaskolski M: **Human cystatin C, an amyloidogenic protein, dimerizes through three-dimensional domain swapping**. *Nat Struct Biol* 2001, **8**:316-320.

92. Knaus KJ, Morillas M, Swietnicki W, Malone M, Surewicz WK, Yee VC: **Crystal structure of the human prion protein reveals a mechanism for oligomerization**. *Nat Struct Biol* 2001, **8**:770-774.

93. Sanders A, Jeremy Craven C, Higgins LD, Giannini S, Conroy MJ, Hounslow AM, Waltho JP, Staniforth RA: **Cystatin forms a tetramer through structural rearrangement of domain-swapped dimers prior to amyloidogenesis**. *J Mol Biol* 2004, **336**:165-178.

94. Staniforth RA, Giannini S, Higgins LD, Conroy MJ, Hounslow AM, Jerala R, Craven CJ, Waltho JP: **Three-dimensional domain swapping in the folded and molten-globule states of cystatins, an amyloid-forming structural superfamily**. *Embo J* 2001, **20**:4774-4781.

95. Sambashivan S, Liu Y, Sawaya MR, Gingery M, Eisenberg D: **Amyloid-like fibrils of ribonuclease A with three-dimensional domain-swapped and native-like structure**. *Nature* 2005, **437**:266-269.

96. Nenci A, Gotte G, Bertoldi M, Libonati M: **Structural properties of trimers and tetramers of ribonuclease A**. *Protein Sci* 2001, **10**:2017-2027.

97. Gotte G, Bertoldi M, Libonati M: **Structural versatility of bovine ribonuclease A. Distinct conformers of trimeric and tetrameric aggregates of the enzyme**. *Eur J Biochem* 1999, **265**:680-687.

98. Park C, Raines RT: **Dimer formation by a "monomeric" protein**. *Protein Sci* 2000, **9**:2026-2033.

99. Louie GV, Yang W, Bowman ME, Choe S: **Crystal structure of the complex of diphtheria toxin with an extracellular fragment of its receptor**. *Mol Cell* 1997, **1**:67-78.

100. Liu Y, Eisenberg D: **3D domain swapping: as domains continue to swap**. *Protein Sci* 2002, **11**:1285-1299.

101. Laskowski RA, Moss DS, Thornton JM: **Main-chain bond lengths and bond angles in protein structures**. *J Mol Biol* 1993, **231**:1049-1067.

102. Glickman MH, Ciechanover A: **The ubiquitin-proteasome proteolytic pathway: destruction for the sake of construction**. *Physiol Rev* 2002, **82**:373-428.

103. Pickart CM: **Back to the future with ubiquitin**. *Cell* 2004, **116**:181-190.

104. Martin PR, Singleton CK, Hiller-Sturmhofel S: **The role of thiamine deficiency in alcoholic brain disease**. *Alcohol Res Health* 2003, **27**:134-142.

105. Butterworth RF: **Thiamin deficiency and brain disorders**. *Nutrition Research Reviews* 2003, **16**:277-284.

106. Xi J, Ge Y, Kinsland C, McLafferty FW, Begley TP: **Biosynthesis of the thiazole moiety of thiamin in Escherichia coli: identification of an acyldisulfide-linked protein--protein conjugate that is functionally analogous to the ubiquitin/E1 complex**. *Proc Natl Acad Sci U S A* 2001, **98**:8513-8518.